CR-128734

N73-17510

TRINITY BAY STUDY:
DYE TRACING EXPERIMENTS

Submitted to:

Earth Observations Division
Manned Spacecraft Center
National Aeronautics and Space Administration
Houston, Texas

November, 1972

TRACOR

6500 Tracor Lane, Austin, Texas 78721, AC 512/926-2800

Contract Number NAS 9-12724
TRACOR Project 077-021
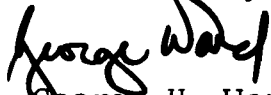Document Number T72-AU-9601-U

TRINITY BAY STUDY:

DYE TRACING EXPERIMENTS

By

George H. Ward, Jr.

Submitted to:

Earth Observations Division
Manned Spacecraft Center
National Aeronautics and Space Administration
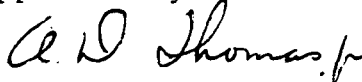Houston, Texas

November, 1972

Submitted by:

George H. Ward, Jr.
Project Director

Approved by:

A. D. Thomas, Jr., Ph.D.
Acting Director, Ocean Sciences
and Water Resources Department

TABLE OF CONTENTS

TABLE OF CONTENTS (CONT'D)

LIST OF ILLUSTRATIONS

LIST OF ILLUSTRATIONS (CONT'D)

LIST OF ILLUSTRATIONS (CONT'D)

LIST OF TABLES

1. INTRODUCTION

The NASA/MSC Trinity Bay Study (NASA, 1971) has focused upon the heat balance and temperature distribution within Trinity Bay, particularly as affected by the Houston Lighting and Power (HL&P) Cedar Bayou Generating Station, which draws its cooling water from behind Atkinson Island in upper Galveston Bay and discharges into upper Trinity Bay above Point Barrow (Fig. 1.1). One of the predominant factors governing the distribution of temperature (and, especially, the thermal plume configuration at the Cedar Bayou discharge) is the hydrodynamics of the Trinity Bay System. This is conventionally dichotomized as advective and dispersive. Among the former are included the effects of tidal currents, wind-driven circulations, and large-volume inflows. Among the latter are the effects of turbulent diffusion and local shears in the currents. In practice, there is no clear separation between these two classes of hydrodynamic processes; this depends, in part, upon the resolvable scales of motion, which in turn is determined by methods of measurement and the mathematical representation (the "model").

The dye tracing experiments reported here address specifically the dispersion processes, although advective information is extracted as well when appropriate. The fundamental approach was to perform an instantaneous release (a "slug") of dye, producing a patch whose subsequent growth is determined by the dispersive processes. By tracking the patch and obtaining quantitative measures of the dye distribution, one can infer the values of parameters (dispersion coefficients) characterizing dispersion.

These activities were conducted with an eye to a projected study of the Galveston Bay system, planned to be a unified examination of mass, momentum, and energy exchange

1
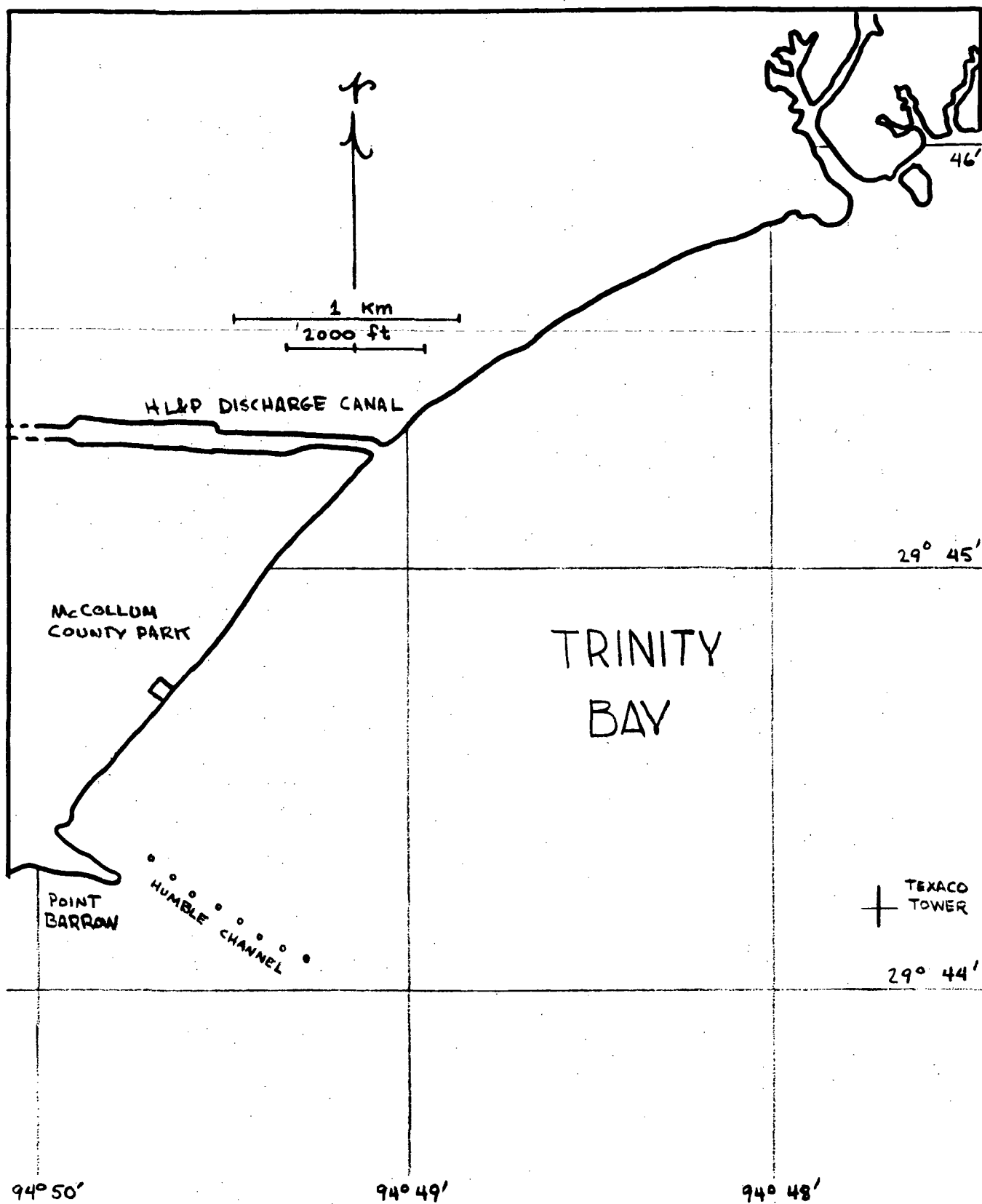
FIG. 1.1   OPERATING AREA

processes in the estuary. While the dye data collected has value in itself for analyzing dispersion processes, an alternate, even overriding, application was to be the formulation of measurement strategies for the projected program. Of central importance to this was determination of how the vast remote sensing capabilities of NASA could be used to maximal benefit. Accordingly, several variations in the field techniques were tried during the course of this study. Some failed, and the data obtained was consequently inferior. However, it is felt that the cost of poorer data is more than compensated by gaining information on the feasibility of certain techniques.

The analysis of the data reported here represents an effort to make the most of what we have. Some of the data sets perhaps should not have even been attempted because of their incompleteness; nevertheless the philosophy is followed that a little information is better than none at all. Accordingly, when detailed information was missing, approximations were made; if not an approximation, an assumption; if not an assumption, a guess. For this reason, an effort has been made to indicate clearly the quality of various computations.

The greatest difficulty in executing the field work was weather conditions, which continually frustrated the operations. It seemed that every mission encountered an exceptional condition. Most of the data here represents near-calm conditions, which limits the potential applicability. Hopefully, as this type of exercise is continued, more representative data sets will be accumulated.

2.   FIELD OPERATIONS

As one of the objectives of this series of experiments was the development of dye tracing methods adequate for studies in Trinity Bay, a number of different procedures were employed on the various missions. In general, the approach was to perform a slug release of dye (i.e., an approximately instantaneous release of a volume of diluted dye) and then follow the subsequent development of the dye patch by means of fluorometry supplemented by aerial photography as available.

2.1   Equipment

The principal piece of equipment used in this work is a fluorometer equipped for continuous monitoring of dye concentration. A fluorometer is an instrument for measuring the fluorescence intensity of a substance, in this case a tracer dye, exposing the tracer to a beam of light and measuring the light intensity emitted by the tracer by means of an optical bridge. The fact that fluorescent substances emit light at a different wave length (usually longer) than that at which they absorb means that the separation of the excitation beam and the emission beam within the fluorometer is a matter of selection of proper filters. The measured quantity, intensity of fluorescence, can be related to the concentration of tracer matter present. This, therefore, provides a quantitative assessment of dye concentration which is necessary to carry out the calculations described in Section 3.

The fluorometer used in this study is a Turner Model 111 equipped with a flow-through door and a strip chart recorder to allow continuous monitoring of dye concentration. The fluorometer system is comprised of the fluorometer itself, a pump, a gasoline alternator to provide power for both the fluorometer and

pump, and various hoses, couplings, and screens. The entire
system is mounted within a boat with intake hose fore and the
discharge aft so that dye is continuously pumped through the
fluorometer as the boat moves. Fig. 2.1 shows the fluorometer
in place in the boat; the pump is visible in front of the
fluorometer. Shading is required as the instrument is sensitive
to direct sunlight.

The boat used throughout this work was a 15' Glastron
with maximum draft of about a foot. Selection of a boat for this
kind of operation is obviously a matter of trade-offs. On the
one hand, large deck space and stability are desirable; on the
other hand, too large a boat or one with a large displacement
will disrupt the dye patch as it is being traversed. The Glastron
used in this study was found to be generally adequate provided
one is careful not to began sampling the patch prematurely. On
one occasion, Mission 186, waves coming over the bow shorted out
the pump and terminated the operation. This was more the fault,
however, of inadequately locating and protecting the pump than
the low topsides of the boat per se.

The type of fluorescent dye used in these experiments
is Rhodamine WT, manufactured by Du Pont. This is presently one
of the most popular dyes for tracer studies in surface waters
because of its high detectability, its relatively low decay, and
its good sorptive properties. Rhodamine WT has a peak in its
excitation spectrum at about 560 mμ, and in its emission spectrum
at about 580 mμ.

2.2   Procedures

For each release a quantity of dye was diluted with
ethacol and ambient water so as to adjust the buoyancy of the
mixture. At the selected release point the dye was poured into the

FIG. 2.1   BOAT MOUNTED FLUOROMETER IN OPERATION

FIG. 2.2   "SLUG" RELEASE OF DILUTED DYE

water at a steady, relatively slow rate, Fig. 2.2. The boat was held stationary and the release performed so as to confine the dye to as small an area initially as practical. Thus, in its initial stages, the developing patch was almost circular, and any subsequent development along preferred axes would, therefore, be a consequence of different diffusion processes, not the configuration of the dye at its release. Fig. 2.3 is an aerial photograph of one of the patches twenty-five minutes after its release.

After the patch has been allowed to develop for about an hour, the sampling is initiated. Ideally, one would like to obtain the instantaneous horizontal spatial distribution of the dye. When sampled from a boat, this must be approximated by a series of intercepts crisscrossing the patch from which the dye contours are then constructed. The greater the number of intercepts the greater the detail in the dye distribution that can be inferred, but, on the other hand, the longer the time necessary for the boat to complete the set of traverses. A compromise is necessary, therefore, between these two extremes. In these operations the number of intercepts for each patch configuration was about three or four. When the patch appeared symmetric this was reduced to two, i.e., the longitudinal and lateral axes. However, when the dye distribution appeared complex and irregular, more traverses were necessary.

As the output of the fluorometer is basically concentration versus time, some additional information is required to transform this into concentration versus spatial position. Several methods for accomplishing this were employed in this study but they basically divide into two kinds: first, the boat track is noted relative to fixed reference points, e.g., marker buoys, poles, etc.; and second, the relative movement of the boat throughout the set of traverses

FIG. 2.3   PATCH A AT 0914 (8 OCTOBER 1971), MISSION 186, 25 MINUTES AFTER RELEASE

FIG. 2.4   DUCTED FLOWMETER

is determined using the (magnetic) course together with the boat
velocity. The most accurate means of accomplishing the latter
was found to be a series of rectilinear passes in which the boat
track is limited to lines along perferred directions at right
angles to each other. An integrated measure of the boat velocity
was obtained by using a ducted impeller flowmeter, Fig. 2.4, in
a continuous run from the start of the first traverse to the
completion of the last.

The end product of the above procedure is the distribution
of dye in a horizontal plane at the depth of the intake, about 8"
or 0.2 m. Some knowledge of the vertical distribution of dye is
useful as well in analyzing the data. When time permitted, there-
fore, vertical soundings were made in the dye patch. The boat
returned to the patch center, as indicated by the fluorescence peak,
where the intake hose was lowered from surface to bottom to obtain
a fluorescence-versus-depth trace on the chart record. This was
done both by lowering the intake continuously at a slow rate and
by holding the intake at discrete levels for several seconds.
The latter proved to yield the better data as the fluctuations in
concentration could be averaged out.

Most of the operations discussed in this report were
conducted in conjunction with missions of the NASA/MSC Trinity
Bay Study. Accordingly, the data collected by the dye boat
was supplemented by transit positioning and by helicopter and
P-3 photography. One of the aims of this work was to develop
techniques by which these remote-sensing capabilities could be
used to maximal advantage in conducting tracer studies. This
hope was repeatedly frustrated by poor conditions, which either
limited the utility of the remote photography or eliminated it
altogether. For this reason, the use of this kind of supporting
information, unfortunately, has been limited to qualitative rather
than quantitative applications.

2.3   Data Reduction

The immediate information acquired from the fluorometer
system is a strip chart record of fluorescence versus time. The
problem of data reduction devolves then to relating the fluores-
cence to dye concentration and relating the time record to spatial
position. An example of the strip chart output from the fluorometer
is given in Fig. 2.5. In this case the patch was traversed along
its longitudinal axis. Upon exiting the patch, the boat reversed
its course and went back through the patch in the same direction
but slightly to one side of the original track. The near mirror-
image symmetry of the two traces emphasizes the fact that the
fluorometer system time constant introduces no hysteresis in the
data (at least at these space scales). Thus, the measured
concentration gradients are not significantly distorted as a
consequence of the direction of the traverse.
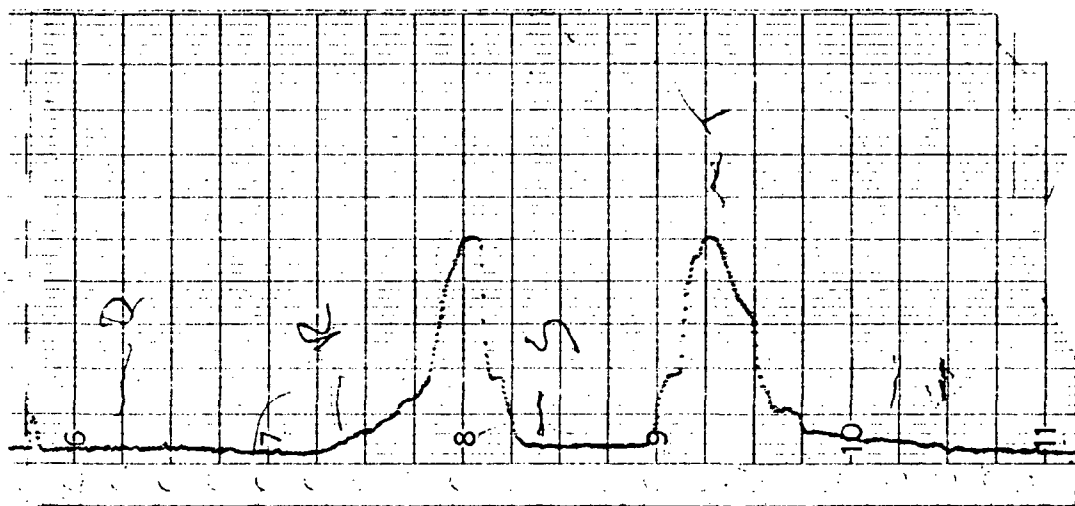
FIG. 2.5   EXAMPLE OF FLUORESCENCE VERSUS TIME FROM
             FLUOROMETER STRIP CHART RECORD

10

Fluorescence is dependent upon concentration, of course, but also upon the presence of other fluorescing substances in the water, upon scattering and absorbing materials in the water, and upon the water temperature. Insofar as this work is concerned, the quantity of interest is the fluorescence elevation above the "background." The background fluorescence is determined by monitoring ambient water at the start of the experiments before any dye is released. This is then subtracted from the total fluorescence before the data is analyzed. Thus, the first effect, the problem of fluorescing materials other than dye in the water, is not of practical importance for this work. The third difficulty, the temperature dependence of the fluorescence, can become a problem in natural waters when the dye patch moves through a large temperature gradient. Because all of these releases were made sufficiently far from shore (and from the HL&P discharge), and because the vertical variation in temperature in Galveston Bay is so slight, this potential difficulty was eliminated. This does mean, however, that the fluorescence observed in summer waters may be different from that observed in winter even though the concentration of dye is the same. The second difficulty, that of scattering or absorptive matter in the water, is of most concern to these experiments because of the high and variable turbidity of water in Trinity Bay. Care was taken in selecting the release points to minimize the probability of the patch moving through areas of changing turbidity. Ultimately, of course, this circumstance is beyond the control of the experimenter; he can only observe the turbidity and try to correct for it in his data. Fortunately, in all of the patches analyzed in this report (except for Patch C of Mission 204) there is no evidence that changing turbidities corrupted the data. The effect of turbidity does, however, prevent direct comparison of concentrations measured in nearshore releases to those made further out (cf. Mission 186, Patch A_1 and Patch B_1).

Relation of concentration to fluorescence is established by laboratory calibration curves determined by running known concentrations in the particular fluorometer to be used (with the continuous-flow cuvette) for each of the four intensity ranges available. Because, for the analysis performed in this study, the feature of interest is the relative development of the patch, not its absolute concentration, these calibration curves were used without any correction for temperature, etc. Accordingly, the "calibration" should be regarded as a means to relate the fluorescence at the four scales of intensity to a common base, with the recognition that the relation of that common base to absolute concentration may vary. When grab samples were obtained in lieu of pump-through monitoring (Mission 186), the samples were restored to approximate bay temperature and shaken before analysis to restore turbidity, then analyzed with the flow-through cuvette. Therefore the same set of calibration curves should apply and the measurements obtained be comparable to those that would have been obtained <u>in situ</u>.

From the calibration of the fluorometer, therefore, one may convert the fluorescence versus time (e.g., Fig. 2.5) to concentration versus time. The next step is to relate the time scale to a distance scale and locate the traverses geographically. When a traverse is run between two reference points whose absolute positions are known, the time corresponding to the boat's passage at each point is marked on a strip chart. It is a simple matter then to mark concentration versus distance along the line connecting the reference points on an appropriate map. From several such traverses the dye contours may be constructed, e.g., Fig. 4.14. Usually, though, all that is available is a record of the boat's track, each change in course being marked on the strip chart when it was effected, and the magnetic direction being recorded in the field notes. One must now use the mean boat

velocity to plot the boat movement throughout the set of traverses. Some adjustment is usually required as time is lost in executing the turns, as there are occasional errors in direction, and as the velocity may vary slightly during the run, e.g., depending on whether the boat is moving against the wave crests or with them. Once the boat's track has been adequately established, the concentrations from the strip chart record are marked along the corresponding traverses. From the resulting plot, isopleths of dye concentration are developed. Thus, the final product of this analysis is a diagram showing contours of dye concentration in the horizontal plane at intake depth.

It must be remarked that the construction of isopleths is a highly subjective matter which depends considerably upon the experience and judgement of the individual. From the same set of concentration-versus-distance intercepts, different interpretations yield different contour configurations; the differences are sometimes in detail only, but sometimes are significant. The techniques of data analysis (Section 3.3) were selected in part to minimize the effects of such isoplething variations. More important is that the contouring be carried out by personnel experienced with isopleth construction who also are familiar with the analysis to which the data will be subjected. It may be comforting (or maybe not) that in this study this task was left to meteorologists.

Data reduction for the vertical profiles follows the same approach as that for the horizontal traverses. Fluorescence is converted to concentration, and as the individual depths (or the end-points of a surface-to-bottom profile) are marked on the chart record, the conversion to spatial distribution is straight-forward.

13

3. METHODS OF ANALYSIS

3.1 Theoretical Considerations

The purpose of analyzing the dye distributions measured in this study is to infer properties of turbulent mixing and their dependence upon ambient conditions. To accomplish this, a theoretical model of the diffusion process is employed, which is summarized, rather superficially, in this section. The distribution of concentration of a dilute, neutrally buoyant, conservative tracer is governed by the continuity equation; in the well-known Reynolds form this is

$$\frac{\partial c}{\partial t} + u_i \frac{\partial c}{\partial x_i} = - \frac{\partial}{\partial x_i} \overline{u_i' c'} \qquad (3.1)$$

Here the overbar denotes an ensemble average, which may be reduced to a spatial or temporal average under appropriate conditions, c and u_i denote the ensemble-mean values of concentration and velocity, and c' and u_i' denote the instantaneous departures from the respective ensemble means. Thus $c + c'$ is the (total) concentration at a particular time and point, and $u_i + u_i'$ is the corresponding (total) velocity.

The usual approach, adopted here, is to regard the net effect of the mean nonlinear advective fluxes $\overline{u' c_i'}$ on the mean concentration distribution as being diffusive in character, i.e., proportional to the spatial gradients in the mean concentration. The "constants" of proportionality are called eddy diffusivities, denoted here ϵ_{ij}. With this definition, (3.1) becomes

$$\frac{\partial c}{\partial t} + u_i \frac{\partial c}{\partial x_i} = \frac{\partial}{\partial x_i} \epsilon_{ij} \frac{\partial c}{\partial x_j} \qquad (3.2)$$

This is the most general form for such a diffusive flux, since the possibility of the i-flux depending as well upon cross-gradients of c is accomodated through the tensor character of ϵ_{ij} . We may, however, rotate the axes to align with the principal axes of ϵ_{ij} , in which case (3.2) reduces to

$$\frac{\partial c}{\partial t} + u_i \frac{\partial c}{\partial x_i} = \frac{\partial}{\partial x_i} \epsilon_I \frac{\partial c}{\partial x_i} \tag{3.3}$$

where ϵ_I denotes the principal value of ϵ_{ij} corresponding to x_i in the new coordinates.

Variations in $c + c'$ and $u_i + u_i'$ in geofluid systems exist over a wide, continuous range of space and time scales. In an estuarine system such as Trinity Bay one does not expect to find the smooth $\frac{5}{3}$-law spectral roll-off predicted by similarity theory, because there are energy inputs at preferred scales, e.g., tidal action, wind stress, density currents. There may in fact be spectral "gaps," certain ranges of the spectrum whose energy content, though not zero, is an order-of-magnitude or so less than that of the neighboring regions. Application of the ensemble-mean Reynolds equation (3.1) to a set of data such as dye concentrations where the averaging is in space and time, requires, for example, $\overline{c'} = \overline{u_i'} = 0$, the overbar now denoting a space-time mean. This is satisfied only if the mean quantities c and u_i exhibit variations on larger scales than those of the averaging, that is, only if there is a spectral gap between the scales of motion in c and u_i and those scales represented in the Reynolds fluxes. (De Fériet, 1951, has initiated a discussion of some aspects of this problem.)

This condition is satisfied by and large for the dye releases analyzed here, because the patch development was followed only for the first few hours of its lifetime. Some averaging is

15

imposed by the response of the fluorometer system itself, then
the strip chart record is further averaged by eye when the
concentrations are read off. The necessary smoothing attending
isopleth construction represents both a time and space average,
the former since data taken sequentially over a 30-minute period
are used to establish an "instantaneous" mean distribution. The
final computation (as will be seen) involves further averaging
in that the isopleths are effectively replaced by equi-areal
ellipses. All told, the dye data are subjected to time averages
on the order of 10^3 seconds and space averages on the order of the
patch radius. Significant variations in the mean current u_i
above these scales were usually on orders of 10^4 sec or more and
on scales of many radii, so that (3.1) or (3.3) are applicable.
There were, however, some notable exceptions (Patch B_2 of Mission
186, for example) that are discussed later.

Another effect of the continuous spectrum over wide
ranges of scales is that as a dye patch grows it becomes under
the influence of motions at larger scales, in addition to those
motions which have accomplished its dispersion so far. Thus
with the increase in size, diffusion is accelerated. This is a
particularly prominent effect in the horizontal plane, but not
so much in the vertical because of other complications. This is
manifested as an increase in the horizontal eddy diffusivities
with scale, which dimensional analysis predicts as a $\frac{4}{3}$-dependence
on horizontal scale ℓ ,

$$\epsilon_{1,2} \propto \ell^{4/3}$$

This seems to be obeyed locally by oceanic dye diffusion data
(see Okubo, 1971).

The three-dimensional equation (3.3) is too cumbersome
for the purposes of this study, which is principally restricted

to horizontal processes. Accordingly, we suppress the vertical dependence by integrating with z (= x_3) between the surface h and a level below which no dye penetrates, whose depth we denote D . Since the vertical flux of dye at h and at $h - D$ is zero, (3.3) becomes

$$\frac{\partial [c]}{\partial t} + [u] \frac{\partial [c]}{\partial x} + [v] \frac{\partial [c]}{\partial y} = \frac{\partial}{\partial x} \left[\epsilon_1 \frac{\partial c}{\partial x} \right] - \frac{\partial}{\partial x} [u'' c'']$$

$$+ \frac{\partial}{\partial y} \left[\epsilon_2 \frac{\partial c}{\partial y} \right] - \frac{\partial}{\partial y} [v'' c'']$$

where $[f] \equiv \frac{1}{D} \int_{h-D}^{h} f \, dz$, the vertical mean of f , and $f'' \equiv f - [f]$, the local departure in f from its vertical mean value. (Suffix notation has also been replaced.) It has become conventional to treat the combined fluxes on the right as being <u>diffusive</u>, in analogy to the definition of eddy diffusion. That is, the effect of these fluxes on the vertical mean concentration $[c]$ is assumed to be proportional to the gradient of $[c]$,

$$\left[\epsilon_1 \frac{\partial c}{\partial x} \right] - \left[u'' c'' \right] = E_x \frac{\partial [c]}{\partial x}$$

$$\left[\epsilon_2 \frac{\partial c}{\partial y} \right] - \left[v'' c'' \right] = E_y \frac{\partial [c]}{\partial y}$$

(3.4)

where E_x and E_y are called the "effective" diffusion coefficients or "dispersion" coefficients. (More generally, one defines a dispersivity tensor, analogous to the derivation of (3.2) above, but as only the principal values are of concern in this study, equation (3.4) was referred to its principal axes.) There is less justification for the assumption (3.4) than for the introduction of eddy coefficients; however, (3.4) has enjoyed considerable empirical success, and its utilitarian value is certain. With this definition, the vertical mean continuity equation for c becomes

$$\frac{\partial c}{\partial t} + u \frac{\partial c}{\partial x} + v \frac{\partial c}{\partial y} = \frac{\partial}{\partial x} E_x \frac{\partial c}{\partial x} + \frac{\partial}{\partial y} E_y \frac{\partial c}{\partial y} \qquad (3.5)$$

in which the brackets have been omitted.

Since (3.5) is to be applied to a diffusing patch of dye over short periods of time, the further simplification is made that the axes are embedded in the center of the patch and move with the mean velocity (u, v) . Then (3.5) reduces, finally, to

$$\frac{\partial c}{\partial t} = \frac{\partial}{\partial x} E_x \frac{\partial c}{\partial x} + \frac{\partial}{\partial y} E_y \frac{\partial c}{\partial y} \qquad (3.6)$$

expressing the relative horizontal dispersion of the vertical-mean concentration c . If E_x and E_y have no spatial dependence, then

$$\frac{\partial c}{\partial t} = E_x \frac{\partial^2 c}{\partial x^2} + E_y \frac{\partial^2 c}{\partial y^2} \qquad (3.7)$$

A common behavior of a release of dye is that the patch tends to elongate as it diffuses. This is obviously an indication that $E_x \neq E_y$. The underlying physical cause is implicit in (3.4), which shows that an enhanced flux along one axis is produced by either anisotropy in the turbulence (i.e., $\epsilon_1 \neq \epsilon_2$) or by a correlation in the vertical structure of (u, v) and c .

The latter circumstance, [u" c"] $\neq$ 0 , say, is known as the "shear effect" because of the central importance of vertical shear in the mean current. A thorough discussion may be found in, e.g., Bowden (1965). For the present context, it is sufficient to note that this effect is thought to be responsible for the large differences between E_x and E_y observed in oceanic diffusion

18

experiments. It is also the effect responsible for the inflated longitudinal dispersion coefficients necessary for (one-dimensionally) modeling the saline region of coastal plain estuaries.

The former possibility, anisotropy in the turbulence, is generally discounted in favor of the shear effect because it is expected that $\overline{(u')^2} \cong \overline{(v')^2}$, the difference not being large enough to account for the large eccentricities exhibited by elongated patches. In a system such as Trinity Bay, this possibility cannot be so readily discounted, however. If momentum is supplied with a preferred component, e.g., in the direction of the tidal current or in the direction of wind drift, the preservation of (horizontal) isotropy depends upon the vigor of the turbulent redistribution processes, viz.

$$\overline{\frac{u'}{\rho_o}\frac{\partial p'}{\partial x}} + \frac{1}{2}\left\{\frac{\partial}{\partial x}\overline{(u')^3} + \frac{\partial}{\partial y}\overline{v'(u')^2} + \frac{\partial}{\partial z}\overline{w'(u')^2}\right\}$$

etc., see Phillips (1966). In near-calm conditions, with only bulk tidal motion, it is not inconceivable that significant anistropy could occur.

3.2   Gaussian Models

Determination of the coefficients E_x and E_y from observed distributions of c using either (3.6) or (3.7) must involve some assumptions about the nature of the solution of the governing equation. One of the most ubiquitous practical methods is to assume a Gaussian distribution of the dye,

$$c = \frac{A}{t}\exp\left\{-\frac{1}{4t}\left(\frac{x^2}{E_x} + \frac{y^2}{E_y}\right)\right\}$$ (3.8)

19

or, equivalently,

$$
c = A4\pi \sqrt{E_x E_y} \left(\frac{1}{2\pi\,\sigma_x\,\sigma_y} \exp\left\{ -\tfrac{1}{2}\left[\left(\frac{x}{\sigma_x}\right)^2 + \left(\frac{y}{\sigma_y}\right)^2 \right] \right\} \right) \tag{3.9}
$$

where $\sigma_x = \sqrt{2E_x t}$, $\sigma_y = \sqrt{2E_y t}$, see Mood (1950, pg. 165 f), Okubo (1968), Diachishin (1963). Equation (3.8) may be readily verified to be <u>one</u> solution of (3.7) subject to the boundary condition that $c \to o$ as $x^2 + y^2 \to \infty$. Since the quantity in parentheses in (3.9), the Gaussian distribution, integrates to unity over the entire x-y plane, we have the total mass (or volume) of dye added M given by

$$
M = \int_{h-D}^{h} \int_{-\infty}^{\infty} \int_{-\infty}^{\infty} c\ dx\ dy\ dz = DA\ 4\pi\sqrt{E_x E_y} \tag{3.10}
$$

where D is the "depth" of the patch (as defined in the preceding section). Substituting back into (3.9) yields

$$
c = \frac{M}{2\pi\,D\,\sigma_x\,\sigma_y} \exp\left\{ -\tfrac{1}{2}\left[\left(\frac{x}{\sigma_x}\right)^2 + \left(\frac{y}{\sigma_y}\right)^2 \right] \right\} \tag{3.11}
$$

We note that the peak concentration is

$$
c_o = \frac{M}{2\pi\,D\,\sigma_x\,\sigma_y} \tag{3.12}
$$

From the logarithm of (3.11)

$$
\log \left(\frac{c_o}{c}\right)^2 = \left(\frac{x}{\sigma_x}\right)^2 + \left(\frac{y}{\sigma_y}\right)^2
$$

20

which for c constant is the equation of an ellipse with semi-axes given by

$$a^2 = \sigma_x^2 \log \left(\frac{c_o}{c}\right)^2$$

(3.13)

$$b^2 = \sigma_y^2 \log \left(\frac{c_o}{c}\right)^2$$

Thus the isopleths of concentration are ellipses in the x, y-plane; for specificity, we take the major axis of the ellipse to coincide with the x-axis.

One grapples with real dye data for only a short time before he recognizes that ellipitical contours are rarely, if ever, encountered. Instead real dye patches assume the contortions of a tormented amoeba, and the equations (3.8-11) derived from the Gaussian form are consequently poor models. Fortunately, dispersion coefficients are rarely required to stringent precision (the assumptions involved merely to arrive at (3.7) are crude approximations in themselves), so that the convenience and simplicity of using Gaussian "fits" largely justify the roughness of the approximation.

The dispersion coefficients are given in terms of the respective variances

$$E_x = \frac{\sigma_x^2}{2t} \quad , \quad E_y = \frac{\sigma_y^2}{2t}$$

(3.14)

where t is the total elapsed time from the release, or, differentiating,

$$E_x = \tfrac{1}{2} \frac{d \, \sigma_x^2}{dt} \quad , \quad E_y = \tfrac{1}{2} \frac{d \, \sigma_y^2}{dt}$$

(3.15)

21

Both of these expressions assume E_x , E_y to be invariant with time, i.e., Fickian diffusion, which is not strictly valid since E_x , E_y generally increase with time as the scale of the patch enlarges. For a short interval, however, the Gaussian model is approximately valid and (3.15) is an adequate means of computing the dispersion coefficients. Equation (3.14) is not as good since t is measured from the time of release, during which E_x and E_y vary significantly with time. We can estimate the error incurred by using (3.14) if it is assumed that $E \propto \sigma^{4/3}$ (omitting the subscripts), i.e., the spatial standard deviation is taken as a measure of the scale of diffusion, and that (3.15) applies throughout the diffusion process. Upon integration,

$$E(t) = \frac{3}{2} \frac{\sigma^2}{t}$$

so that evaluation of E by (3.14) underestimates its magnitude by about a factor of three. This is a soft number actually, because to carry out the above integration one is implicitly assuming that $E(t)$ varies sufficiently slowly that (3.8) is still a valid solution for (3.7), a WKB-type approximation, whereas in reality c_o , σ^2 and E probably have about the same time scales in their variation. Nonetheless, we anticipate that (3.14) will be an underestimate, and prefer to use (3.15) whenever the data permits.

3.3   Computational Techniques

As E_x and E_y are given in terms of the horizontal variances σ_x^2 and σ_y^2 , the problem of data analysis devolves to an estimation of these variances. If variances are known at two different times, t_1 , and t_2 , E is computed by the finite-difference approximation of (3.15),

$$E_x \cong \tfrac{1}{2} \frac{\sigma_x^2(t_2) - \sigma_x^2(t_1)}{t_2 - t_1}$$

$$E_y \cong \tfrac{1}{2} \frac{\sigma_y^2(t_2) - \sigma_y^2(t_1)}{t_2 - t_1}$$

(3.16)

If the configuration of dye is known at only one time, t_1 , say, then E is calculated from (3.14)

$$E_x = \frac{\sigma_x^2}{2 (t_1 - t_0)}$$

$$E_y = \frac{\sigma_y^2}{2 (t_1 - t_0)}$$

(3.17)

where t_0 is the time of release. In the following data summaries, the first method (3.16) is abbreviated by $E = \sigma \dot{\sigma}$ and the second (3.17) by $E = \sigma^2/2t$. As noted above, the former is preferable.

The properties of the Gaussian distribution (3.9) suggest a number of approaches to estimating σ^2 from dye data (e.g., Diachishin, 1963; Okubo, 1968; Ward, 1972; see also Kullenberg, 1969, 1971 for related methods). We note, for example, that (3.11) may be rewritten

$$\frac{c(x,y)}{c_0} = 2\pi \, n\left(\frac{x}{\sigma_x} \; ; \; 0,1\right) \cdot n\left(\frac{y}{\sigma_y} \; ; \; 0,1\right)$$

(3.18)

where $n(t \; ; \; p,q)$ denotes a normal density function in t with mean p and variance q . With the origin at c_0 , the x-axis along the major axis and y-axis along the minor axis, (3.18) implies

23

$$\frac{1}{\sqrt{2\pi}} \frac{c\ (x,o)}{c_o} = n\left(\frac{x}{\sigma_x}\ ;\ 0,1\right)$$

$$\frac{1}{\sqrt{2\pi}} \frac{c\ (o,y)}{c_o} = n\left(\frac{y}{\sigma_y}\ ;\ 0,1\right)$$

Now where the standard Gaussian density $n\ (t\ ;\ 0,1) = .242$ there $t = 1$ (see, e.g. Mood, 1950, or any probability table). Consequently when $c\ (x,o)/c_o = \sqrt{2\pi}\ \cdot\ .242 = .607$, $x/\sigma_x = 1$ or $x = \sigma_x$. Similarly when $c\ (o,y)/c_o = .607$, $y = \sigma_y$. One may select other convenient σ - levels by consulting a tabulation of $n(t;0,1)$. When the corresponding concentration is calculated, the distance between the centroid and that concentration isopleth is measured along the patch axes, and the standard deviations computed.

On some occasions the value of peak concentration c_o may not be known, e.g., if the traversals were off-peak or if the center portion of the patch were off-scale. In this case, c_o can be estimated from the properties of the Gaussian distribution. If the first equation of (3.13) is evaluated for two different concentrations c_1 and c_2 , and σ_x^2 eliminated, one obtains

$$\log c_o = \frac{X_1^2\ \log c_2 - X_2^2\ \log c_1}{X_1^2 - X_2^2} \qquad (3.19)$$

where X_1 and X_2 denote either the semi-major axis (distance from peak to $c_{1,2}$ contour along x-axis) or the major axis (distance between intercepts of $c_{1,2}$ contour and x-axis). A similar equation holds for the minor axis.

The method generally used in this study is derived from the geometric properties expressed by (3.13). Since the

area of an ellipse is πab , the area enclosed by a contour of concentration c is

$$A_c = \pi \, \sigma_x \, \sigma_y \, \log \left(\frac{c_o}{c}\right)^2 \qquad (3.20)$$

Furthermore the ratio of the major to minor axis is

$$\frac{a}{b} = \frac{\sigma_x}{\sigma_y}$$

which implies

$$\sigma_x{}^2 = \frac{a}{b} \, \sigma_x \, \sigma_y$$

$$\qquad (3.21)$$

$$\sigma_y{}^2 = \frac{b}{a} \, \sigma_x \, \sigma_y$$

The method used is:

    (1)   Planimeter the area enclosed by various concentration isopleths.

    (2)   Plot these areas versus the logarithm of the corresponding concentration on log-linear paper. The zero-intercept is c_o .

    (3)   Choose a best-fit straight line to the data points. The slope of this line is $- (2\pi \, \sigma_x \, \sigma_y)^{-1}$ from (3.20). Compute $\sigma_x \, \sigma_y$.

    (4)   Estimate the ratio a/b of major axis to minor axis from the horizontal configuration of the patch.

(5) Compute $\sigma_x{}^2$ and $\sigma_y{}^2$ from the values of $\sigma_x \sigma_y$ and a/b, using equations (3.21).

This method has several advantages. It is largely graphical so can be implemented quite easily. It basically replaces the contours with ellipses having equivalent areas and smoothes the distribution of these areas by an exponential fit. Thus the data is subjected to a very effective graphical averaging process. As a by-product several important parameters of the patch configuration are obtained, e.g., $\sigma_x \sigma_y$, c_o and a/b.

4.   MISSION 186, 6-8 OCTOBER 1971

4.1   General Conditions, Operations and Observations

        Dye operations in support of Mission 186 were conducted
throughout the period 6-8 October 1971. Weather conditions during
this period were generally good. A weak front had passed through
the area earlier in the week, leaving in its wake scattered
showers and weak variable winds, generally northerly at less than
10 knots. Throughout the operations on the 6th and 7th clearing
continued and the wind was generally calm. (The 500 mb charts for
this period show less than a 60 m potential drop over the entirety
of Texas, Louisiana, and Oklahoma.) On the 8th, a zone of weak
convergence began moving into the region in advance of an approaching
trough. The resulting gusty wind in conjunction with thunderstorms
over the bay produced somewhat heavier chop which eventually was
responsible for abortion of the fluorometric operations that day.
Tidal variation during the period was dominantly diurnal with a
mean increase in water level over the entire period of about a
foot. The tidal record from the USCE station at Point Barrow is
shown in Fig. 4.1. The wind observations noted by NASA personnel
at McCollum Park Pier are shown in Fig. 4.2. Miscellaneous
observations transcribed from the dye boat field notes for this
period are listed in Table 4.1 (all times given in this section
are CDT unless specified otherwise).

        On the afternoon of 6 October some preliminary work
was performed near Point Barrow. A small dye release was made
and tracked for about two hours to check out the operation of the
fluorometer system. On 7 October five slug releases from three
stations were made throughout the day. The three release points
were placed on a line straight out from the HL&P discharge at
intervals of about a kilometer, and were marked with large
anchored buoys. Two of these buoys, A and B, were left in the

27

FIG. 4.1 TIDE RECORD AT POINT BARROW

FIG. 4.2 WIND OBSERVATIONS AT McCOLLUM PARK

TABLE 4.1

MISCELLANEOUS OBSERVATIONS
(Transcribed from Field Notes)

Times CDT[*]

6 October 1971

1330	Current ca. 0.2 knots, choppy
1440	Wind down, water smooth. Tide out, water <u>very</u> low. 6" depth near County Park pier, about 1' of barnacles exposed on pilings.
1535	Humble work boat passed thru patch, may have caused separation.
1600	At Humble Channel, water temperature 28.4°

7 October 1971

0730	High water. No wind. Some chop and old swell.
0915	Calm, clear.
1121	Conditions calm, very few waves.
1129	Between points B and C, salinity 17 $^{\circ}$/oo.
1135	Incredibly calm.
1345	SE wind ca. 10 knots. Some chop.
1453	Between A and B, salinity 18 $^{\circ}$/oo.
1540	Clear, calm, few waves.
1700	Water level down 9"-12" from morning. Clear, calm.

8 October 1971

0830	Wind from NE, ca. 5 knots gusting. Chop. Waves down coast at Crawleys (Umbrella Point) much more pronounced (SWH ca. 1' at 0730). Clear, some Ci wisps.

29

TABLE 4.1 - Continued

0850	At A. Wavefronts appear to run NNW to SSE.
0858	Point B, salinity 16 ^{o}/oo.
0928	Waves and chop. Taking waves over bow.
0935	Alternator shorted out by wave.
0945	Underway.
1000	Alternator out, pump smoking.

*CDT = GMT - 5 hours.

water to serve as release points for operations on 8 October.
The position of these release points, as well as the release
off Point Barrow on 6 October, are shown in Fig. 4.3. In Table
4.2 is summarized the series of dye releases performed in this
period. The times of these dye releases are indicated in Figs.
4.1 and 4.2.

In addition to the slug releases analyzed here, a
continuous release was made from the end of the HL&P groin on
both 7 and 8 October and a series of slug releases were made at
Red Bayou up the coast. The purpose of these operations was to
provide qualitative indications of water movement; they are not
amenable to quantitative analysis so are not treated any further
here. The behavior of the groin release of 7 October does,
however, merit some mention. Fig. 4.4 shows the time evolution
of this release as photographed from the helicopter. The billowing
patterns formed is suggestive of the instability of a vortex sheet,
e.g., Kelvin-Helmholtz instability and Karmán vortices, on the
down-coast side of the plume. Unfortunately, there are no direct
measurements of currents in this area to provide details of the
hydrodynamics of this phenomenon.

Traverses of the morning releases of 7 October were
performed by setting marked poles on the boundaries of the patch
and running transects between the poles. The locations of the
poles were then shot in by the transit team. Thus, so long as
the traverse was made at a constant velocity, the fluorometric
record could be related directly to distance by the correspondence
of its end points with the absolute positions of the markers.
This eliminated the need for careful tracking of the boat movements.
Unfortunately, the marker poles proved to be so unwieldy and so
much time was consumed in placing and retrieving these poles that
this approach had to be abandoned. This does appear to be an
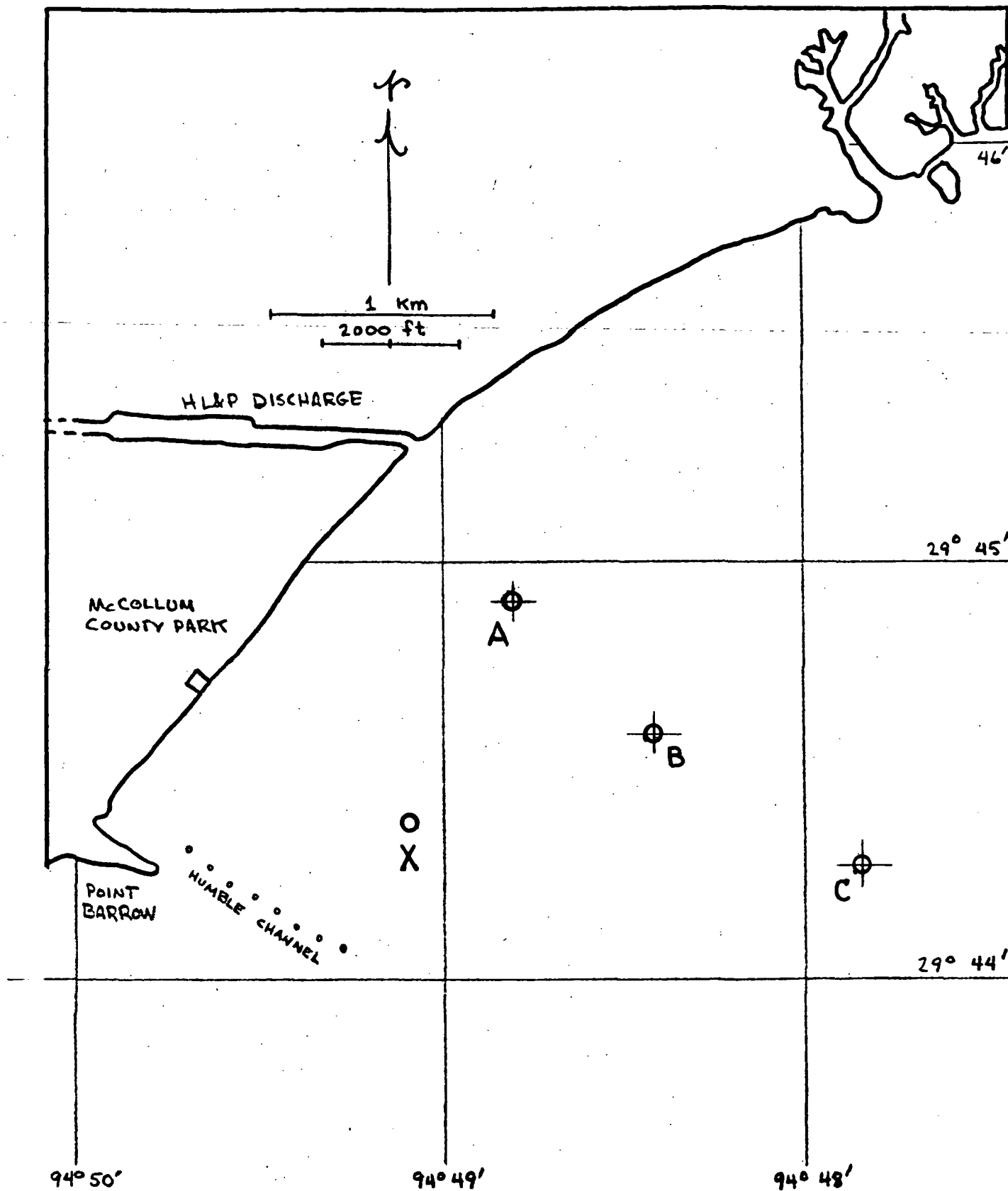
FIG. 4.3   MISSION 186, DYE RELEASE POINTS

32

TABLE 4.2

DYE RELEASES PERFORMED IN MISSION 186

Date (1971)	Designator	Release Point (See Fig.4.3)	Time (CDT)	Quantity (Liters)	Concentration (Parts per thousand)	Remarks
6 Oct	Point Barrow	X	1440	20.	10.	n
7 Oct	A_1	A	0934	20.	50.	n
	B_1	B(RO2)	0936	20.	~40.	b
	C	C	0943	20.	20.	n
	groin	outer end of groin structure at discharge	0922 (start) 1006 (replenish)	30?	100?	b,continuous
	A_2	A	1345	20.	20.	n
	B_2	B(R18)	1400	20.	20.	n
8 Oct	groin	same as above	0845	30?	100?	b,continuous
	A		0850	20.	10.	n
	B(RO1)		0858	20.	10.	n

b: slightly buoyant, by dilution with methanol

n: neutral buoyancy, adjusted to ambient salinity

Slug release unless otherwise noted
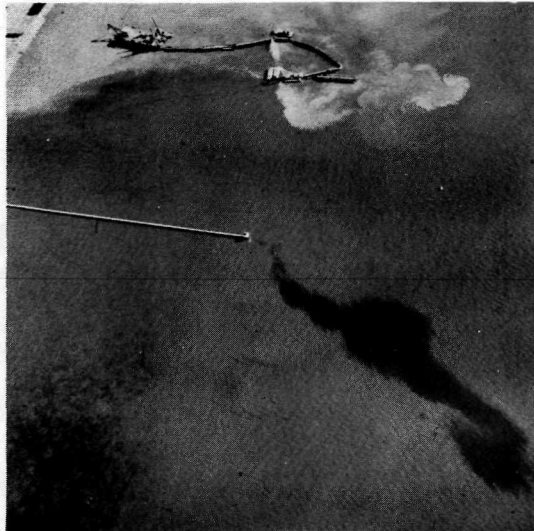
0935

1015

1055

FIG. 4.4   GROIN RELEASE, MISSION 186 (7 OCTOBER 1971)

excellent approach to the problem of locating the boat traverses, but a second boat is imperative for handling the markers. Traverses of the remainder of the dye patches were carefully annotated with both velocity and direction and boat positions were shot in by the transits as often as possible so as to provide an absolute location.

On 8 October waves became a serious problem. As noted in Table 4.1, water was taken over the bow several times, eventually shorting out the pump. Thus, the fluorometer system became inoperable early on this day and it was necessary to instead collect a sequence of discrete samples. These were collected in jars which were taken back to the laboratory and later analyzed for concentration with the fluorometer.

FIG. 4.5   PATCH A_1 (MISSION 186) AT 0938,
15 MINUTES AFTER RELEASE

4.2   Release and Movement of Patches

The morning release from point A, designated here Patch A_1, was a rather concentrated, neutrally buoyant quantity of dye. Fig. 4.5 shows this patch about 15 minutes after its release. Two subsequent series of traverses were made of this patch, the first at 1040, the second at 1200. In Fig. 4.6 is shown the general movement and development of this patch. The patch moved due south at an average velocity of about half-a-foot per second, no doubt with the ebbing current. The approximate centroids of the patch are indicated by the bold circles in Fig. 4.6. These were used to determine the mean patch velocities listed in Table 4.3.

The early morning release at location B was also a rather concentrated solution that was diluted with methanol to be slightly more buoyant than the receiving water. The movement of this patch relative to the release point is shown in Fig. 4.7. Like Patch A_1, this dye patch also moved due south from its point of release but at a considerably slower mean velocity, roughly .2 feet per second. Release C behaved in a similar manner moving due south with a mean velocity about .3 feet per second as shown in Fig. 4.8. Locating and tracing three widely spaced dye patches proved to be more than one boat could handle. As a consequence only one set of traverses were obtained for both Patch B_1 and C_1. Patch C separated into two lobes (discussed later), the centroid positions of each of which are indicated in Fig. 4.8. The mean of these two positions was used in computing the velocity of Table 4.3.

Because of the difficulty of tracking three separate patches, the afternoon releases were reduced to two, made from positions A and B. The general movement of each of these releases, A_2 and B_2, are shown in Figs. 4.6 and 4.7. These positions were

36

RELEASE POINT A (R01)
  RELEASES:
    0934 CDT
    1355 CDT

⊙ (R19)
1453

• A1 (R05)

A4
(R09) •

○
1040

• A3
(R07)

A2 •
(R06)

500 ft

1200
○
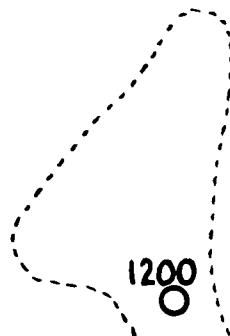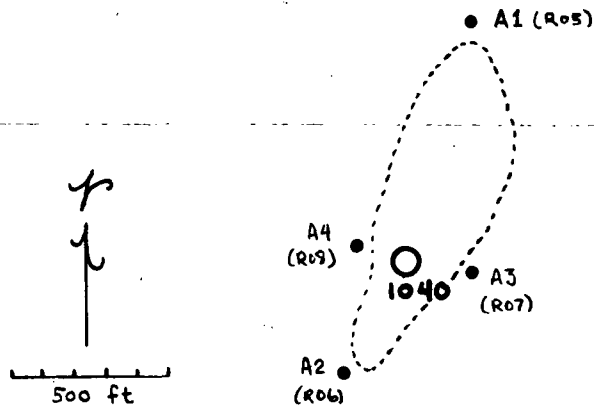
FIG. 4.6 TRAJECTORIES OF PATCHES RELEASED AT "A", 7 OCTOBER 1971

37

TABLE 4.3

MEAN VELOCITIES OF PATCH CENTROIDS[*]

MISSION 186

Patch	Time	Magnitude (fps)	Direction
		6 October 1971	
Point Barrow	1517	.44	210
		7 October 1971	
A_1	1007	.48	180
A_1	1120	.68	190
B_1	1018	.22	190
C	1031	.26	180
A_2	1424	.32	255
B_2	1448	.23	240
		8 October 1971	
A	0952	.33	185
B	~ 1000	nil	-

[*]The convention is observed that current directions are that to which the current flows, in contrast to wind direction which are that from which the wind blows.
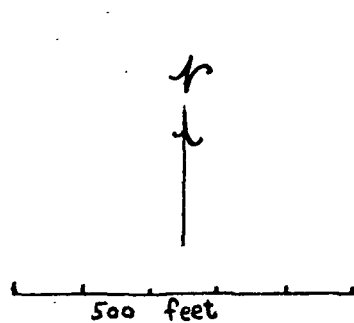
RELEASE POINT B
(R18)
1400 CDT

RELEASE POINT B
(R02)
0936 CDT

(R20)
1536

B1 (R09)

B3
(R11)

1100

B4 (R12)

B2 (R10)

500 feet
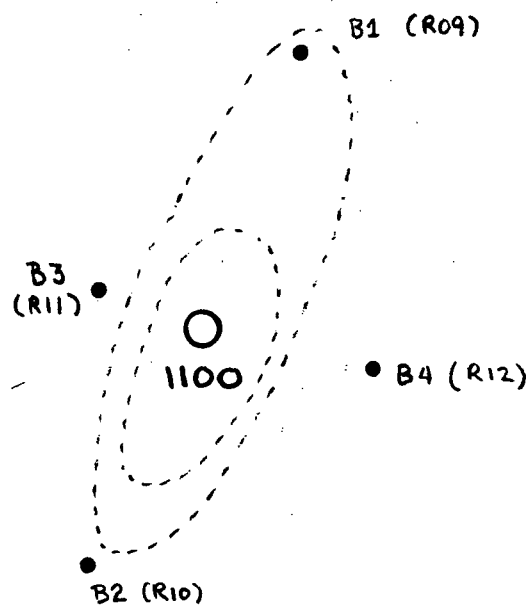
FIG. 4.7 TRAJECTORIES OF PATCHES RELEASED AT "B", 7 OCTOBER 1971

RELEASE POINT C
(R03)
0943 CDT

500 ft

G2 (R14)

C3
(R15)

C4
(R16)

1120

C1
(R13)

1120

C5
(R17)
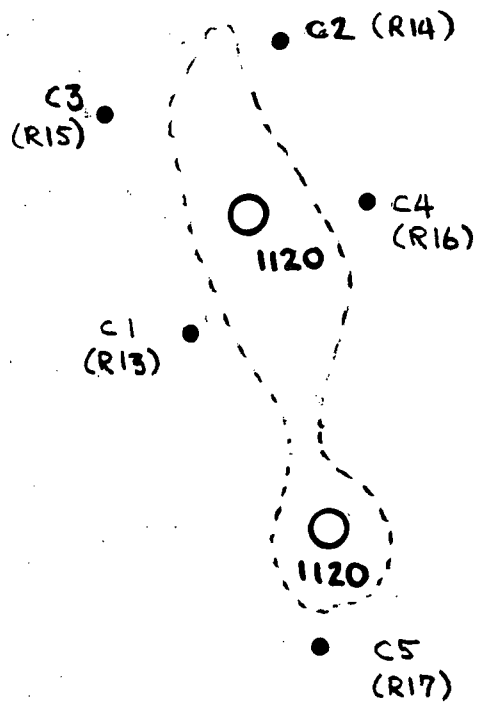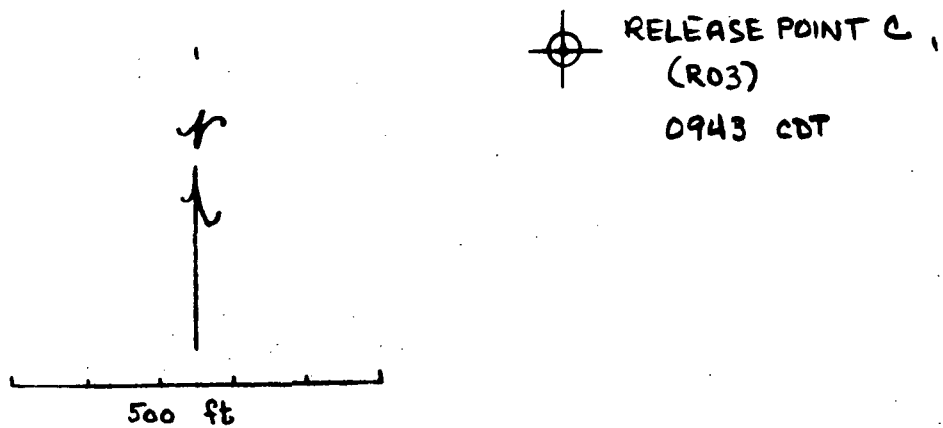
FIG. 4.8   TRAJECTORY OF PATCH RELEASED AT "C", 7 OCTOBER 1971

obtained by siting the boat over the point of maximum concentration
where its location was shot by the transit crew. Direction of the
current at both points A and B had now swung around to the WSW.
The current magnitude at B was about the same as in the morning,
.2 feet per second, while the magnitude at A slacked somewhat to
about .3 feet per second. It should also be noted that release
point B was moved north some 400 feet from the position of the
morning release. The reason for this is unknown; perhaps the
marker was moved by one of the crews but there is no record of
this in the field notes.

Both the releases of 8 October were neutrally buoyant
and of somewhat low concentration. The patch released at point A
developed considerably within the next two hours and moved nearly
due south with a mean velocity around .3 feet per second. The
relative position of patch A, some two hours after its release,
is indicated in Fig. 4.9. The behavior of the release at point
B was quite bizarre. Very little net movement was experienced
by the dye patch. The discrete samples at 1110 (see Fig. 4.10)
locate the patch within a few hundred feet of the point of
release. Helicopter photography verifies that this patch remained
very near release point B throughout the morning. Moreover, very
little development of the patch took place, as indicated both
by the helicopter photography and the extremely high concentrations
in the discrete samples.

Current velocities computed from the movement of patch
centroids are summarized in Table 4.3. The time given is the mean
of the times of the patch positions used to derive the velocity.
The information in this table was developed from Figs. 4.6 through
4.10. Positions in these figures were determined from the transit
data.

RELEASE
POINT "A"
0850 CDT

φ

500 ft

● position of discrete
sample

APPROXIMATE
ORIENTATION
FROM HELICOPTER
PHOTOGRAPHY

●2   ●5●6
       ●1
   ○ ●   1055
      ●4
  ●3   ●7
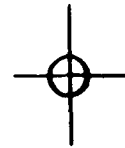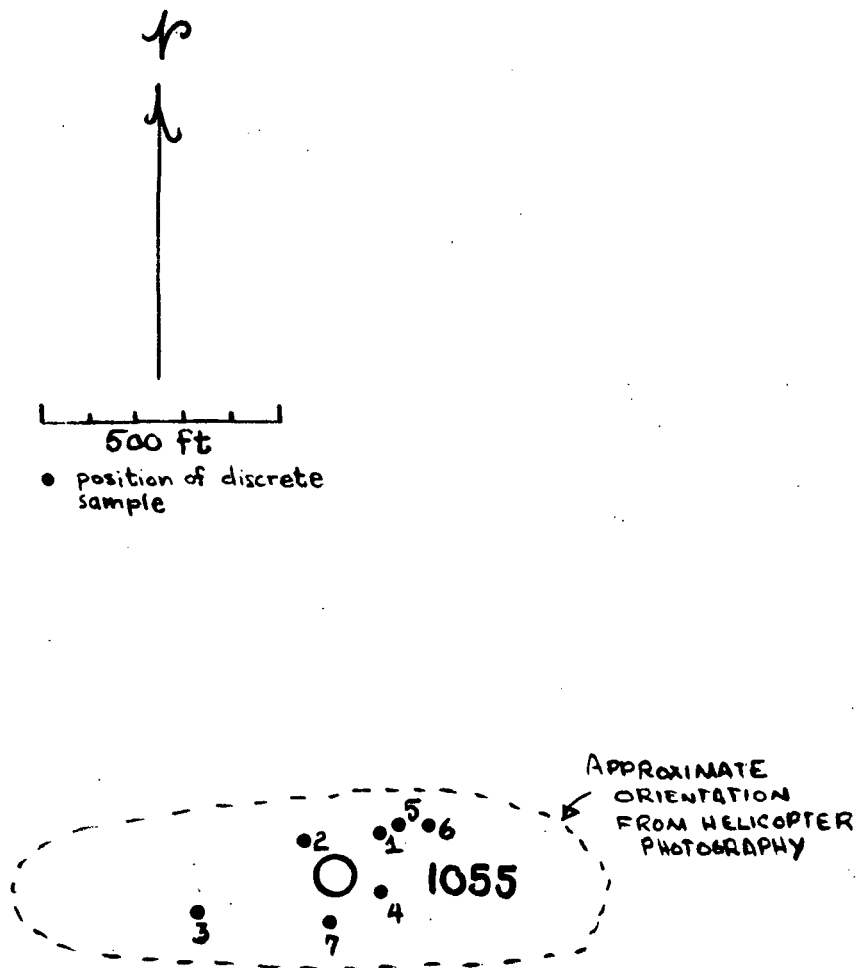
FIG. 4.9   POSITIONS OF PATCH A, 8 OCTOBER 1971

42

100 ft

● Position of discrete sample

5
●

1
●

3
●

○ 1110

4●

●2

RELEASE POINT B
0858 CDT
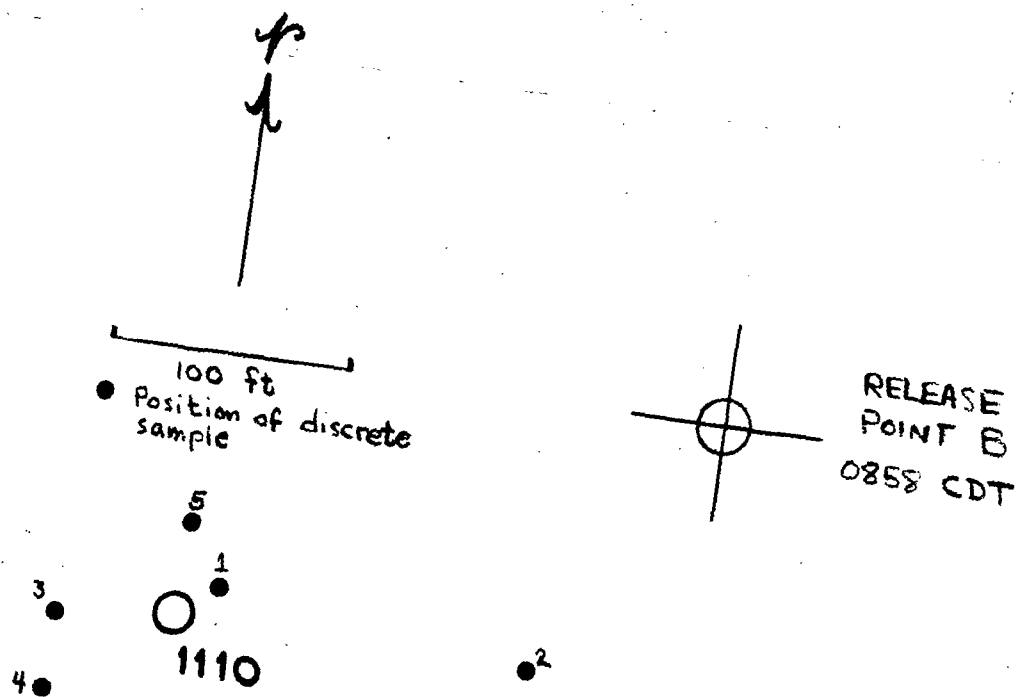
FIG. 4.10 POSITIONS OF PATCH B, 8 OCTOBER 1971

4.3   Patch Development

In this section are presented the patch configurations
constructed from the fluorometric data following the procedures
described in Section 3.1. The distribution of dye is indicated
by concentration isopleths marked in units of parts per billion
which are drawn at intervals appropriate to the gradients and
concentrations of the individual patches. The boat track associated
with each transect is indicated on these figures by the straight
lines traversing the contours.

A relatively detailed set of traverses was made of the
Point Barrow release, 6 October, 1.25 hours after its release.
The resulting isopleths are shown in Fig. 4.11. The patch has
clearly separated into two large lobes, very likely because a
deep-draft work boat passed through the patch some twenty mintues
before (see Table 4.1). Such separation is often caused by the
passage of a boat, particularly when a patch is still in its
early stage of development and the dye is not well mixed vertically.

The second set of traverses of this patch was initiated
at 1700. Unfortunately, the center of this patch lay in the
Humble Camp Channel, and before the patch could be completely
traversed a second work boat moved through the dye. Fig. 4.12
displays the isopleths constructed from the transects made before
the passage of this work boat. As more work boats were on their
way in, the patch was abandoned. Fig. 4.13 shows the vertical
distribution of dye in this patch at 1715. Even though the patch
has been in the water some two-and-a-half hours, the dye is still
largely confined to the top three feet. This is a consequence of
the very light wave action of that day.

Patch A_1 of 7 October evidenced considerable development
during its lifetime. Fig. 4.14 displays the concentration contours
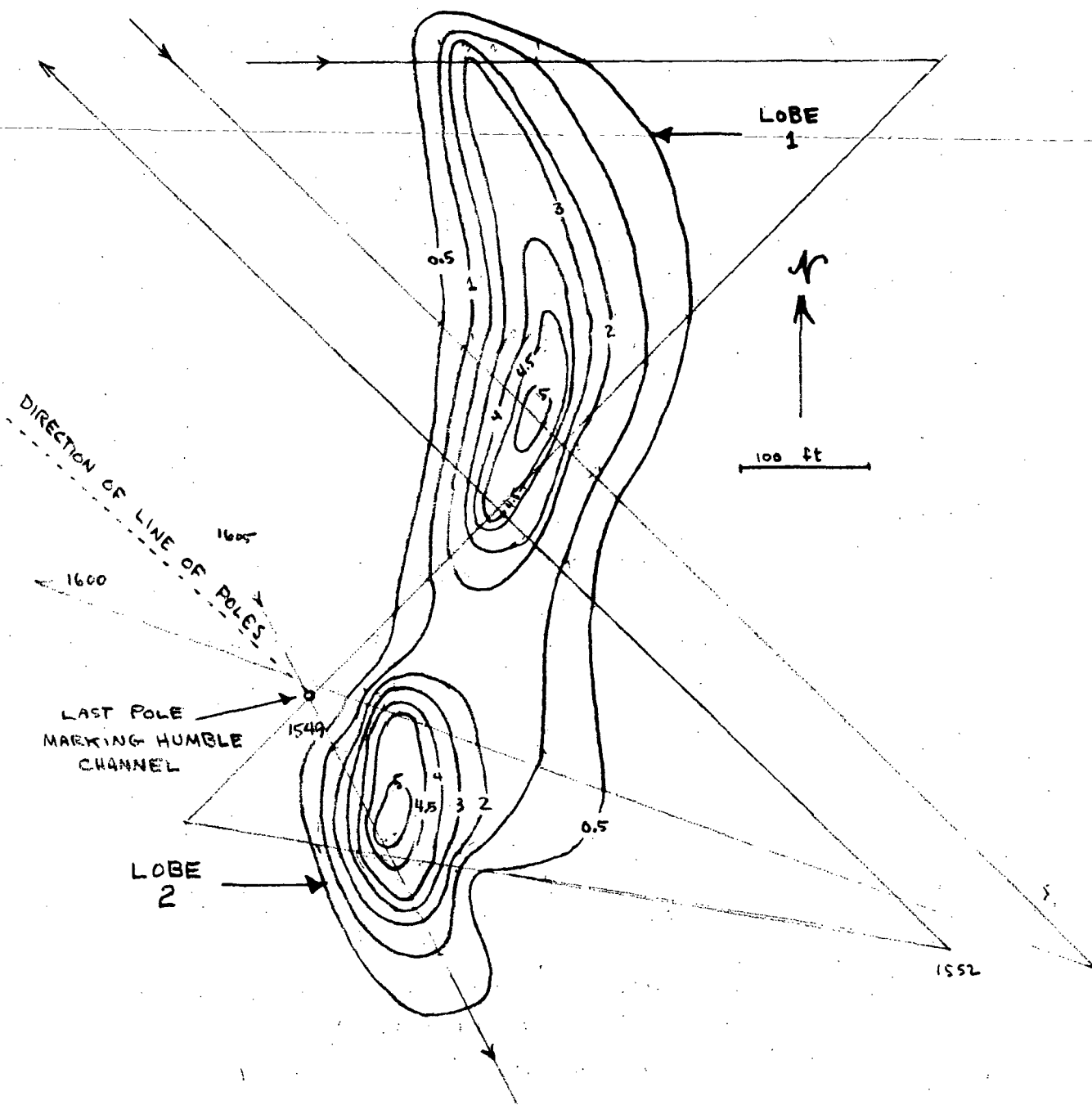
FIG. 4.11 RELEASE OFF POINT BARROW, 6 OCTOBER 1971
PATCH CONFIGURATION AT 1555

45
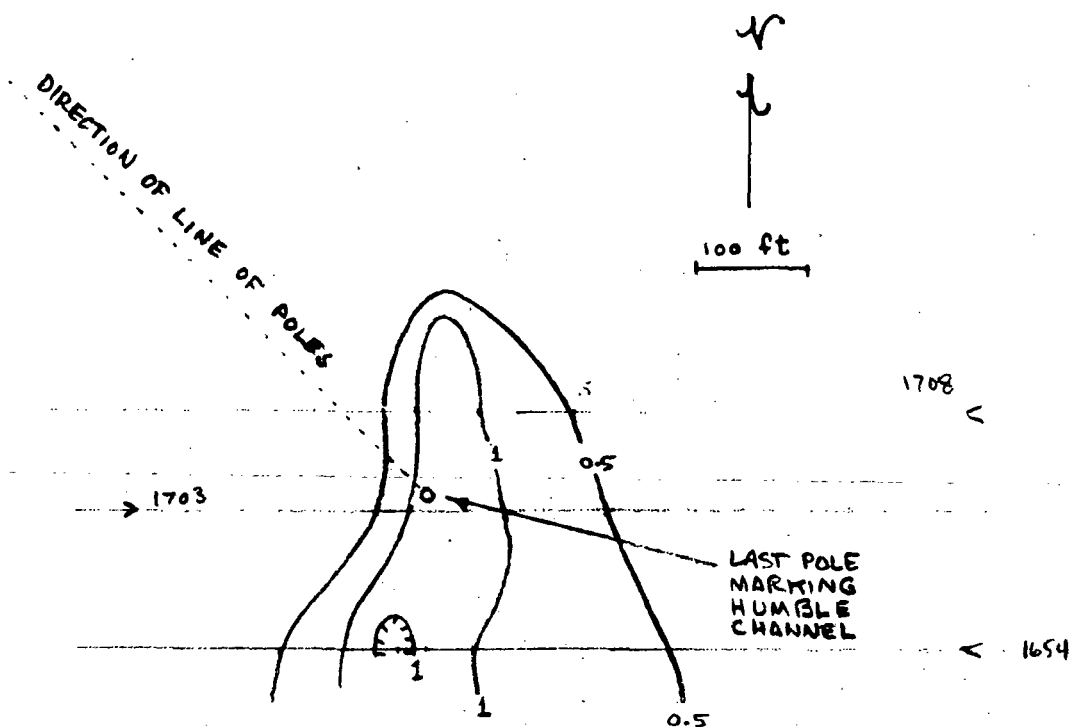
FIG. 4.12   RELEASE OFF POINT BARROW, 6 OCTOBER 1971
PATCH CONFIGURATION AT 1700   (Note: Passage
of work boat in Humble Channel interrupted
traverses.)
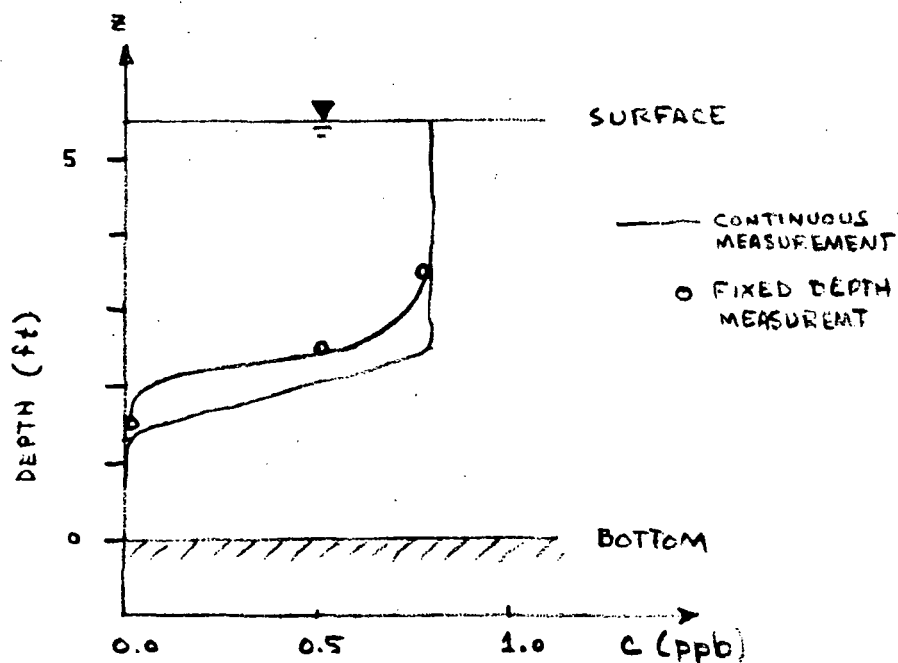
FIG. 4.13   VERTICAL PROFILE IN POINT BARROW
PATCH, 1715, 6 OCTOBER 1971

46
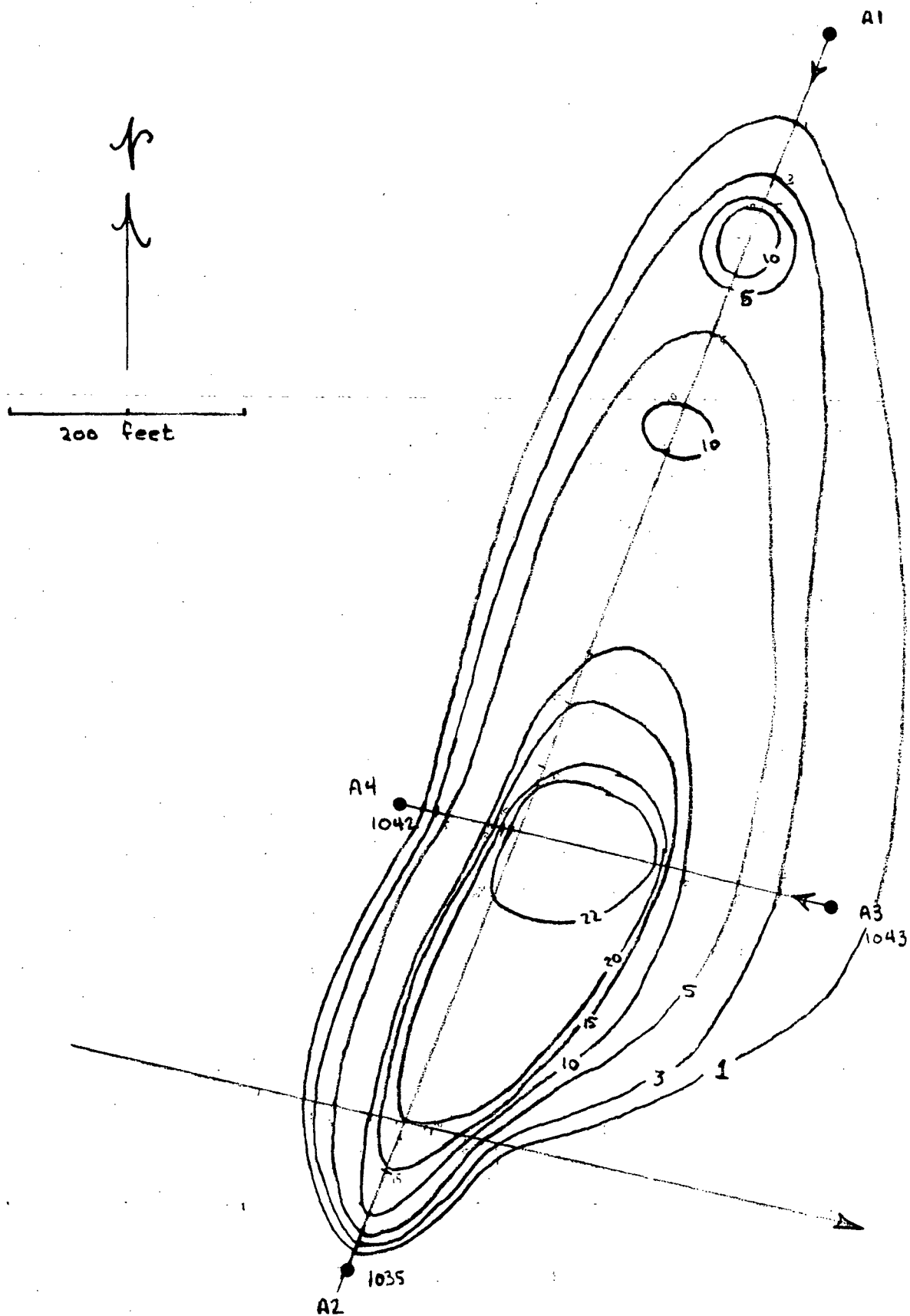
FIG. 4.14　　RELEASE A$_1$, 7 OCTOBER 1971, PATCH
　　　　　　　　CONFIGURATION AT 1040 CDT

47

at 1040, about an hour after the release, and Fig. 4.15 shows
the concentration contours at 1200, about 2.5 hours after release.
The dark circles in Fig. 4.14 indicate positions of the marker
poles plotted from transit data. The general asymmetry of the
contours of both these figures should be noted. This is a
common characteristic of a patch subjected to strong current
action. The maximum concentration gradient occurs on the leading
side of the patch while the wake becomes highly irregular with
very shallow concentration gradients. Thus, even without the
information of Table 4.3, one could infer from these contours
that the patch is moving in a southerly direction. Note also
that the elongation is parallel to the prevailing current.

Only one set of traverses was obtained for Patch B_1;
these consisted of two transects, roughly through the center of
the patch, at nearly right angles, again between marker poles
whose absolute positions were known. The concentration contours
constructed from these intercepts are displayed in Fig. 4.16.
The symmetry is probably unrealistic, but with only two intercepts
the information is inadequate to assess the detailed structure.
Once again we note the maximum concentration gradient on the
leading (down-current) side of the patch and the shallow concen-
tration gradient in the wake; and again the elongation is in
the direction of the prevailing current.

Fig. 4.17 shows the concentration isopleths of Patch C
about 1.5 hours after the time of release. Like the preceding
two, this patch shows an elongation in the direction of the
current; however, it has separated into two lobes. The cause
of this separation is unknown; very likely the patch was inadver-
tently crossed by one of the boats in the area.

The first release of the afternoon series was Patch A_2.
An initial transect was made at 1445, one hour after the time of

FIG. 4.15   RELEASE A₁, 7 OCTOBER 1971
PATCH CONFIGURATION AT 1200 CDT

49

FIG. 4.16   RELEASE B$_1$, 7 OCTOBER 1971
PATCH CONFIGURATION AT 1100 CDT
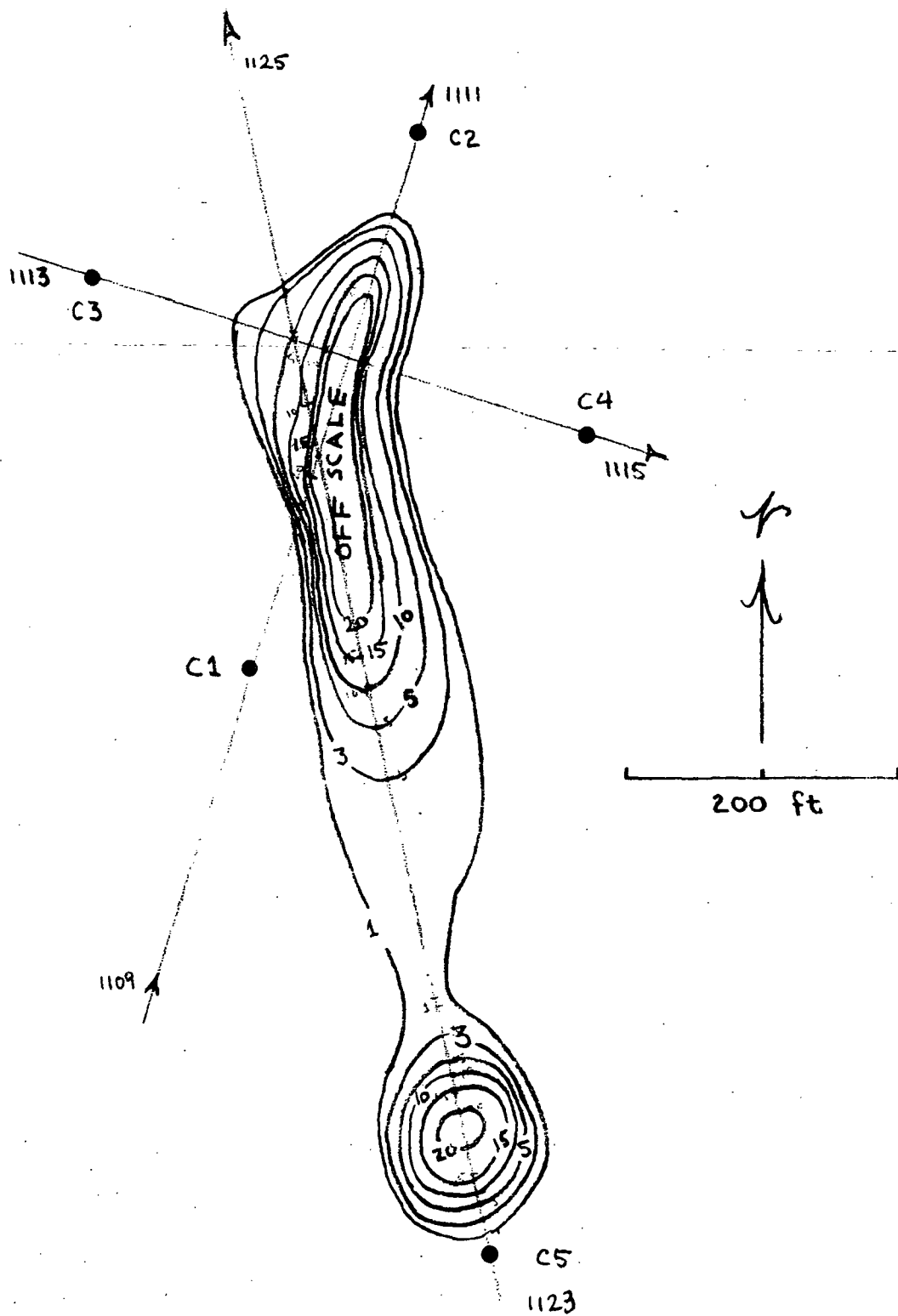
FIG. 4.17   RELEASE C, 7 OCTOBER 1971
PATCH CONFIGURATION AT 1120 CDT

51

release, but the dye proved to be still too concentrated for a
profitable series of traverses. This transect was across the
minor axis of the patch and is shown in Fig. 4.18. The first
complete set of traverses of Patch A_2 was obtained about an hour
later, and the isopleths so obtained are given in Fig. 4.19.
The vertical distribution, Fig. 4.20, indicates the dye was
present throughout the depth, although at somewhat lower concen-
trations near the bottom. Again, it should be noted that the
patch has elongated in the direction of the prevailing current
with its maximum gradient on the leading edge.
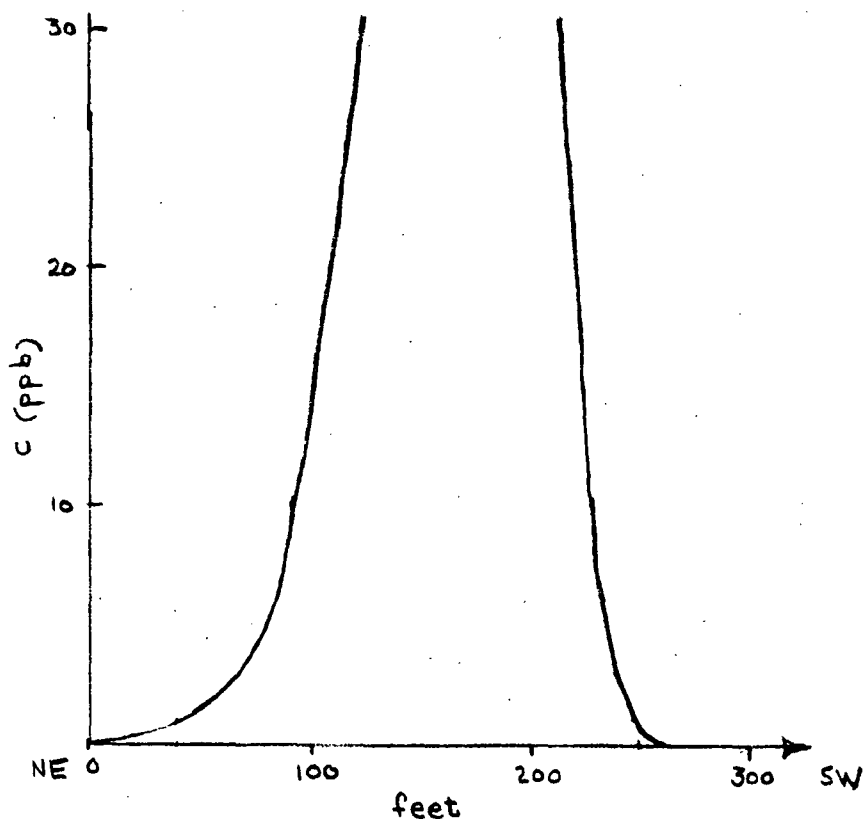
FIG. 4.18 LATERAL TRANSECT OF PATCH A_2
1445, 7 OCTOBER 1971
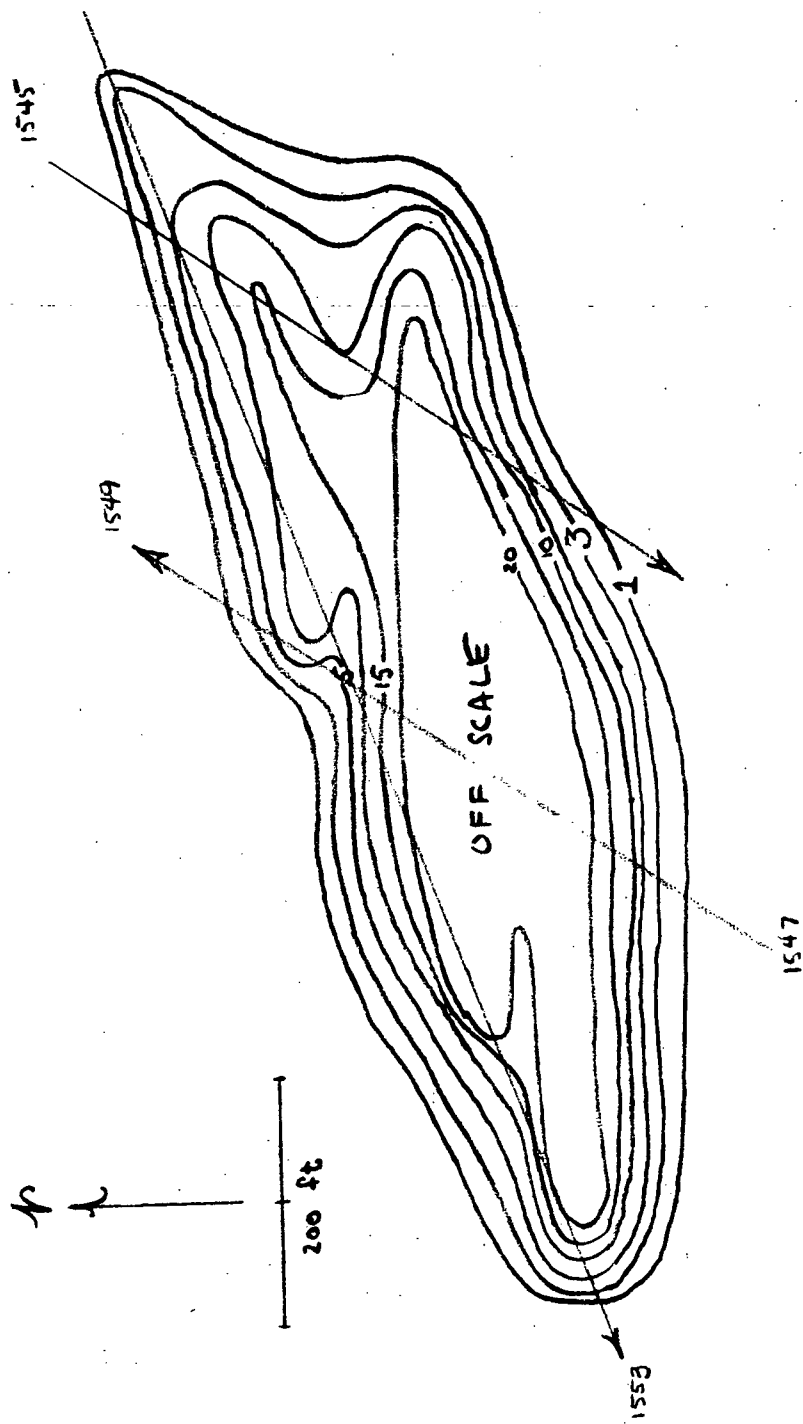
FIG. 4.19   RELEASE A$_2$, 7 OCTOBER 1971
PATCH CONFIGURATION AT 1550 CDT
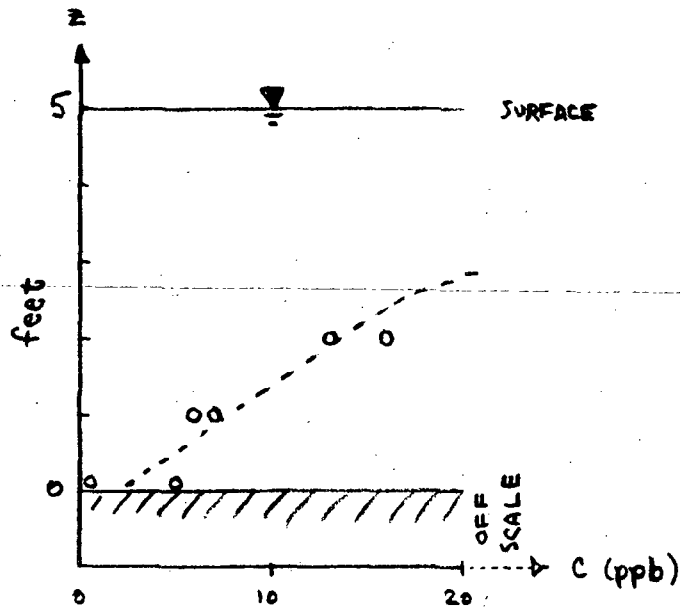
FIG. 4.20   VERTICAL PROFILE IN CENTER OF
             PATCH A_2, 7 OCTOBER 1971, 1610 CDT

Patch B_2 exhibited extremely peculiar behavior which should serve to warn us of the simplifications latent in our conceptual view of diffusion. Figs. 4.21 and 4.22 display the concentration isopleths at, respectively, 1.5 and 2.5 hours after release. The patch in both cases is elongated in the direction of the current with its maximum gradient leading, however its distribution is tighter and its concentration is higher (but not significantly) at the later configuration of 1625. That this really took place can be verified from the helicopter photography shown in Figs. 4.24 and 4.25. The scale of the patch can be easily estimated due to the fortuitous presence of the dye boat (length 15 feet) in each photograph. Obviously there is inadequate data to explain this behavior. The dye was clearly subjected to some kind of organized convergence, such as might be expected with, for example, a Langmuir-type circulation. Whatever the cause in this instance, it is clear that this is an organized hydrodynamic
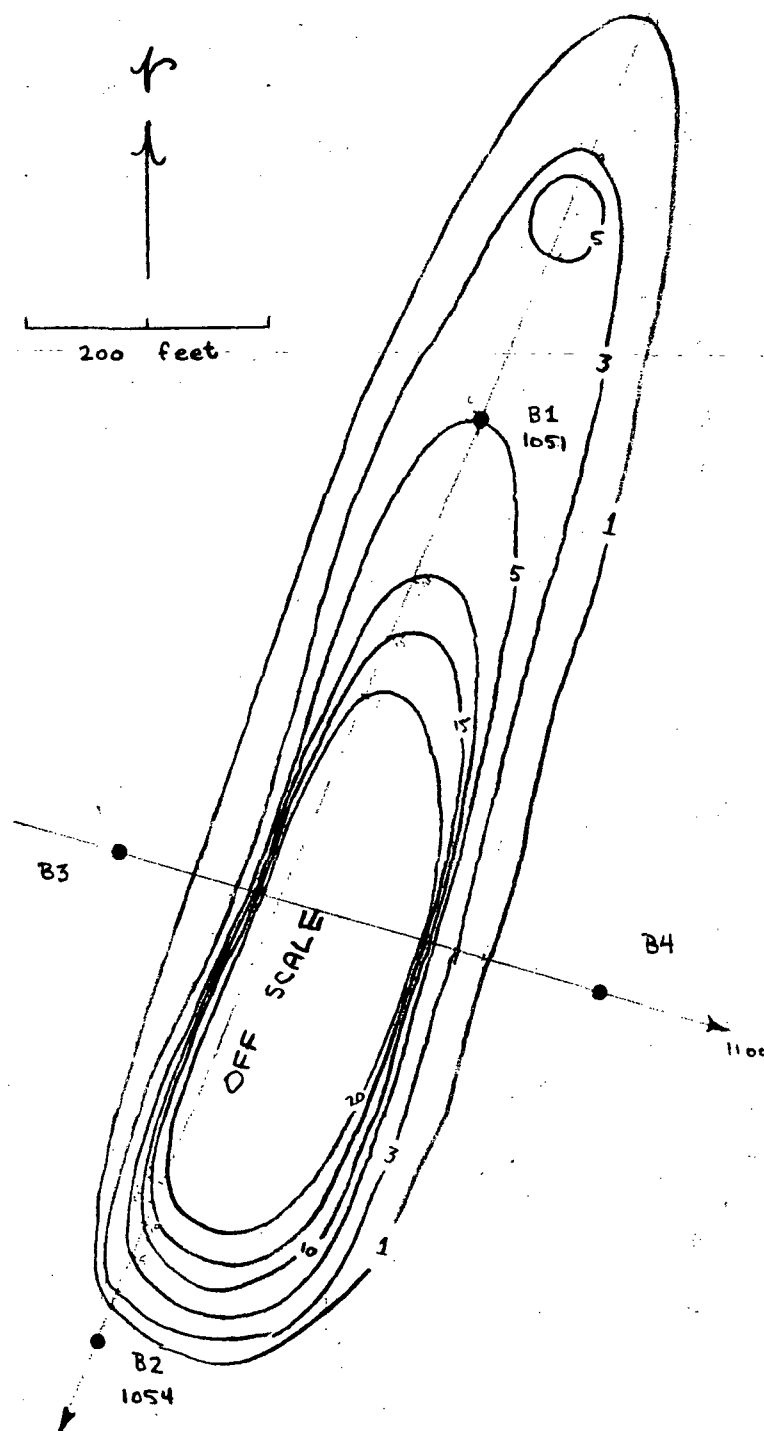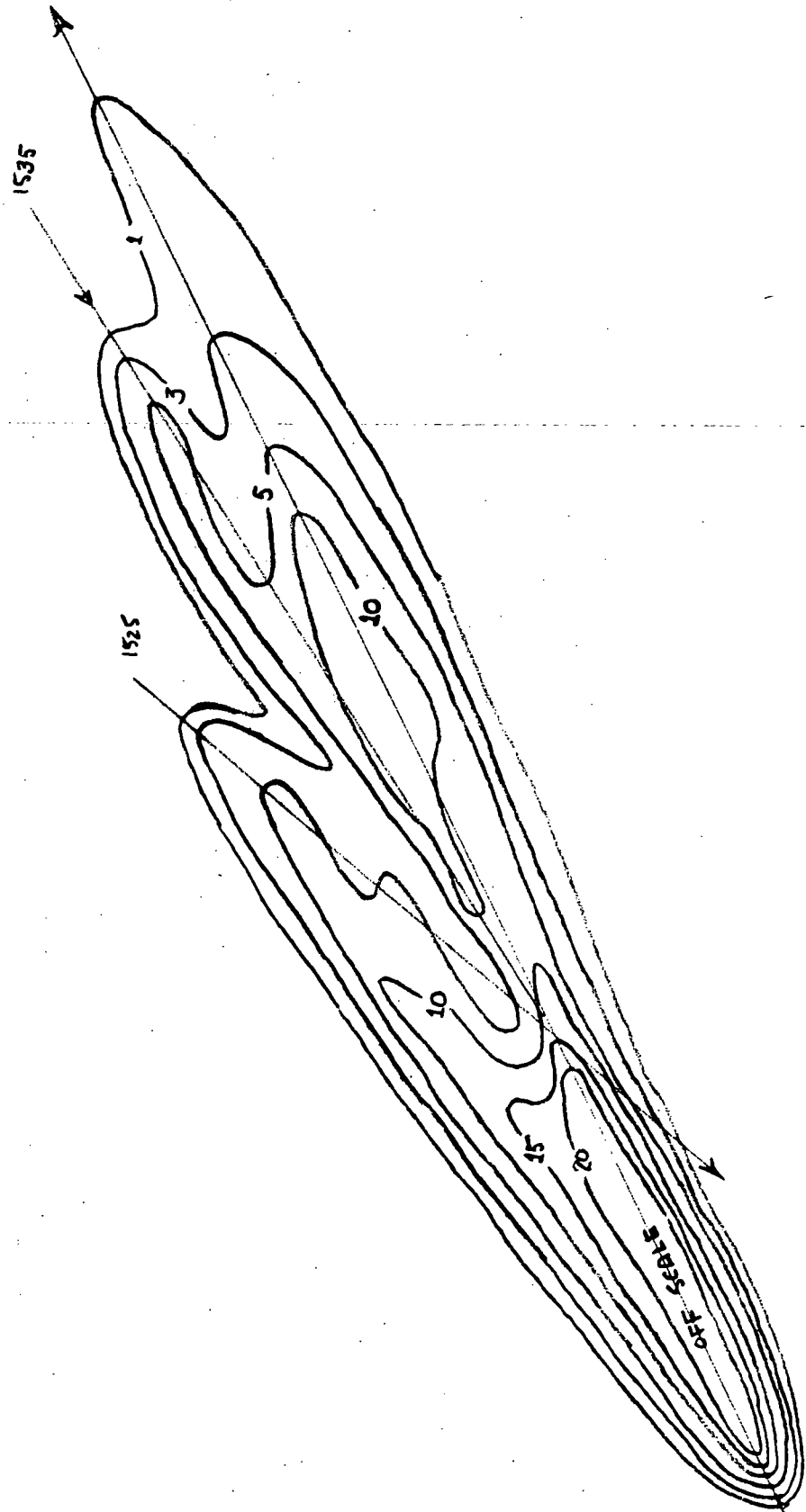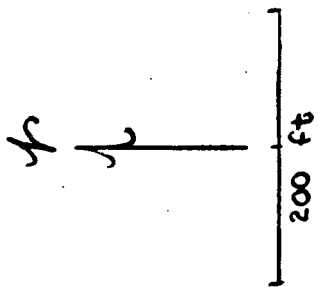
FIG. 4.21   RELEASE B2, 7 OCTOBER 1971,
PATCH CONFIGURATION AT 1530 CDT
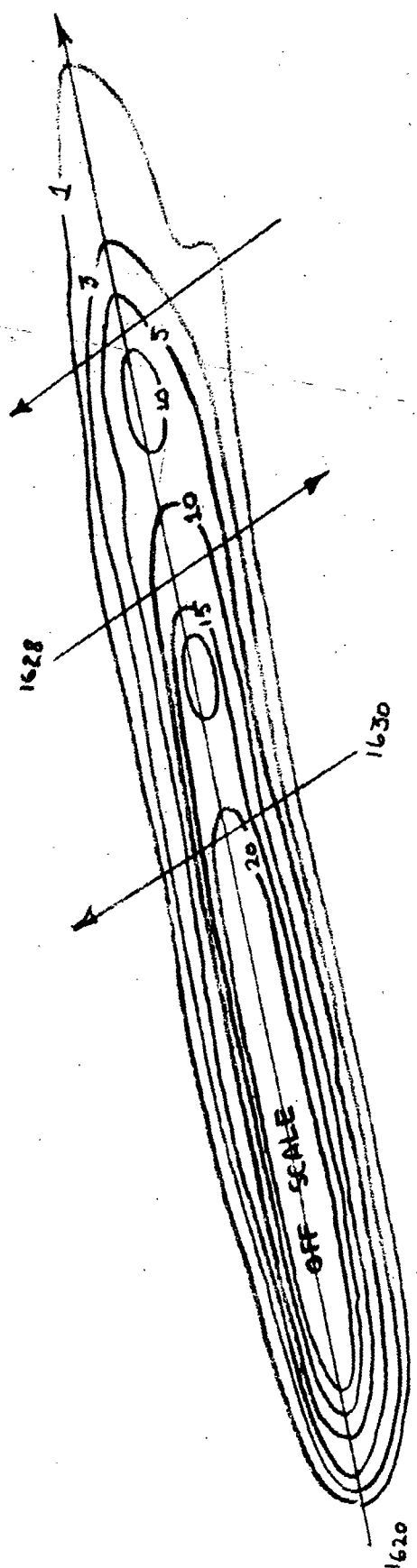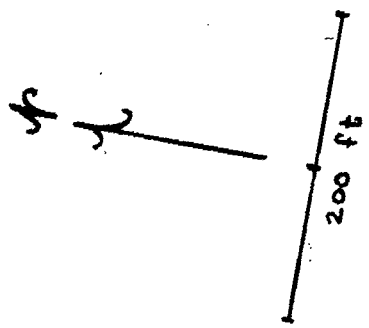
FIG. 4.22 RELEASE B₂, 7 OCTOBER 1971, PATCH CONFIGURATION AT 1625 CDT
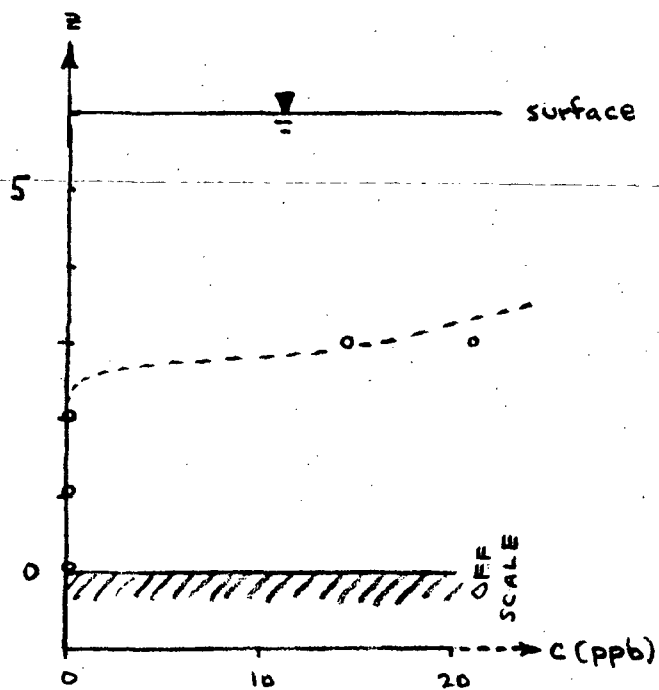
FIG. 4.23   VERTICAL PROFILE IN CENTER OF
PATCH B_2, 7 OCTOBER 1971, 1540 CDT

FIG. 4.24   PATCH B$_2$ (MISSION 186) AT 1531

FIG. 4.25   PATCH B$_2$ (MISSION 186) AT 1615

phenomenon operating at scales on the order of, or less than that of the dye patch, thus violating the assumption underlying this analysis that all motions on these scales are turbulent. Certainly if organized convergence can exist, so also can divergence, which would presumably contribute much faster spreading and dilution of the patches than can be strictly attributed to dispersion. This must be borne in mind in interpreting the diffusion coefficients derived from this data. In passing, it is comforting to note the general similarity between the contours of Figs. 4.21 and 4.22, derived solely from fluorometer data and boat tracks, and the photographs of Figs. 4.24 and 4.25.

As noted in the preceding section, failure of the fluorometer system on the 8th precluded the conduct of continuous transects; instead, series of discrete samples were obtained. The spatial density of these samples, however, is so sparse that contour isopleths analogous to those preceding cannot legitimately be constructed. The laboratory measurements of concentration of each grab sample are given in Table 4.4. The location at which each sample was obtained was shot in by the transit crew, and the positions obtained from these data are shown in Figs. 4.9 and 4.10. As noted in the preceding section, very little activity, either diffusive or advective, was associated with Patch B. This is also exemplified by the helicopter photography, Figs. 4.26 and 4.27. The only development apparent in these photographs is some striation of the patch due to local gusts of wind (cat's paws).

TABLE 4.4

FLUOROMETRIC ANALYSIS OF DYE CONCENTRATION
GRAB SAMPLES FROM OPERATIONS
OF 8 OCTOBER 1971, TRINITY BAY

Sample	Concentration (ppb)
Patch A:	
A-1	8.2
A-2	14.1
A-3	1.0
A-4	3.9
A-5	8.6
A-6	8.5
A-7	9.7
Patch B:	
B-1	58.0
B-2	71.8
B-3	49.9
B-4	11.2
B-5	14.5

FIG. 4.26   PATCH B (MISSION 186) AT 1041

FIG. 4.27   PATCH B (MISSION 186) AT 1107

4.4   Dispersion Coefficients

As discussed in Section 3.3, the methods of analysis selected for these data rely upon replacing the individual concentration isopleths with an ellipse of the same area. Fundamental to carrying out this replacement is the determination of the distribution of concentration versus the area enclosed by the concentration isopleth. For a Gaussian distribution, this relation should be exponential and thus should become a straight line on semilog paper. Thus, for the contours given in Section 4.3 graphs have been constructed plotting the logarithm of concentration against the enclosed area. These graphs are presented here in Figs. 4.28 through 4.34. From this plot and the ratio of the major-to-minor axis is derived the longitudinal and lateral variance of the dye distribution, σ_x^2 and σ_y^2. An example of the computation of variance from a log c versus area graph is given in Table 4.5 for Patch A_1. When patch configurations are available for two subsequent times, the corresponding variances are determined for each configuration and the dispersion coefficient calculated from the time derivative of the variance, according to equation (3.16). When only one configuration is available, the dispersion coefficient is computed from the corresponding variance and the total elapsed time from the release, according to equation (3.17).

Table 4.6 summarizes the physical parameters of the dye configuration determined from the boat traverses. These include the peak concentration determined from the zero intercept of the log c versus A graphs, Figs. 4.28 through 4.34; the longitudinal and lateral spatial variances; and the aspect ratio (ratio of major-to-minor axis). Only rarely throughout the operation was it possible to obtain vertical soundings through the dye patches due to the severe time constraints. When available, these depths are
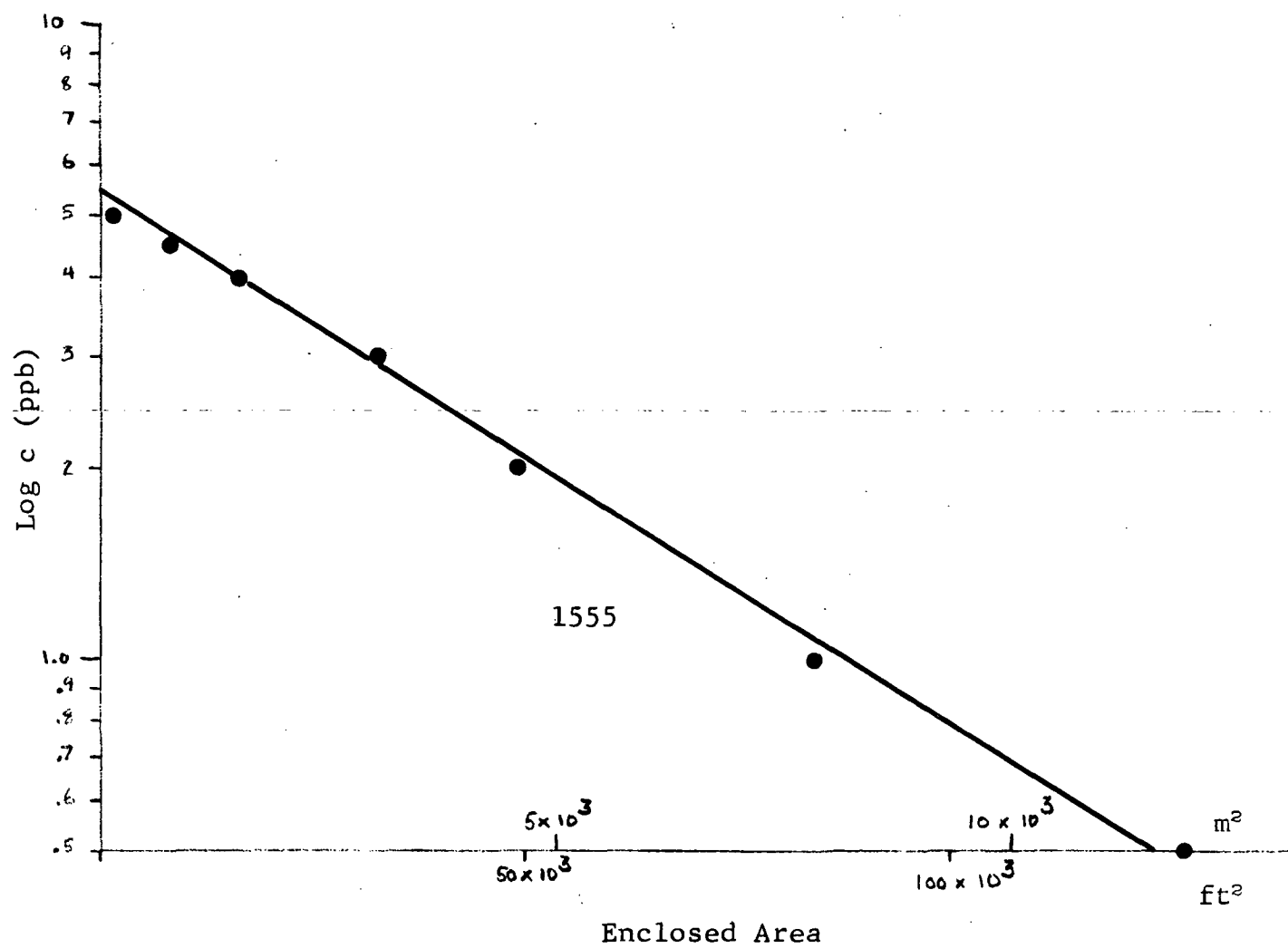
FIG. 4.28   POINT BARROW PATCH, 6 OCTOBER 1971, LOG c VERSUS AREA
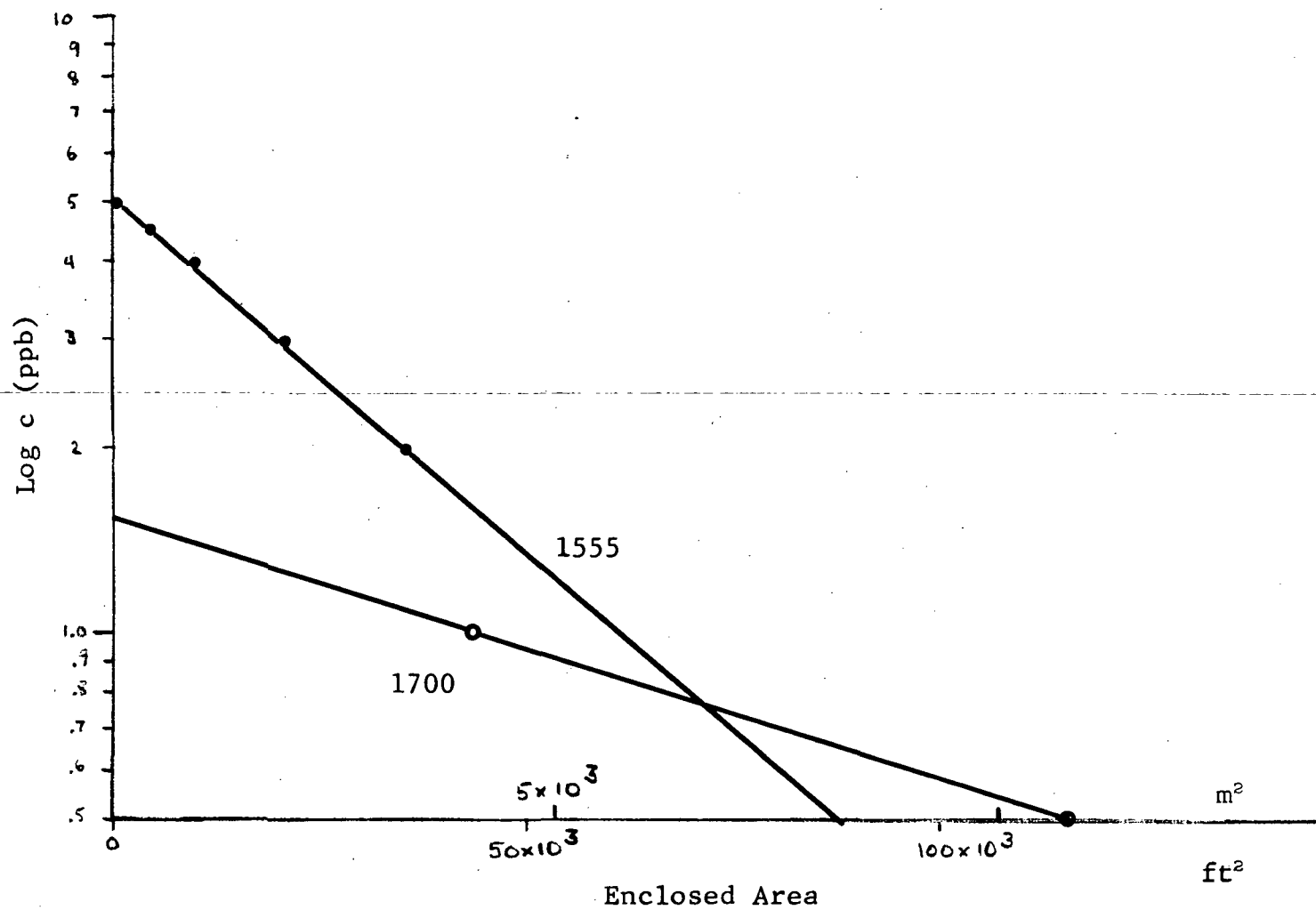
FIG. 4.29 POINT BARROW PATCH, LOBE 1, 6 OCTOBER 1971
LOG c VERSUS AREA
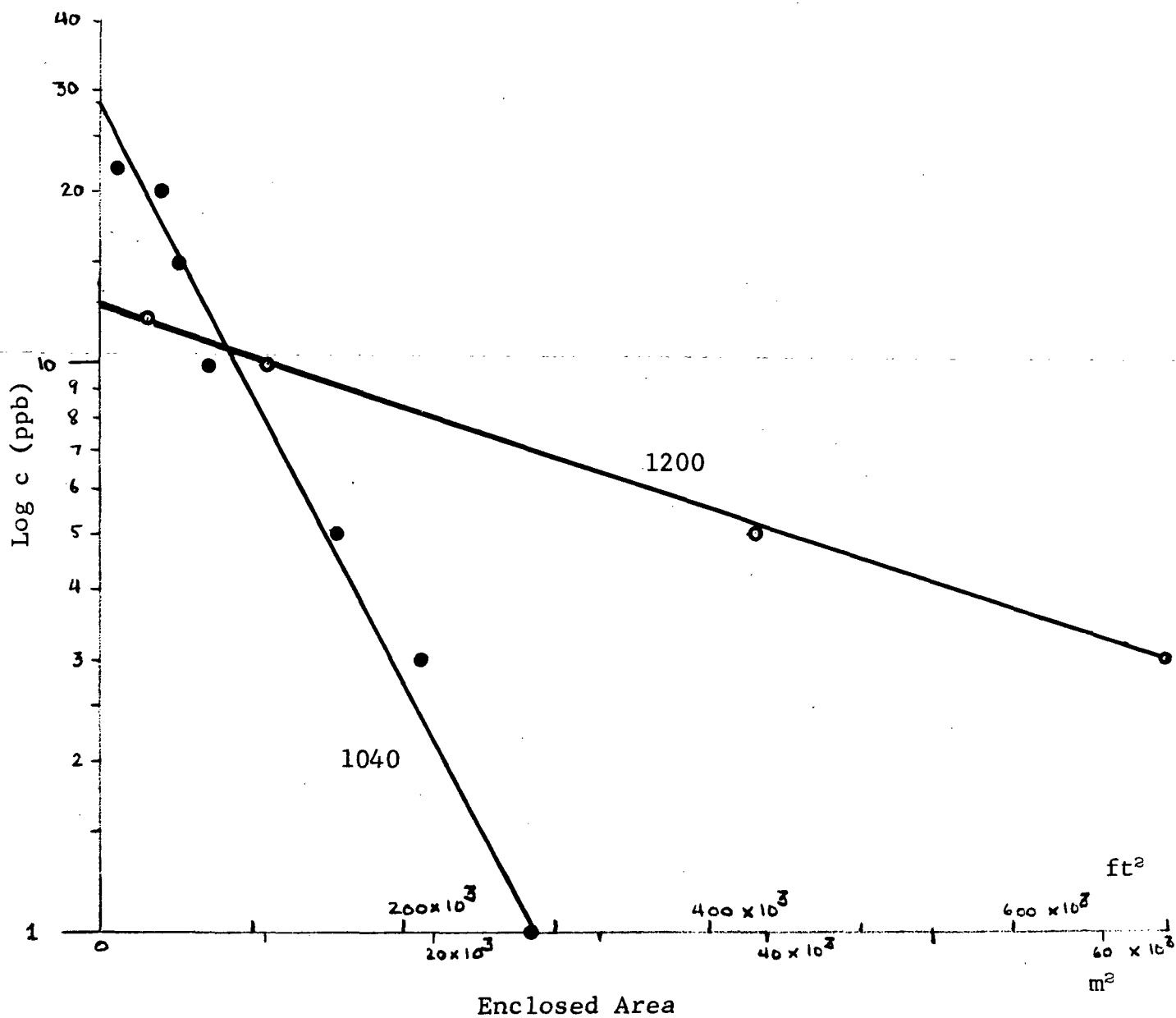
FIG. 4.30   PATCH A_1, 7 OCTOBER 1971, LOG c VERSUS AREA

65
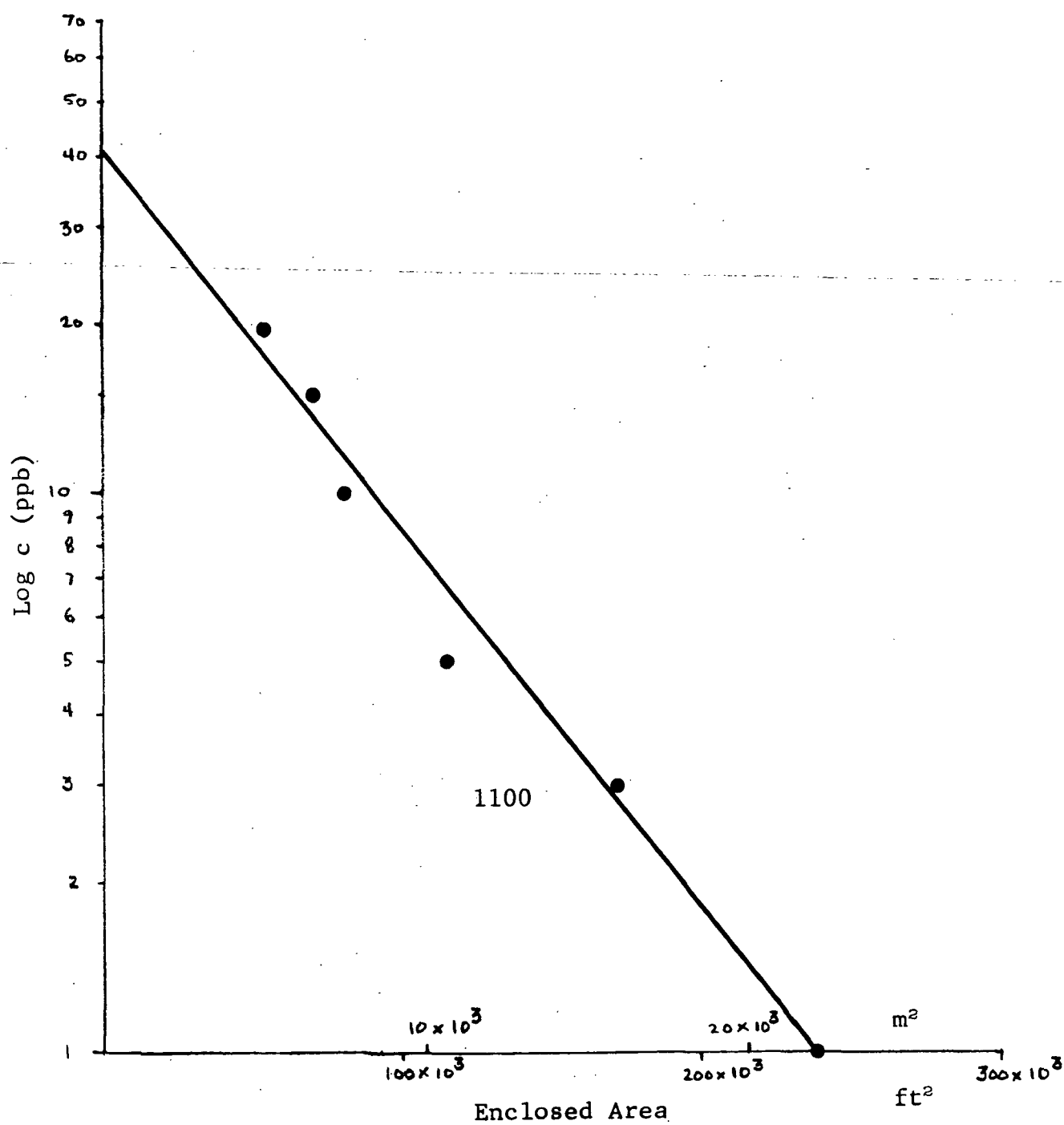
FIG. 4.31   PATCH B$_1$, 7 OCTOBER 1971, LOG c VERSUS AREA
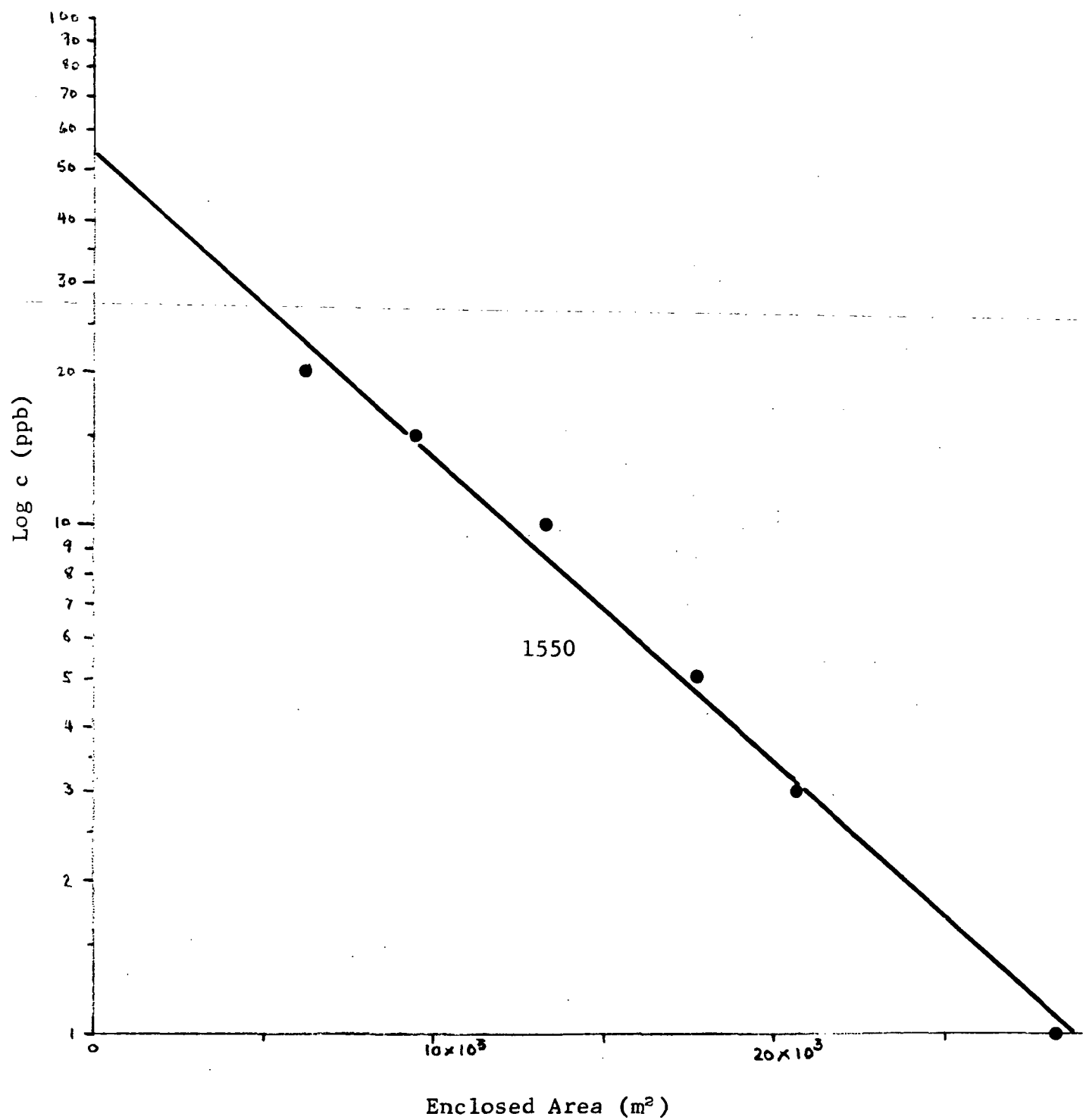
FIG. 4.32   PATCH A$_2$, 7 OCTOBER 1971, LOG c VERSUS AREA

67
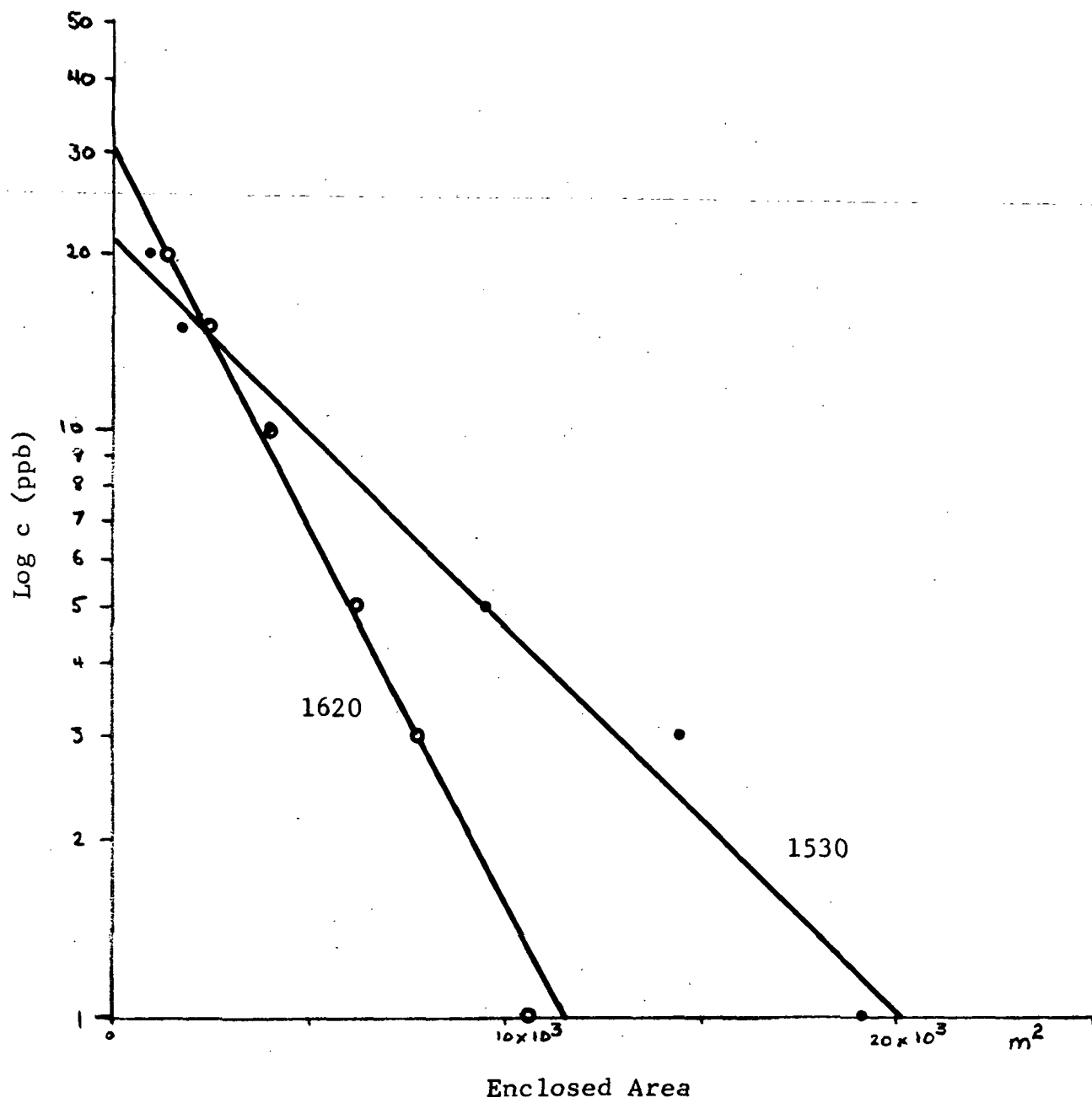
FIG. 4.33 PATCH B_2, 7 OCTOBER 1971, LOG c VERSUS AREA
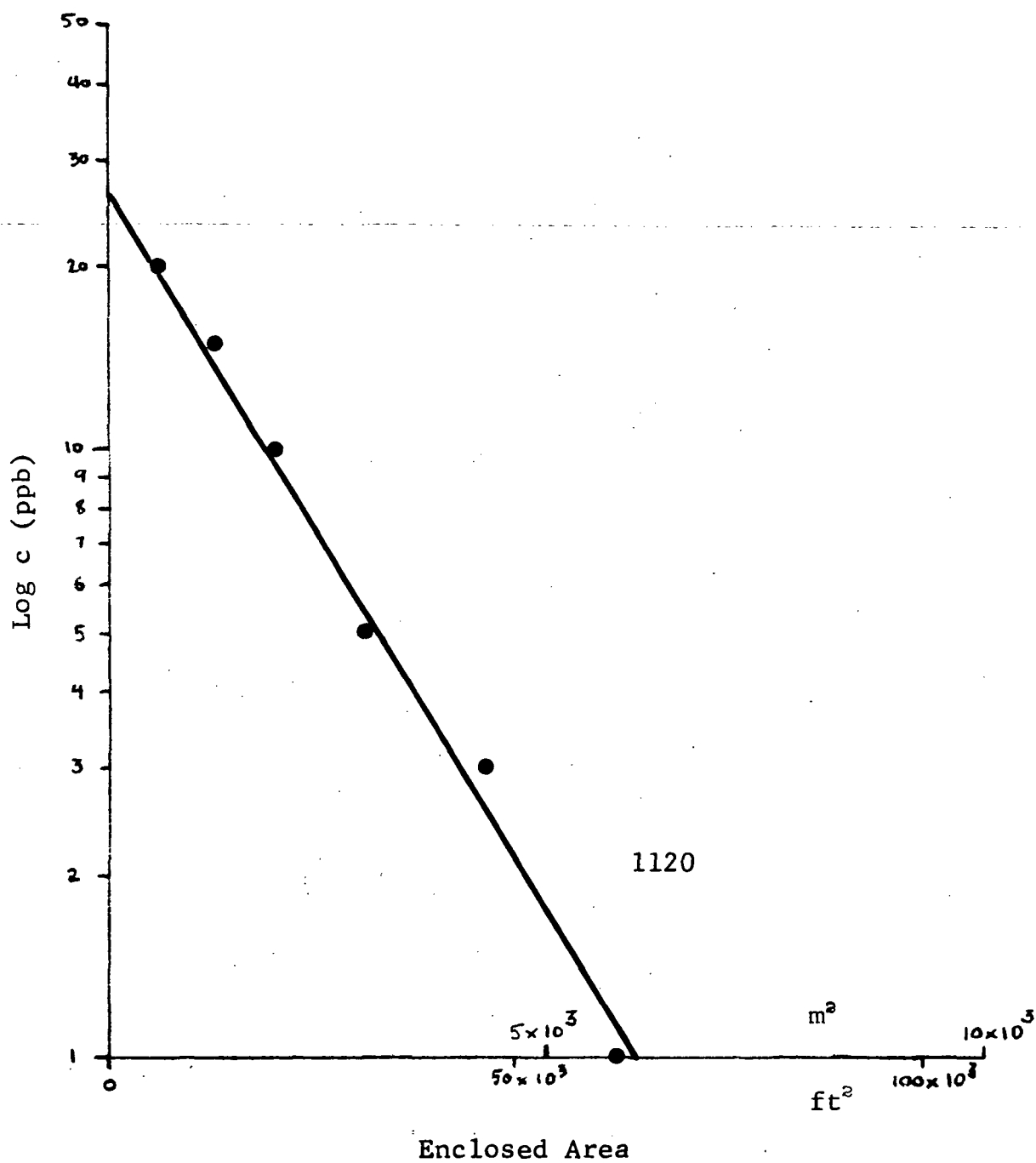
FIG. 4.34   PATCH C, 7 OCTOBER 1971, LOG c VERSUS AREA

69

TABLE 4.5

EXAMPLE COMPUTATION OF VARIANCE
PATCH A_1, 7 OCTOBER 1971, 1040 CDT

1. Determine slope of best-fit line to log c versus area
   distribution. From Fig. 4.30, $m = -1.144 \times 10^{-5}$

2. Compute $\sigma_x \sigma_y = \frac{1}{2\pi} \left(-\frac{1}{m} \right)$. For this case,

$$\sigma_x \sigma_y = \frac{1}{2\pi} (.875 \times 10^5) = 13.93 \times 10^3 \text{ ft}^2$$

3. Estimate "aspect ratio" a/b (ratio of major-to-minor axes)
   from concentration contours. From Fig. 4.14,

$$\frac{a}{b} \cong 3.3$$

4. Compute longitudinal variance,

$$\sigma_x^2 = \frac{a}{b} \sigma_x \sigma_y = (3.3) (13.93 \times 10^3) = 4.6 \times 10^4 \text{ ft}^2$$

5. Compute lateral variance

$$\sigma_y^2 = \frac{b}{a} \sigma_x \sigma_y = \left(\frac{1}{3.3} \right) \left(13.93 \times 10^3 \right) = 4.2 \times 10^3 \text{ ft}^2$$

70

TABLE 4.6

PHYSICAL PROPERTIES OF PATCHES

MISSION 186

Date	Patch	Time (CDT)	Peak Concentration (ppb)	σ_x^2 (m²)	σ_y^2 (m²)	Aspect Ratio a/b	Depth of Patch at Center (m)	Lateral Axis at c = 1ppb (m)	Computed Volume, M (m³)
6 Oct	Point Barrow	1555	5.4	2.82×10^3	2.06×10^2	3.7	1.	50	2.64×10^{-5}
	Point Barrow, Lobe 1	1555	5.0	1.79×10^3	1.79×10^2	3.2	1. (e)*	50	1.77×10^{-5}
		1700	1.5	2.26×10^4	1.22×10^4	1.4	1. (e)	35	1.56×10^{-5}
7 Oct	A_1	1040	28.	4.27×10^3	3.92×10^2	3.3	.5(e)	120	1.14×10^{-4}
		1200	15.	2.40×10^4	2.07×10^3	3.4	.5(e)	240	3.33×10^{-4}
	B_1	1100	40.	4.89×10^3	2.04×10^2	4.9	.3(e)	25	7.6×10^{-4}
	C	1120	26.	1.34×10^4	7.56×10^2	4.2	.5(e)	45	2.6×10^{-4}
	A_2**	1445	79.	1.78×10^3	1.11×10^2	4.	1 (e)	20	2.2×10^{-4}
		1550	53.	3.46×10^3	3.84×10^2	3.0	1 (e)	90	3.83×10^{-4}
	B_2	1530	21.	4.66×10^3	2.41×10^2	4.4	1.	75	1.40×10^{-4}
		1620	30.	4.46×10^3	6.47×10	8.3	1. (e)	35	1.01×10^{-4}
8 Oct	A***	1110	14.1	2.26×10^3	1.41×10^2	4.	2. (e)	20	1×10^{-4}
	B	no development							

* (e) denotes "estimated." See text for discussion.

** σ_y^2 computed from one lateral transect (Fig. 4.18). a/b estimated from helicopter photography and longitudinal variance computed from $\sigma_x^2 = (a/b)^2 \sigma_y^2$.

*** Very rough, see text for explanation.

given in Table 4.6. When vertical soundings are not available, the depth of the patch is estimated from the behavior of the other patches, the buoyancy of the initial release, and the known conditions of wind and waves. These estimated depths are marked with an "e" in Table 4.6. These are necessarily rough estimates. Also given in Table 4.6 is the approximate width of the patch at 1 ppb contour (the lateral axis). This is useful as an estimate of the largest scales of motion contributing to the diffusion of the patch.

The last column in Table 4.6 is the computed volume of dye which is estimated from the equation $M = 2\pi D \sigma_x \sigma_y c_o$. D here is the mean depth of the patch which is taken for this estimate to be the depth of the patch at its center although this is an overestimate since dye patches are usually lenticular in shape. The number M is based upon the assumed Gaussian distribution and the gross physical parameters of the patch, and is, therefore, at best a very rough estimate. Its utility lies in the fact that for two configurations of the same patch (a short time apart) the values of M should be about the same so that M provides a quick consistency check of the data and an indicator as to whether any of the dye has been lost. It should be remarked that when a patch is still in its early stages of development the dye near the center may be extremely concentrated, far more than that expected from the Gaussian distribution, and consequently M will be underestimated by this formula.

The computed volume M can not be compared directly to the volume of dye released because the latter is determined by dividing down the barrel concentration, whereas the former is determined from the measured fluorescence in the water body. Thus, anything in the receiving water which alters the fluorescence, e.g. turbidity, will change the effective peak concentration and hence M . Indeed, one notes from Table 4.2 that the volumes

of dye released in the Point Barrow patch on 6 October and Patch A_1 on 7 October are, respectively, 2. x 10^{-4} and 1. x 10^{-3} m^3. In contrast, however, the computed volumes in Table 4.6 for the same patches are roughly an order of magnitude lower than these values. Both of these are near-shore releases, and this poor comparison is undoubtedly due to the concomitantly high turbidity.

For all the patches except B_2 of 7 October and B of 8 October, dispersion coefficients were computed from the distribution of dye. These computed dispersion coefficients are tabulated in Table 4.7. The inclination of the major axis from a north-south line is given along with the values of the dispersion coefficients parallel and perpendicular to that axis. This specifies the direction of the principal axes of the dispersivity tensor as well as the principal horizontal values. As noted above, the dispersion coefficients are computed by one of two methods. The first by equation (3.16) which is denoted in the table $\sigma\dot{\sigma}$, and the second by equation (3.17) denoted in the table by $\sigma^2/2t$. The former is considered superior, but in most cases two serial configurations of the same patch were not available so the second method had to be used. The times in Table 4.7 are the effective times of the computed dispersion coefficient; that is, for method 1, $\sigma\dot{\sigma}$, this is the mean of the times of the two configurations, and for method 2, $\sigma^2/2t$, this is the time corresponding to the patch configuration used in the computation. The last column of Table 4.7 represents an attempt to evaluate the quality of the computed dispersion coefficient on the basis of the adequacy of the data and the methods used in the calculation. This is, of course, a strictly subjective judgement, but it is felt that the computed coefficients should not be regarded as equally weighted data points, as some are derived from definitely inferior data or tenuous assumptions.

73

TABLE 4.7

COMPUTED DISPERSION COEFFICIENTS
MISSION 186

Date	Patch	Direction of Major Axis (Degrees E of N)	Time (CDT)	Method of Computation	E_x (m²/s)	E_y (m²/s)	Quality*
6 Oct	Point Barrow	15°	1555	$\sigma^2/2t$	3.13×10^{-1}	2.29×10^{-2}	f
	Point Barrow, Lobe 1	20°	1625	$\sigma\dot{\sigma}$	2.66	1.54	p
7 Oct	A$_1$	10°	1120	$\sigma\dot{\sigma}$	2.06	1.76×10^{-1}	g
		20°	1040	$\sigma^2/2t$	5.40×10^{-1}	4.96×10^{-2}	f
		0°	1200	$\sigma^2/2t$	1.37	1.18×10^{-1}	f
	B$_1$	20°	1100	$\sigma^2/2t$	4.52×10^{-1}	1.89×10^{-2}	f
	C	-20°	1120	$\sigma^2/2t$	2.3	1.3×10^{-1}	p
	A$_2$	70°	1515	$\sigma\dot{\sigma}$	4.3×10^{-1}	7.0×10^{-2}	f
		~90°	1445	$\sigma^2/2t$	2.5×10^{-1}	1.5×10^{-2}	p
		70°	1550	$\sigma^2/2t$	2.3×10^{-1}	2.6×10^{-2}	f
8 Oct	A	~90°	1055	$\sigma^2/2t$	1.51×10^{-1}	9.4×10^{-3}	p

* Subjective judgement of quality of dispersion coefficient, g: good, f: fair, p: poor.

The calculations involved in obtaining Table 4.7 are, for the most part, straightforward application of the methods of Section 3. and the data presented in the preceding sections. The exceptional cases deserve explanation. The Point Barrow patch was divided into two lobes by the passage of a work boat. This fact was ignored in the first entry of Table 4.7, the areas from both lobes being combined as though the patch were unseparated. This was thought to be justified by the fact that the separation occurred only a few minutes prior to running the traverses of Fig. 4.11 so that hopefully the relative distribution and patch elongation were not seriously disrupted. Often after such a separation occurs each lobe develops autonomously, and can be treated as separate patches. Thus, when the data of Fig. 4.12 was obtained, the dye had been advected further south implying that the concentrations detected were those of the uppermost lobe of Fig. 4.11, viz. Lobe 1. Since the configuration of Fig. 4.12 is incomplete, it was assumed that the remainder of this patch was precisely a mirror image of Fig. 4.12. With these assumptions the time history of Fig. 4.29 could then be derived. The dispersion coefficients computed from this information are regarded as being, at best, poor estimates because of our ignorance of the precise history of Lobe 1, and the incompleteness of data concerning its configuration at 1700.

Patch A_1, of 7 October, represents the best set of data collected on this mission. The patch was traversed at two different times, and sufficient data was collected to adequately specify its configuration as well as its location. Accordingly, the computed dispersion coefficients are regarded to be quite good. By way of comparison, the configurations of this patch at 1040 and 1200 were used to compute dispersion coefficients by method 2. These values are also given in Table 4.7, and a comparison of the values from method 1 provides a good indication of the inherent "noise" in this type of calculation.

75

Because of the bifurcation of Patch C, Fig. 4.17, whose cause we can only speculate, very little could be done with this data. The curve of Fig. 4.34 was obtained by ignoring the lobing and combining the areas as though the patch were connected. This is poorly justified, however, because of our ignorance of the patch history. Consequently, the coefficients computed therefrom are labelled as "poor" in Table 4.7.

Strictly speaking, there is only one complete traverse of Patch A_2, namely that performed at 1550. However, the single transect made roughly laterally at 1445 can be used to estimate both the peak concentration and spatial variance. The peak concentration, c_0 , was computed from equation (3.19), using the widths of the patch at 1 ppb and 20 ppb, to be 79. ppb. (Using such widely separated values reduces the effect of errors in measurement.) The lateral standard deviation was then determined from the mean of the widths of the patch at .325 c_0 , .135 c_0 , and .044 c_0 , which correspond respectively to 1.5 σ , 2 σ , 2.5 σ (Ward, 1972). The aspect ratio was estimated from helicopter photography and the remainder of the calculations are as usual. Because the dye configuration and the resulting parameters are only roughly estimated, the dispersion coefficients computed from direct application of method 2, $\sigma^2/2t$, are regarded as poor. However, these estimates of σ_x^2 and σ_y^2 provide at least a fair estimate of the time rate of change of the variances, so that this information combined with the complete configuration of Fig. 4.19 provides a "fair" computation of the dispersion coefficients by method 1.

Because of the failure of the fluorometer system on 8 October, only grab samples from Patch A are available. The spatial variances were estimated from the equation

$$\sigma_x \, \sigma_y \, = \, \frac{M}{2\pi \, D \, c_0}$$

The patch depth D was taken to be 2 meters, i.e. nearly the
depth of the water, because of the higher wave action prevalent
that day. Peak concentration c_o was taken to be 14.1, the
maximum concentration measured among the grab samples. The
volume of dye in the patch M was guessed from the volume
released (2×10^{-4} m^3) divided by 2 to account roughly for the
reduction in fluoresence due to turbidity. (This factor of 2 was
judged by comparing the computed volumes of Table 4.6 with the
initially released volumes of the respective patches. It could be
off as much as a factor of 5.) The aspect ratio was estimated
from helicopter photography. The variances resulting from these
values are given in Table 4.6., and the rest of the calculation
is straightforward. This is obviously very inadequate data upon
which to base this kind of computation, and the resulting coeffi-
cients are regarded as extremely poor. It would be fortuitous
if the order of magnitude is even correct.

5. MISSION 192, 19 JANUARY 1972

5.1 General Conditions, Operations and Observations

Because of poor weather conditions the major operations
of Mission 192 sustained several postponements. Unfortunately,
prior commitments prevented the dye boat and equipment from being
on general standby in support of this mission. For this reason,
on the originally scheduled date, 19 January, dye releases were
performed but without the assistance of transit crews or helicopter
reconnaissance.

The weather conditions which precipitated this unfortunate
circumstance began the previous week when a surge of relatively
cold air pushed through the Galveston Bay area. Temperatures
remained quite cold for several days until the 17th, when the
southerly flow began to return moist warm Gulf air over the area.
As a consequence, the bay water temperature became at or below
the dew point of the overlying air, resulting in a layer of dense
fog several meters deep. Visibility was extremely poor, and opera-
tions on the bay were difficult. Even as the fog dissipated over
the land during the day, it remained over the bay so conditions
became little better (Fig. 5.2). The water was nearly calm due to
the lack of wind hence the development of the patches was sluggish
and limited. Another exceptional condition was the fact that the
waters in Trinity Bay were very nearly zero salinity, as a result
of torrential rains the previous week in the Trinity River water-
shed. The salinities in the discharge canal, however, were on
the order of 9 ^{o}/oo. Some miscellaneous observations transcribed
from the field notes of that day are given in Table 5.1.

Two releases were made on this occasion. The first
from a point about a quarter-mile straight out from the HL&P
discharge canal, and the second from a point about 750 feet
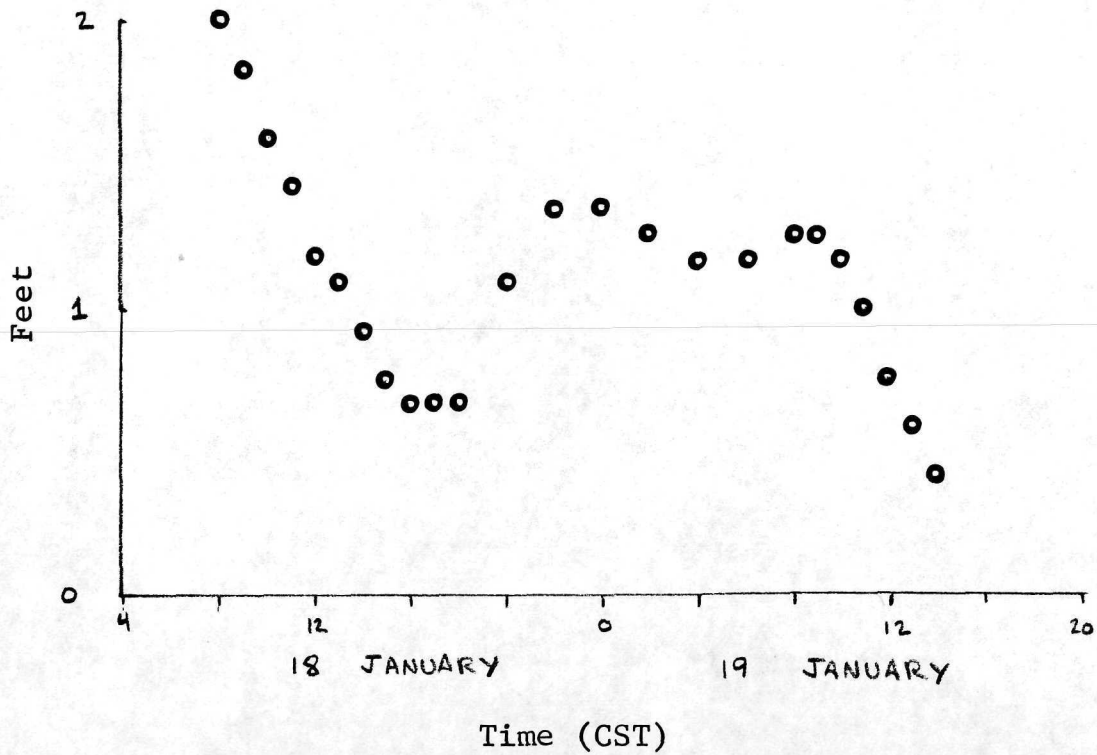
FIG. 5.1   WATER LEVEL OBSERVATIONS (ARBITRARY DATUM)
AT McCOLLUM PARK PIER, MISSION 192

FIG. 5.2   FOG CONDITIONS AT DISCHARGE CANAL (MISSION 192)
TRINITY BAY IS IN BACKGROUND, SOMEWHERE.

TABLE 5.1

MISCELLANEOUS OBSERVATIONS
(Transcribed from Field Notes)

Times CST*

---

19 January 1972

1230	Salinity in discharge 9 ^{o}/oo.
1303	Conditions foggy, cool. <u>Zero</u> salinity. Very little development. May have sunk.
1345	Patch elongating NW-SE with wind, which has picked up to 5 knots within last 1/2 hour.
1405	Waves largely capillary, very slight chop (SWH < 2"). Boat drifts through patch from SE-NW, indicating currents are wind-driven. Distant thunder.

20 January 1972

1500	Salinity at intake 2 ^{o}/oo.

---

*CST = GMT - 6 hours.

further out. The first point was marked with an anchored buoy, B. Approximate locations of these points are shown in Fig. 5.3. When the boat returned to marker B about a half-hour after the release of Patch 1, this patch could not be located. This is not surprising due to the poor visibility that day. Accordingly, a second release was made at 1345, Patch 2, and the boat stayed with this patch for the next two hours to insure that it would not be lost. An initial transect was made about a half-hour later and the dye found to be extremely concentrated. After another half-hour had elapsed, a set of traverses was made of this patch, and the development found to be so poor that the patch was abandoned and further activities terminated for the day.

TABLE 5.2

DYE RELEASES

19 January 1972

Designator & Release Point (See Fig. 5.3)	Time (CST)	Quantity (Liters)	Concentration (parts per thousand)	Remarks
1	1303	20.	20.	d^*, lost
2	1345	20.	5.	d

*d: slightly denser than receiving water. Dye was diluted to be neutral for $9^o/oo$ salinity water but was released in $0\ ^o/oo$ salinity water.
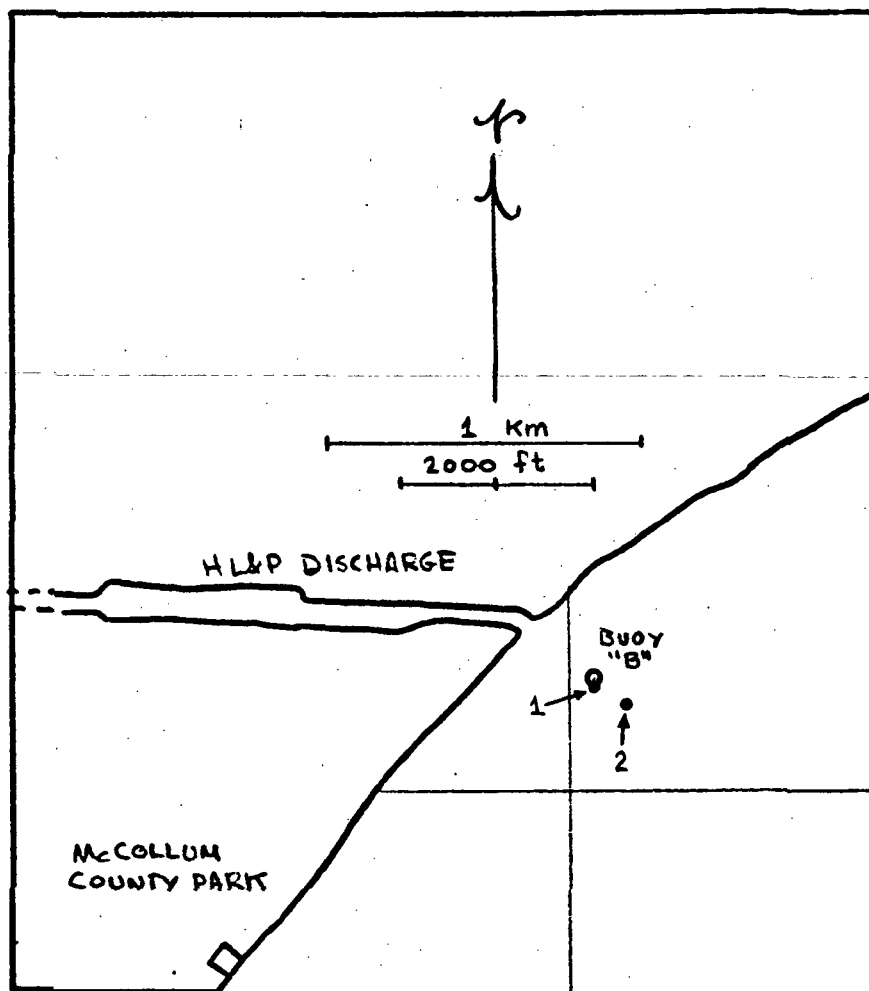
FIG. 5.3   DYE RELEASES OF 19 JANUARY 1972

5.2   Movement of Patches

As there are no transit fixes for these operations, the absolute positioning of the release and subsequent movement of the dye patches is very limited. Fig. 5.4 shows the approximate movement of Patch 2 determined from field observations relative to the fixed buoy B. It can be seen that the patch moved WNW at a rough velocity of .13 fps or about .04 m/s.

5.3   Patch Development

As mentioned above, the development of Patch 2 was limited due to the extremely calm conditions. About the time of release, a slight breeze (about 5 knots from the SE) sprang up over the release area and elongated the patch in a NW-SE direction. At 1418 CST a transect of the patch was made along its longitudinal axis, Fig. 5.5, but the concentrations proved to be too high to merit further traverses. At 1505 the patch was traversed by a series of rectilinear intercepts aligned with the longitudinal and lateral axes. The concentration contours derived from this set of traverses are depicted in Fig. 5.6. The maximum gradient is located along the western side of the patch, in the direction of motion, however the patch shows elongation along the north-south direction, normal to its direction of motion.

Vertical development of the patch was similarly limited. Fig. 5.7 shows the profile derived from a vertical sounding in the center of the patch at 1515. It is evident that the dye is virtually confined to the top two feet.

Buoy
"B"

o

1505 ◯

RELEASE "2"
⊕ 1345 CST

500 ft
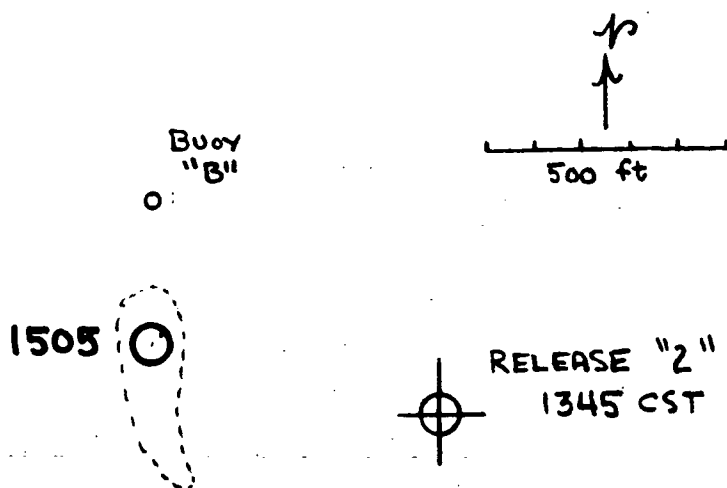
FIG. 5.4   MOVEMENT OF PATCH 2, 19 JANUARY 1972

OFF SCALE

20

c (ppb)

10

0   100   200   m

Distance Along Longitudinal Axis
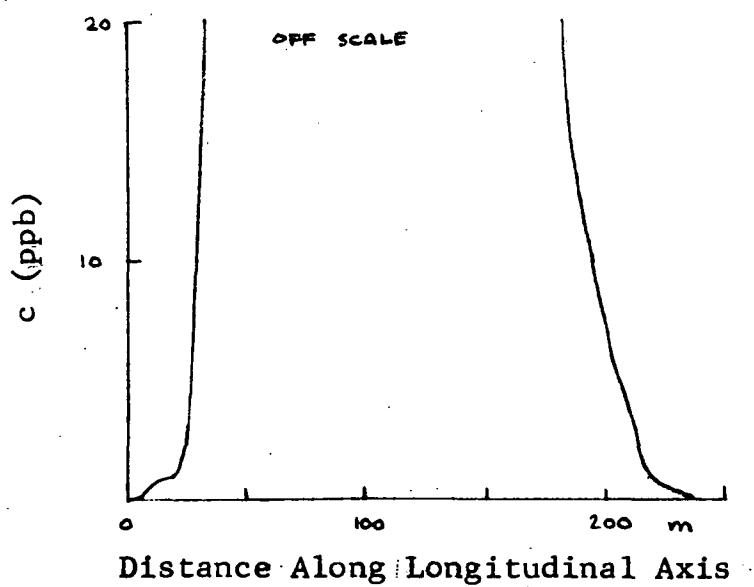
FIG. 5.5   LONGITUDINAL TRANSECT AT 1418 CST

84
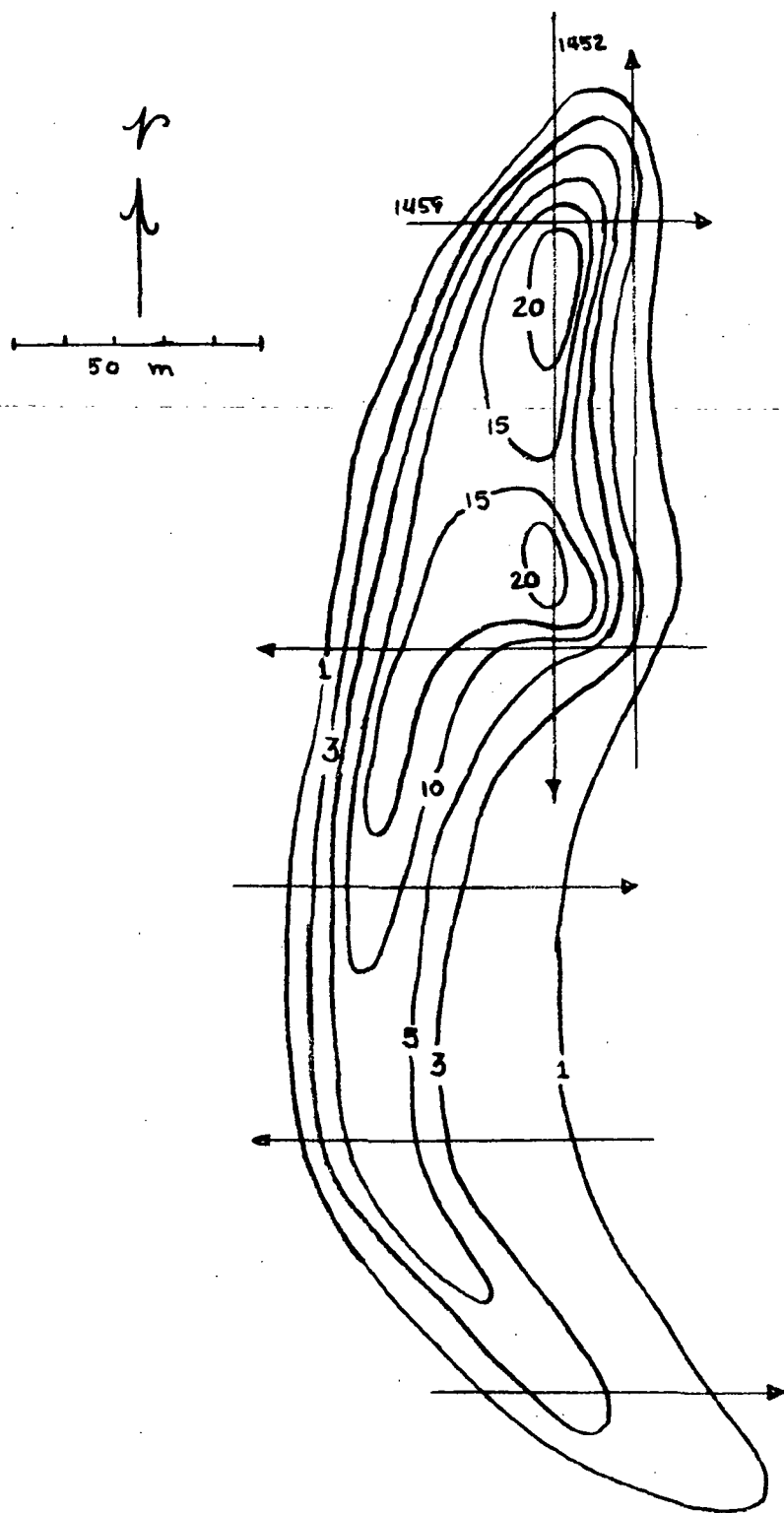
FIG. 5.6   PATCH CONFIGURATION AT 1505 CST
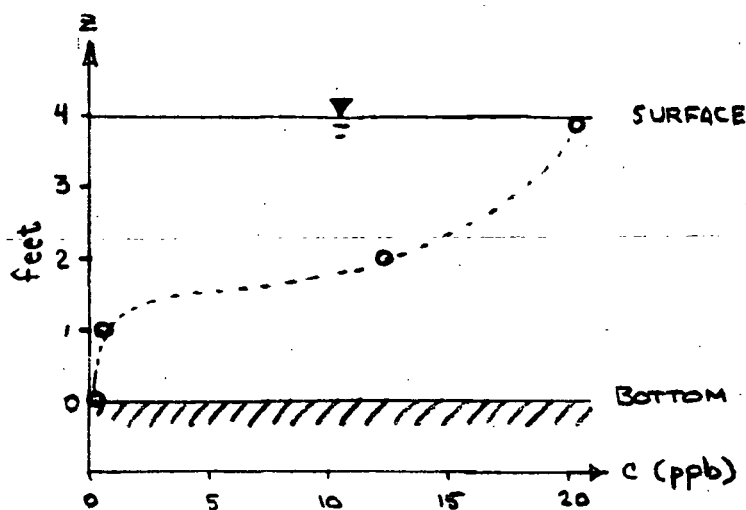
FIG. 5.7   VERTICAL PROFILE IN CENTER OF PATCH 2, 1515 CST

5.4   Dispersion Coefficients

In Table 5.3 are tabulated some of the physical parameters
determined for the patch configurations of 1418 and 1505.   The
reader is reminded that the 1418 data consists of a single transect
along the longitudinal axis of the patch, most of which was off-
scale for the fluorometer.   Because of the sparsity of data,
however, this information was used nevertheless.   From equation
(3.19) the peak concentration was computed to be 1480 ppb, which is
probably much too high in that the gradients near the patch edge
(which basically determined this Gaussian fit) were still quite steep.
Since the length of the semi-major axis where c = .011 c_o =
16.3 ppb has a length of 3 σ_x for the Gaussian distribution,
this axis was measured from the distribution of Fig. 5.5 to be
76 meters giving σ_x^2 = 625 m^2 .   An aspect ratio of 4 was guessed

TABLE 5.3

PHYSICAL PROPERTIES OF PATCH "2", 19 JANUARY 1972

Time (CST)	Peak Concentration (ppb)	σ_x^2 (m²)	σ_y^2 (m²)	Aspect Ratio a/b	Depth of Patch at Center (m)	Lateral Axis at c = 1 ppb (m)	Computed Volume M (m³)
1418*	1480	625	39	4(?)	.3(?)	50	4.33×10^{-4}
1505	24	4.53×10^3	2.83×10^2	4	.6	67	1.06×10^{-4}

*Poor data

87

and $\sigma_y{}^2$ calculated to be 39 m^2 . The total volume M computed from these very shaky estimates is indicative, at best, of order of magnitude.

The configuration of the patch at 1505, Fig. 5.6, is rather complete. The relation of enclosed area to the logarithm of the corresponding concentration is shown in Fig. 5.7. From the fitted distribution indicated by the straight line, the data of Table 5.3 were determined.

Dispersion coefficients calculated from this information are given in Table 5.4. Two methods of computation were used, as before, $E = \sigma \dot{\sigma}$ and $E = \sigma^2/2t$. The time is that applicable to the computed coefficients, i.e., the mean of the times of the two configurations when the first method is used, and the time corresponding to the patch configuration when the second method is used. The meaning of the last column is the same as that for Table 4.7. The first set of values, which employed in addition to the configuration of Fig. 5.6 the spatial variances derived from the single transect of Fig. 5.5, uses the intrinsically better computation. However, the data quality at 1418 is so poor that the computed coefficients are considered to be of little better quality than those determined from the configuration at 1505 by itself.
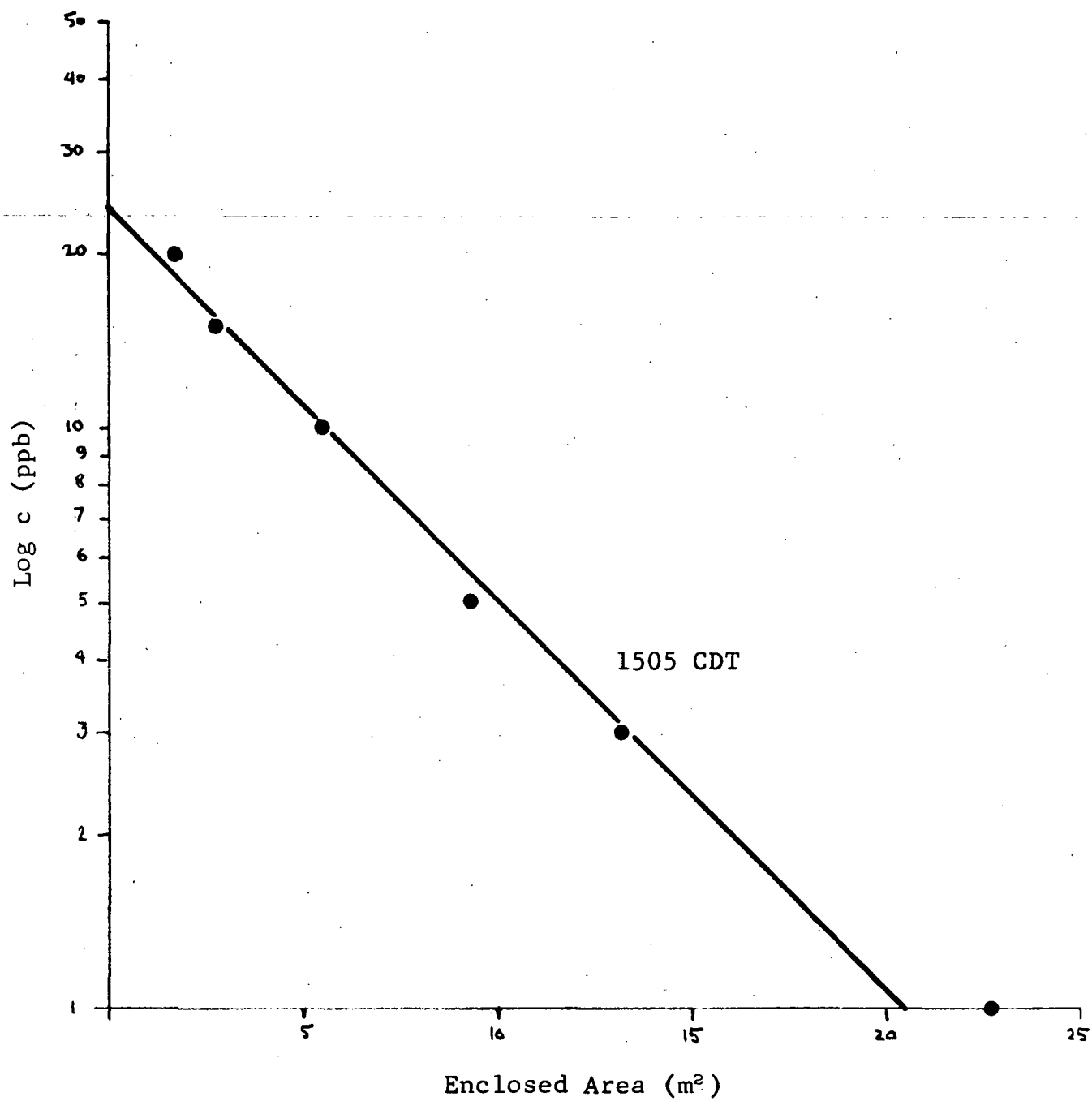
FIG. 5.8   PATCH 2, 19 JANUARY 1972, LOG c VERSUS AREA

TABLE 5.4

COMPUTED DISPERSION COEFFICIENTS

PATCH "2", 19 JANUARY 1972

Time (CST)	Direction of Major axis (Degrees E of N)	Method of Computation	E_x (m²/s)	E_y (m²/s)	Quality*
1442	0°	$\sigma \dot{\sigma}$	6.92×10^{-1}	4.33×10^{-2}	f
1505	0°	$\sigma^2/2t$	9.45×10^{-1}	5.9×10^{-2}	f

*See notes to Table 4.7.

90

6.   MISSION 204, 7-8 JUNE 1972

6.1   General Conditions, Operations, and Observations

Mission 204 was conducted in early June of 1972.
Weather conditions were fair and clear under the domination of
a weak high in the Texas area. The wind was generally from the
east or southeast and very light, an unfortunate circumstance
since it had been hoped that somewhat rougher wave conditions
would be encountered in contrast to the conditions of Mission 186
and 192. The mission, which was originally scheduled for 7 June,
was postponed one day due to mechanical difficulties with the P-3.
Therefore, no dye operations were conducted during the 7th; instead
this opportunity was taken to collect a series of temperature and
salinity measurements encompassing the north part of the operating
area from the HL&P intake around the north shore of Trinity Bay
to the HL&P discharge canal. The measurements obtained, together
with observations in the field notes, are given in Tables 6.1,
6.2, and 6.3. The station locations are shown in Fig. 6.1, and
the salinity profiles depicted graphically in Fig. 6.2. Salinities
in the northern bay area were relatively low (cf. salinities for
Mission 186). It is interesting to note, however, that the HL&P
Cedar Bayou plant is definitely circulating water of slightly
higher salinity which appears to originate in the dredged channels
in the intake area, probably a consequence of density currents.

On 8 June 1972, the dye work was performed. In Table 6.4
are transcribed some observations from the field notes. Conditions
were calm in the morning operations. Shortly after noon, however,
a light breeze began which developed small but short-crested waves.
Wind and tide observations made by NASA personnel at McCollum
Park Pier are shown in Figs. 6.3 and 6.4. One unfortunate feature
of the weather on both the 7th and 8th was the presence of a high

91

TABLE 6.1

T-S SAMPLING STATIONS, 7 JUNE 1972
(See Fig. 6.1)

Station	Description
1	In Bayou at intake of Cedar Bayou Plant
2	Roseland Park
3	Confluence of Cedar Bayou and intake canal
4	Inside mouth of intake canal
5	Intake channel ca. 2,000' out from mouth
6	Confluence of intake channel and Cedar Bayou channel
7	Opposite Mesquite Knoll, between Atkinson Island and Knoll
8	Off Cedar Point, ca. 3,000' out
9	Crawley's, ca. 3,000' out
10	Point Barrow
11a	Opposite discharge, ca. 4,500' out
11b	3,500' out
11c	2,500' out
11d	1,500' out
11e	500' out
11f	At west groin (mid-point)
11g	100' off east groin

TABLE 6.2

TEMPERATURE AND SALINITY MEASUREMENTS
MISSION 204, 7 JUNE 1972

Sta.	Time (CDT)	Depth (ft.)	Temp. (C)	Sal. (º/oo)	Notes
1	1100	1	28.2	10.7	Clear but hazy. Waves
		5	28.0	12.4	light. Wind 7-10 knt. from SE.
		10	27.5	12.5	
		15	27.5	12.6	

NOTE: Depths measured along line. Line slopes about 30° off vertical, due to current.

Sta.	Time (CDT)	Depth (ft.)	Temp. (C)	Sal. (º/oo)	Notes
2	1105	1	28.5	12.9	
		5	28.0	12.8	
		10	27.7	13.2	
		15	27.5	13.4	
3	1115	1	28.0/27.8	11.9	Air temp. 29 C.
		5	27.5	12.3	
		10	27.1	12.6	
		15	27.1	14.2	
		19	27.5	14.5	
4	1125	1	27.1	12.7	
		5	27.0	12.9	
		10	27.0	13.1	
		15	27.5	14.6	
5	1129	1	27.5	12.8	
		5	27.0	12.8	
		10	27.0	12.9	
		15*	27.4	16.2	

*Bottom

93

TABLE 6.2 - Continued

Sta.	Time (CDT)	Depth (ft.)	Temp. (C)	Sal. (o/oo)	Notes
7	1138	1	27.9	12.0	Wind rel. calm. Surface calm, SWH < 2" but slightly short crested.
		5	27.0	12.1	
		10	26.9	12.4	
8	1145	1	28.0	12.0	Wave somewhat choppier, SWH $\cong$ 3". Fronts seem to lie N-S, running W.
		5	27.0	12.2	
		8*	27.0	12.4	
	*Bottom				
9	1155	1	28.0	8.7	
		2.5	27.0	8.9	
		5	27.0	10.5	
10	1215	1	28.5	7.2	Wind EbN (probably was this direction at Sta. 2 also) about 5 knt. Waves rougher with max. height 6-8" and "length" 6-10'.
		5	27.5	7.6	
11a	1227	1	28.5	7.5	
		5	28.0	8.4	
11b	1230	1	28.1	7.7	
		5	28.0	8.4	
		6*			
	*Bottom				
11c	1234	1	28.1	7.3	Wild salinity gradient at about 5 feet. No temperature gradient of merit.
		3		8.0	
		5	27.5	10.$\pm$1.	
		7*			
	*Bottom				

TABLE 6.2 - Continued

Sta.	Time (CDT)	Depth (ft.)	Temp. (C)	Sal. (^{o}/oo)	Notes
11d		1	28.0	7.0	
		3	27.9	9.0	
		5	29.0	13.5	
11e		1	30.0	14.1	
		3	30.0	14.1	
		5	30.0	14.1	
11f		1	30.0	14.0	
		5	30.0	14.0	
11g		1	30.5	14.2	Temp. chart behind drop structure reads 86 F.
		5	30.0	14.3	
8	1354	1	28.5	12.0	
		5	28.0	12.0	
6	1402	1	29.0	12.0	
		5	27.0	14.0	
		3	28.5	12.4	
		10	27.0	16.0	
		12	27.0	16.1	
2	1415	1	28.5	12.9	
		5	28.5	12.8	
		10	27.5	13.0	
		15	27.2	13.2	

TABLE 6.3

WATER LEVEL, 7 JUNE 1972

Read on staff gauge at HL&P intake bridge

(CDT)	(level, ft.)
1122	-2.3
1410	-2.5

Readings relative to line (at 4.34 on gauge) presumably indicating MSL.

TABLE 6.4

MISCELLANEOUS OBSERVATIONS
MISSION 204, 8 JUNE 1972

(Transcribed from Field Notes)

0825 CDT[*] Wind calm, slight waves (very small chop, not smooth).

1114 Still as a graveyard.

1233 Waves somewhat higher (SWH < 2") starting to show coherent fronts.

1337 Waves higher. SWH 4-6".

1437 S-T Measurements SW of "A".

Depth (ft)	Temperature (C)	Salinity (^{o}/oo)
1	30.0	7.1
3	30.0	7.1
5	29.5	7.3

1450 Waves same as at 1337. Some spray. Light breeze

1542 Course S, running into wave crests.

[*]CDT = GMT - 5 hours.

96
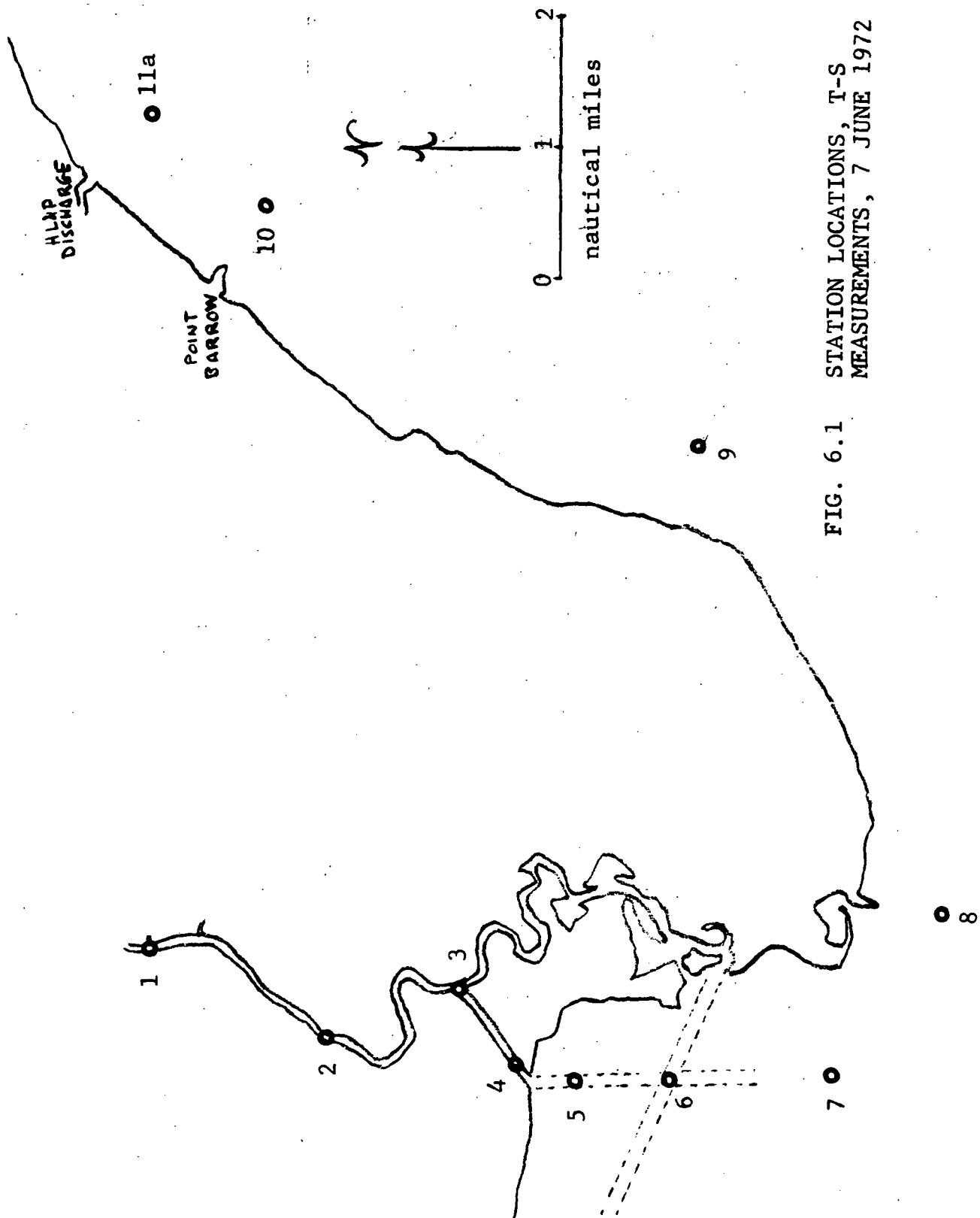
FIG. 6.1   STATION LOCATIONS, T-S
MEASUREMENTS, 7 JUNE 1972

Cedar Bayou
Station Intake

Roseland
Park

Confluence of
Bayou & Canal

Mouth of
Intake Canal

Station S-5 in
Intake Channel

Confluence of
HL&P Channel with
Cedar Bayou Channel

Between Mesquite
Knoll & Atkinson
Island

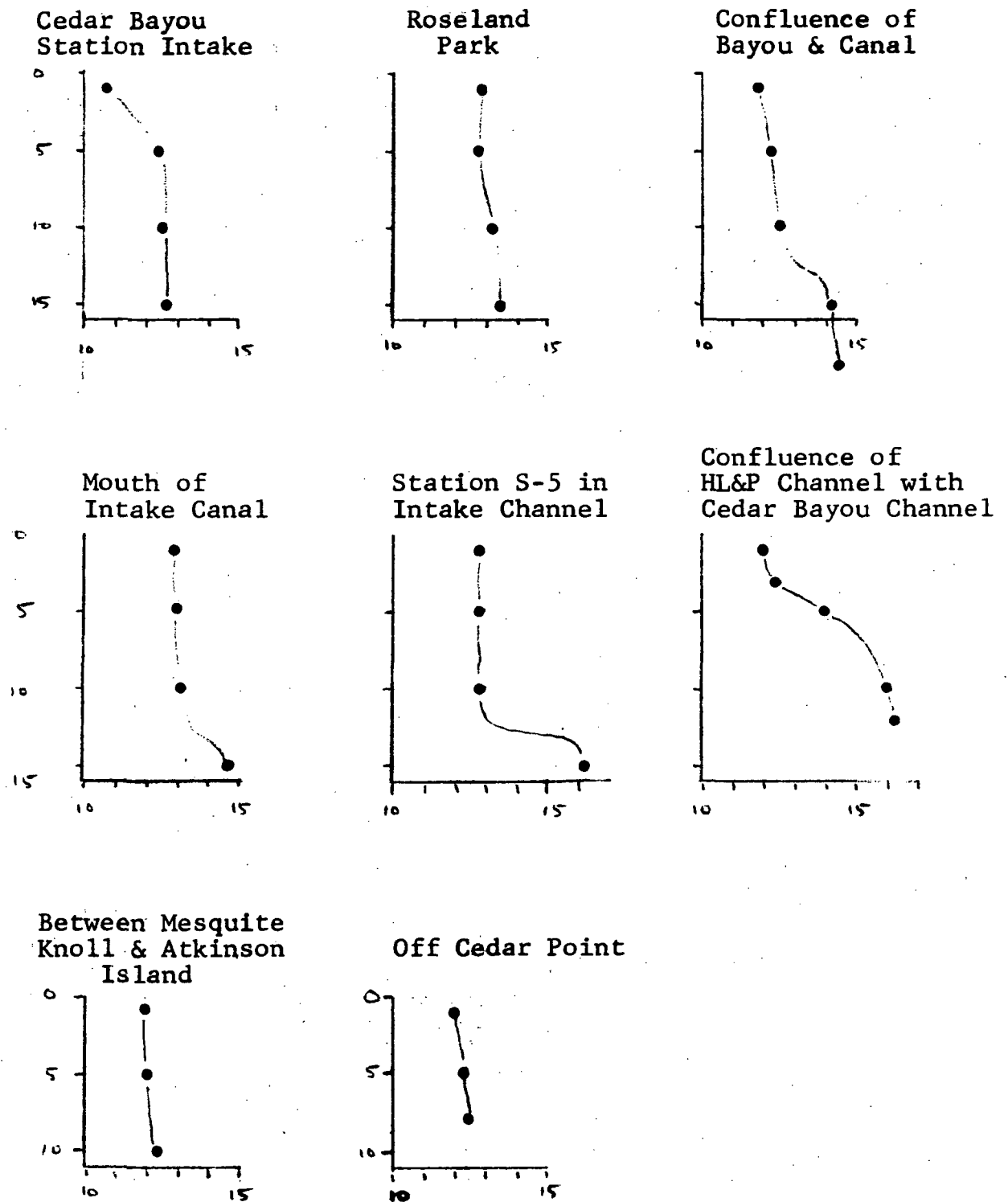Off Cedar Point

FIG. 6.2   SALINITY (°/oo) PROFILES, TRINITY BAY AREA,
7 JUNE 1972, FROM TABLE 6.2.
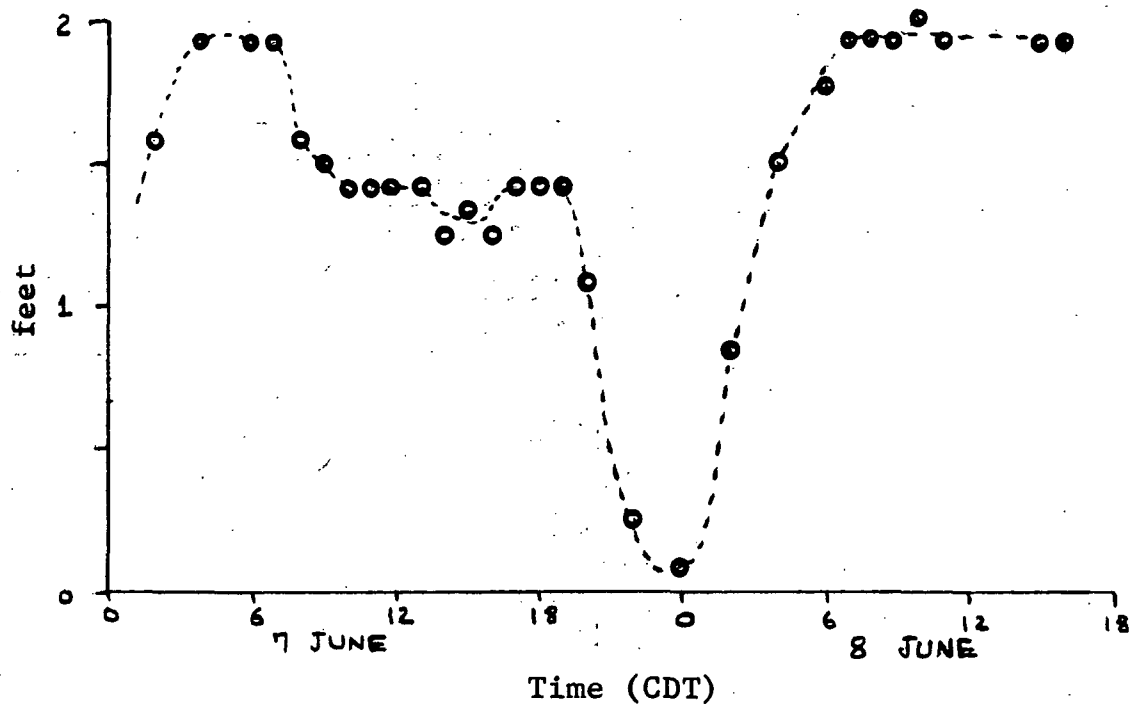
98

FIG. 6.3   WATER LEVEL OBSERVATIONS AT McCOLLUM
            PARK PIER (RELATIVE TO ARBITRARY LEVEL)
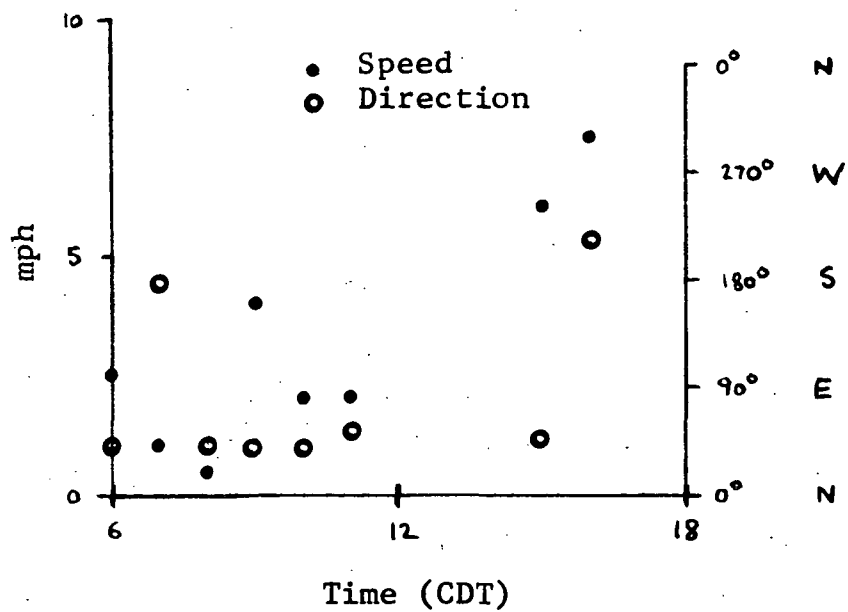

FIG. 6.4   WIND OBSERVATIONS DURING DYE OPERATIONS,
            McCOLLUM PARK PIER, 8 JUNE 1972

99

amount of haze over the bay area. The photography, both from the helicopter and the P-3, failed to show any of the dye releases, probably because of this extreme haziness.

Two releases were made in the morning from points marked by buoys A and B, Fig. 6.5. Because of the still conditions, hence the poor development of the patches, and because the alternator in the fluorometer system was behaving erratically, these patches were not traversed. The patch centroids were, however, tracked to obtain some advective information. These patches proved to be very difficult to locate visually because of the high haze. Therefore only one release was performed in the afternoon operations so that the dye boat could stay with this patch and not risk losing it. Traverses were made by a series of rectilinear intercepts carefully annotated on the fluorometer strip chart while an integrated measure of the boat velocity was obtained with a flowmeter.

The original plan for this mission was to use the helicopter photography as the primary source of information, the concentrations to be determined by densitometry. This data would be supplemented and verified by the fluorometer record. Accordingly, at each traverse buoys were placed within the body of the dye to be used in the photographic analysis, both for orientation and scale. As mentioned above, however, the photography was a failure insofar as detecting the dye, and the fluorometer record became the primary source of information.

6.2   Release and Movement of Patches

The dye releases performed in Mission 204 are summarized in Table 6.5. All of these releases were of relatively low initial concentration. Because of the very calm conditions, it was felt that a more concentrate release would not develop sufficiently to
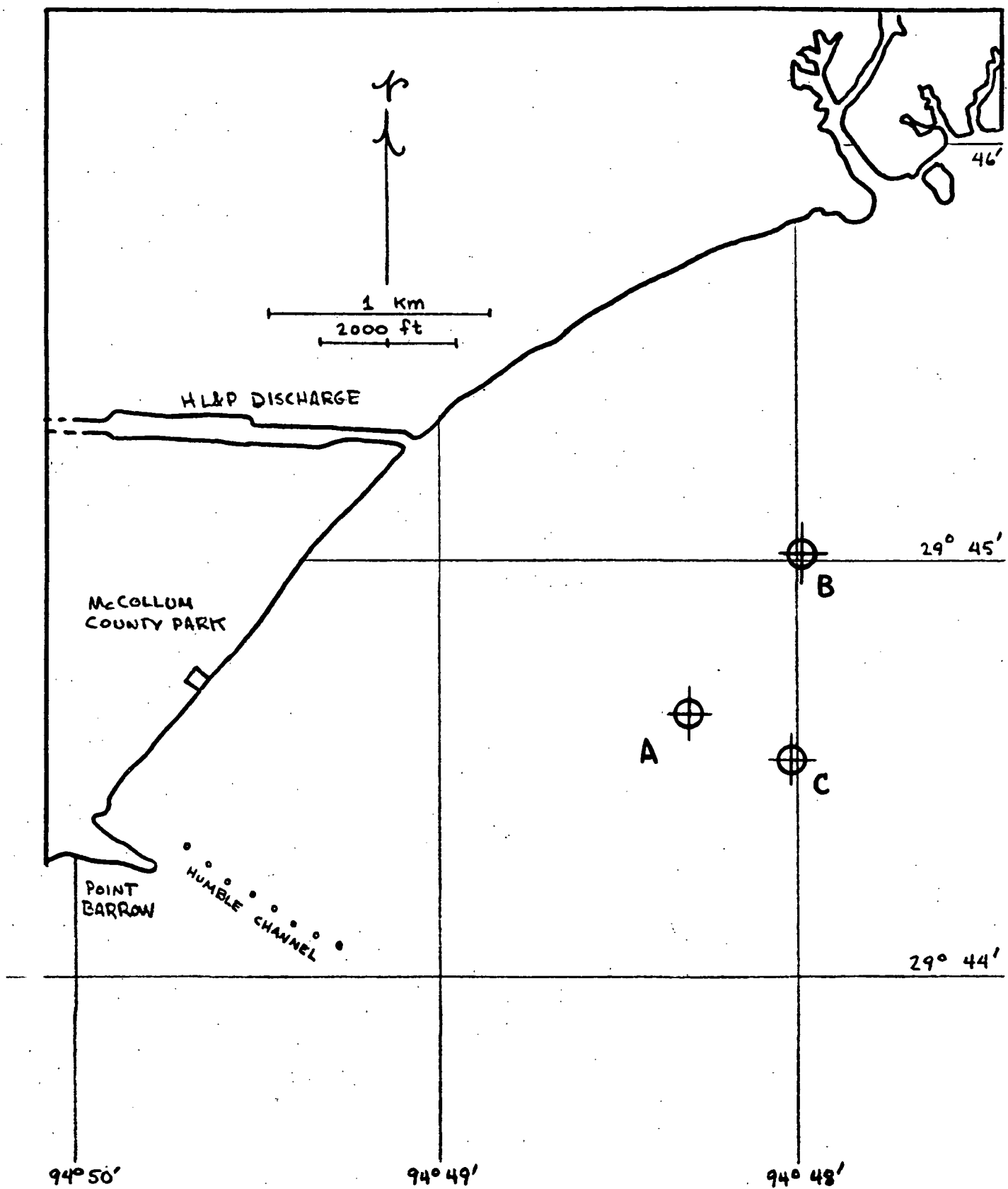
FIG. 6.5   MISSION 204, DYE RELEASE POINTS

TABLE 6.5

DYE RELEASES, MISSION 204
8 June 1972

Release Point (Fig. 6.3)	Time (CDT)	Quantity (Liters)	Concentration parts per thousand
A	0825	20.	10.
B	0830	20.	10.
C	1233	20.	10.

Slug releases, all diluted with ethacol and ambient water to be neutrally buoyant.

TABLE 6.6

MEAN VELOCITIES OF DYE CENTROIDS

Patch	Time (CDT)	Speed (m/s)	Direction (Degrees E of N)
B	0930	.14	255°
C	1320	.080	335°
	1440	.051	30°

be within range of the fluorometer in a reasonable amount of time. In addition to the slug releases of Table 6.5, a continuous low-volume release was made from the north groin throughout the day, being replenished as necessary. Unfortunately, this release is barely discernible from the helicopter photography, and consequently little could be done with it. A very large slug release, about five gallons of 20% Rhodamine WT, was made from the Parks & Wildlife vessel in mid-Trinity Bay with the intention of studying the development of the patch by densitometry of the P-3 photographs. All of the releases conducted thus far in this study have been concerned mainly with diffusion at small scales of motion. It was hoped that such a large release, tracked photographically over the entire day, would provide some information about the larger scales of motion. Unfortunately, this photography, like that of the helicopter, failed to reveal any of the dye.

Both of the morning releases A and B were performed about high-water slack. Both patches moved west by south at about the same velocity. The movement of the centroid of Patch B, as determined from transit fixes, is shown in Fig. 6.6. The average velocity of this patch is .45 fps or .14 m/s. The same kind of transit information is not available for Patch A; however, it was observed in the field that both patches exhibited about the same velocity.

The relative movement of Patch C, also determined from transit data, is shown in Fig. 6.7. This patch exhibited a northerly track with a speed about .26 fps. Specific velocities determined from the information of Figs. 6.6 and 6.7 are given in Table 6.6.
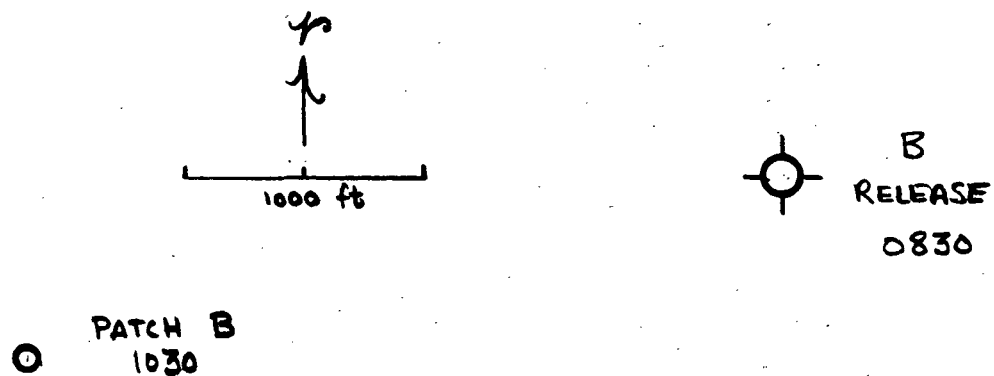
FIG. 6.6   MOVEMENT OF PATCH B, 8 JUNE 1972
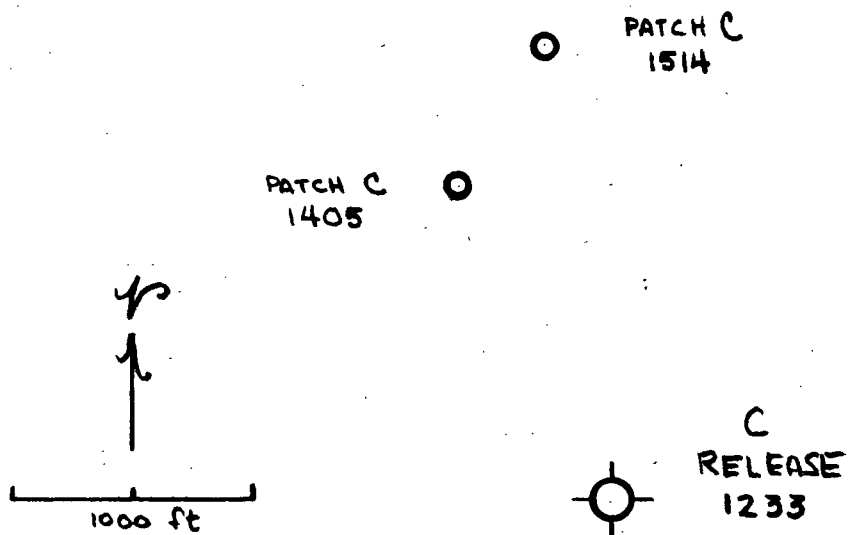
FIG. 6.7   MOVEMENT OF PATCH C, 8 JUNE 1972
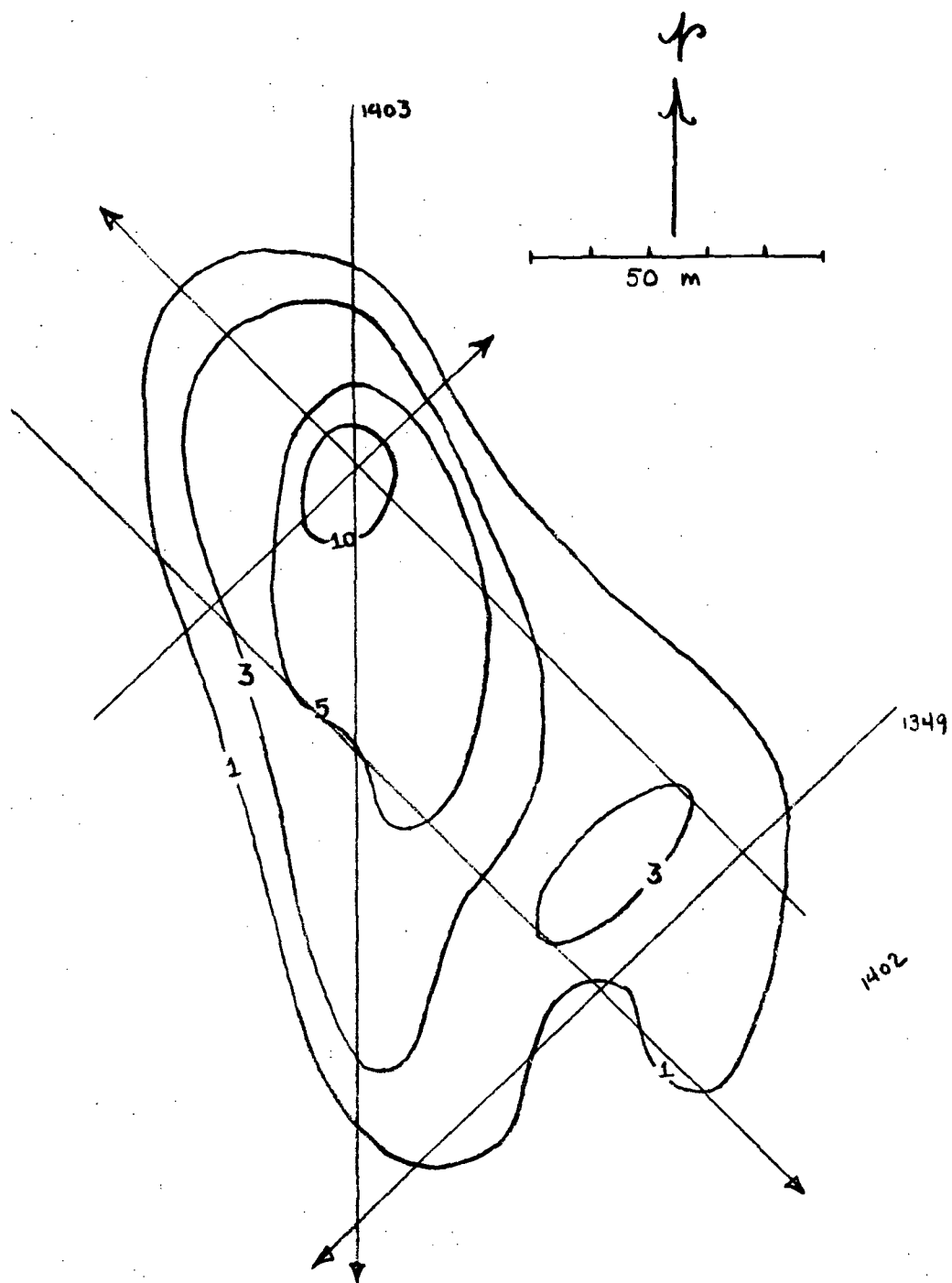
FIG. 6.8   RELEASE C, PATCH CONFIGURATION AT 1400 CDT

6.3   Patch Development

During this mission the only patch traversed was the afternoon release, Patch C. At the time of its release the water was still relatively calm, but under the influence of a southerly breeze, waves were beginning the grow and exhibit coherent fronts. During the next two hours the waves developed further to a slight chop (SWH 4-6") accompanied by some spray and occasional overtopping.

The first set of traverses of release C were made at 1400. The concentration contours, derived from the fluorometer data, are shown in Fig. 6.8. The patch had elongated slightly in the direction of the current, and, as expected, there is a high concentration gradient on the leading edge and shallow confused isopheths in the wake. The vertical profile in the center of this patch, Fig. 6.9, shows the dye to be well mixed through the top three feet and to be present in significant concentrations throughout the top five.

FIG. 6.9   VERTICAL PROFILE IN CENTER OF PATCH C, 1425 CDT

The next set of traverses was made at 1545, nearly
two hours later. The patch at this time was very difficult to
assess in the field, being only marginally visable and having
a confused irregular distribution. More intercepts were required
to adequately locate and identify this patch. The contours
derived from these traverses are shown in Fig. 6.10 several
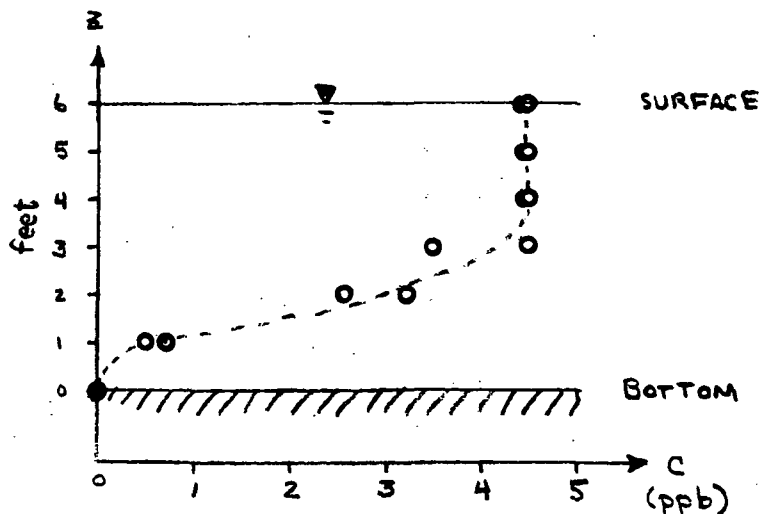features of which are noteworthy. First, the patch possess
about the same areal extent as it did at 1400, but now the
concentrations are reduced by about a factor of 2. This indicates
that the patch was subjected more to dilution due to vertical
mixing than to lateral diffusion. Secondly, the patch no longer
exhibits an apparent elongation or organized patterns of gradients.
This is probably due to a combination of the very low current
velocity extant combined with the enhanced vertical mixing
processes. A rough calculation of total dye volume in this
patch (Section 6.4) shows a reduction of about a factor of 2
from that of the configuration at 1400. Although this difference
is not large enough to establish an inconsistency, it is indicative
of the possibility that some of the dye may have been missed by
the boat traverses. Considering the difficulties of running this
patch configuration, this is indeed a real possibility.

6.4 Dispersion Coefficients

As in the preceding sections, the data from the patch
contours at various times were used to fit Gaussian distributions
from which gross parameters of the patch could be inferred. The
Gaussian fits used are shown in Fig. 6.11. Physical parameters
derived therefrom are given in Table 6.7. The increases in the
horizontal variances from 1400 to 1545 are practically nil; the
differences being of the order of the errors in the computation.
Assuming that by 1545 the dye had been mixed throughout the
two meter depth, the total dye volume in the patch could be
computed as before. The decrease in M from 1400 to 1545 was

107
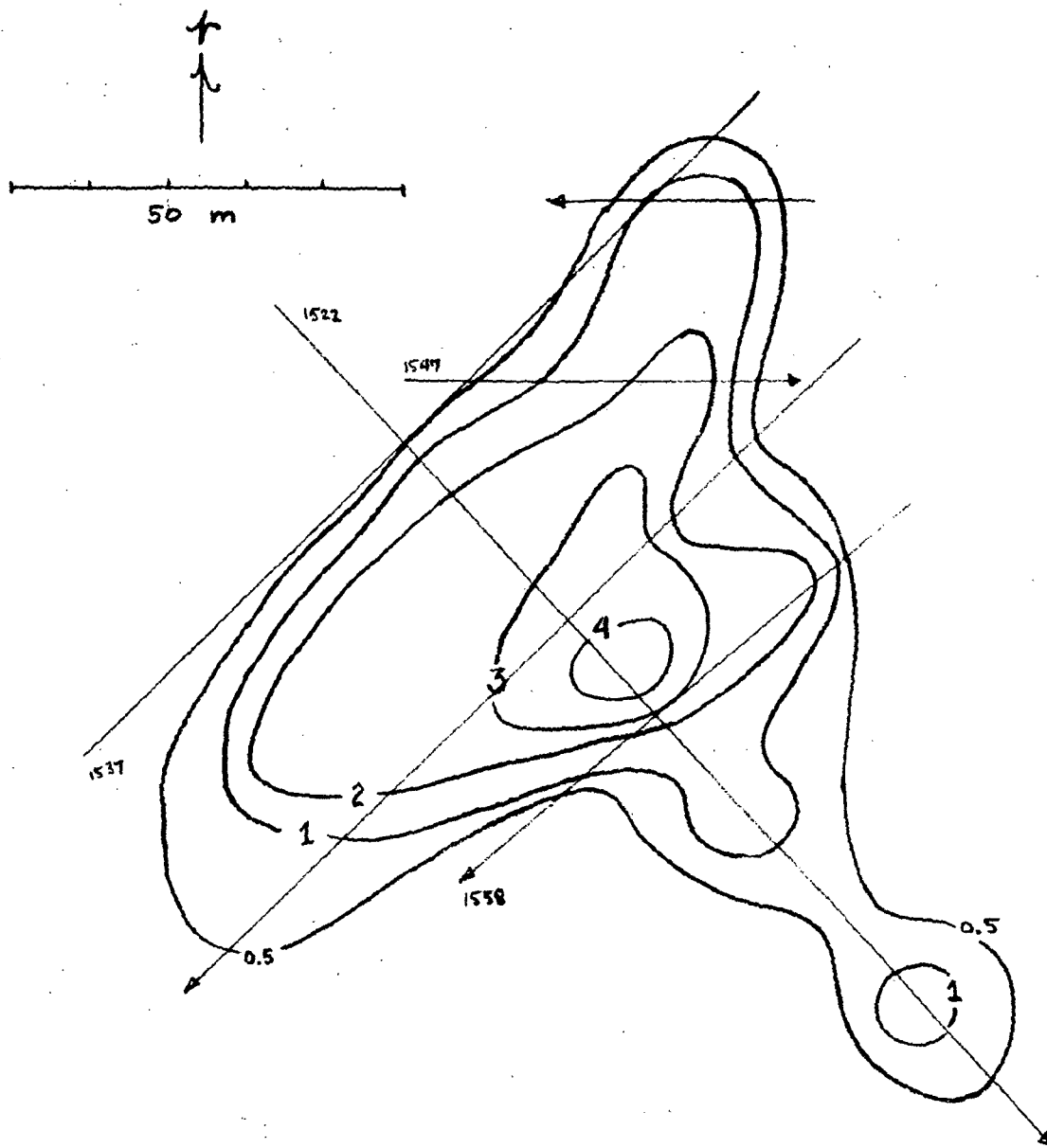
FIG. 6.10 RELEASE C, PATCH CONFIGURATION AT 1545 CDT

108
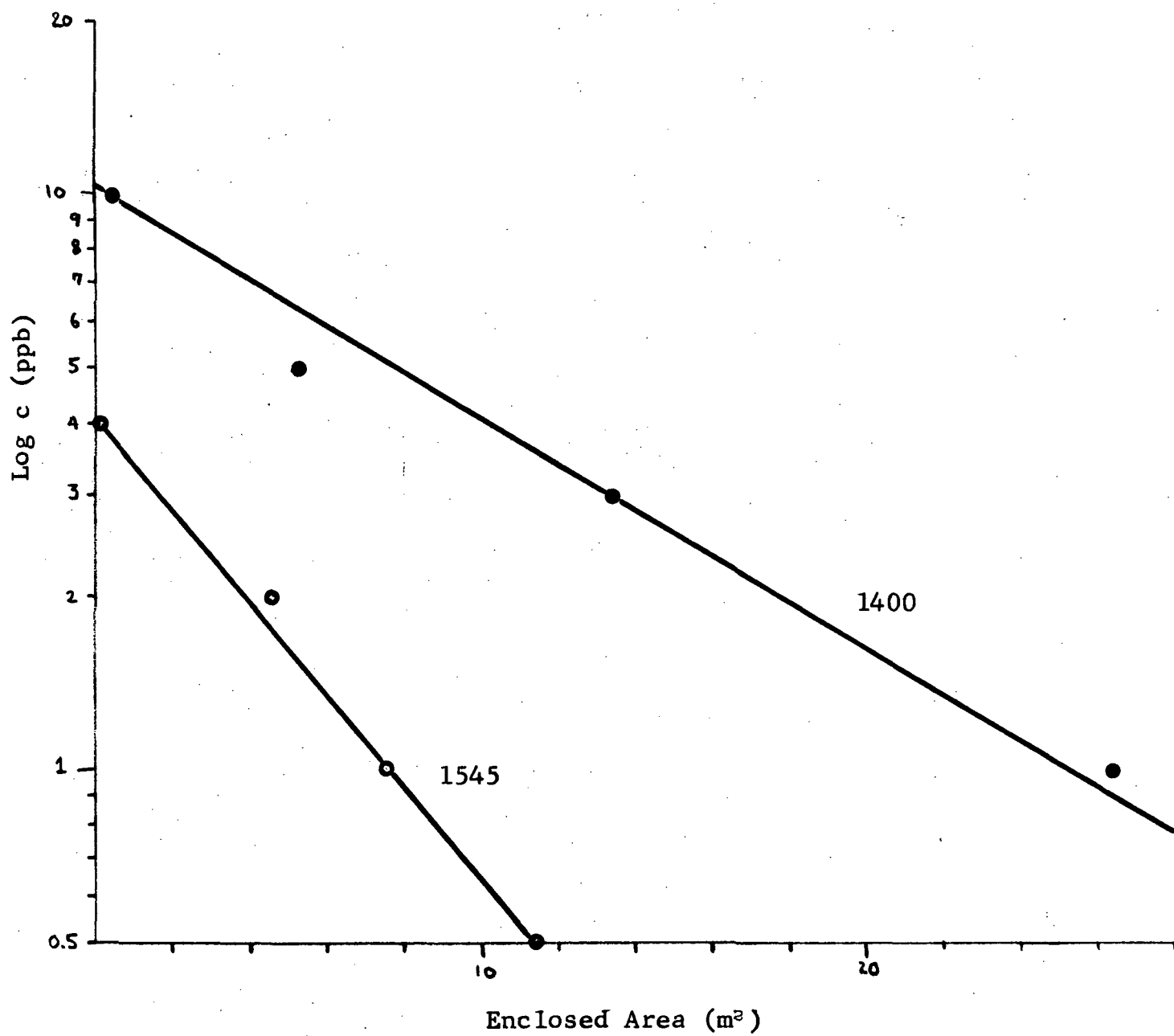
FIG. 6.11   PATCH C, 8 JUNE 1972, LOG c VERSUS AREA

TABLE 6.7

PHYSICAL PROPERTIES OF PATCH C

8 June 1972

Time (CDT)	Peak Concentration (ppb)	σ_x^2 (m²)	σ_y^2 (m²)	Aspect Ratio a/b	Depth at Patch Center (m)	Lateral Axis (m)	Computed Volume M (m³)
1400	10.5	3.55×10^3	8.05×10^2	2.1	1.2	70	1.46×10^{-4}
1545	4.1	1.76×10^3	9.00×10^2	1.4	2.(e)	70	$.65 \times 10^{-4}$

TABLE 6.8

COMPUTED DISPERSION COEFFICIENTS

Time (CDT)	Direction of Major Axis (Degrees E of N)	Method of Computation	E_x (m²/s)	E_y (m²/s)	Quality*
1400	-20°	$\sigma^2/2t$	3.4×10^{-1}	7.7×10^{-2}	f

*See notes to Table 4.7

computed as before. The decrease in M from 1400 to 1545 was
noted in the discussion of the previous section.

Because the patch evidently showed no horizontal
development from 1500 on, the second configuration (1545) was
not used to compute dispersion coefficients. Instead, only
the distribution of Fig. 6.8 was used. The dispersion coefficients
obtained are given in Table 6.8.

7.   DISCUSSION

7.1   Dispersion Coefficients

The pertinent aspects of patch behavior and associated ambient conditions have been summarized in the preceding sections for the individual releases. Little more can be added here. The range of conditions encountered for the three missions was so limited that it is impossible to detect any dependence of the calculated coefficients on current velocity, wind speed or wave height. In general, the patches elongated in the direction of the current, which was in some cases tidal, in some cases wind-driven. For those few exceptions to this, the reason for the cross-current elongation was evident, e.g., Patch 2 of Mission 192. The degree of elongation, as measured by the axis ratio a/b , was, however, not apparently dependent upon the current velocity, as is demonstrated by Fig. 7.1. This is not surprising, since we would expect the patch elongation to be governed more by the _shear_ in the current, rather than the current speed _per se_. This emphasizes the need for detailed current measurements in conjunction with the dye tracer work.

In Table 7.1 is summarized the dispersion coefficients calculated from the preceding data. These coefficients have been scaled to a common base by assuming a four-thirds power dependence on scale and normalizing to 100 m. The scale was taken to be the length of the lateral axis. There is a scatter ranging over an order-of-magnitude in the data, however much of this range is contributed by the "poor" data. The average neglecting poor data is found to be E_x = 1.12 and E_y = 8.25 x 10^{-2} m^2 s^{-1} , although the geometric means E_x = 7.75 x 10^{-1} and E_y = 7.21 x 10^{-2} are probably more meaningful in view of the low-end bias in the data. The higher value of E_x if of course a consequence of not removing the patch elongation before scaling.

112

TABLE 7.1

NORMALIZED DISPERSION COEFFICIENTS

(Lateral Axis Scaled to 100 m by 4/3 - Power Law)

Date	Patch	Time	Quality*	E_x (m^2/s)	E_y (m^2/s)
6-10-71	Point Barrow	1555	f	7.93×10^{-1}	5.8×10^{-2}
	Point Barrow,1	1625	p	8.98	5.2
7-10-71	A_1 ($\sigma \dot{\sigma}$)	1120	g	9.54×10^{-1}	8.15×10^{-2}
		1040	f	4.25×10^{-1}	3.90×10^{-2}
		1200	f	4.26×10^{-1}	3.67×10^{-2}
	B_1	1100	f	2.87	1.20×10^{-1}
	C	1120	p	6.67	3.77×10^{-1}
	A_2 ($\sigma \dot{\sigma}$)	1515	f	9.52×10^{-1}	1.55×10^{-1}
		1445	p	2.13	1.28×10^{-1}
		1550	f	2.63×10^{-1}	2.97×10^{-2}
8-10-71	A	1055	p	1.29	8.04×10^{-2}
19-1-72	2 ($\sigma \dot{\sigma}$)	1442	f	1.37	8.58×10^{-2}
		1505	f	1.52	9.51×10^{-2}
8-6-72	C	1400	f	5.48×10^{-1}	1.24×10^{-1}
<u>Mean</u>				2.09	4.72×10^{-1}
<u>Mean</u> neglecting "p" data				1.12	8.25×10^{-2}
<u>Geometric mean</u>				1.23	1.16×10^{-1}
<u>Geometric mean</u> neglecting "p" data				7.75×10^{-1}	7.21×10^{-2}

*See notes, Table 4.7
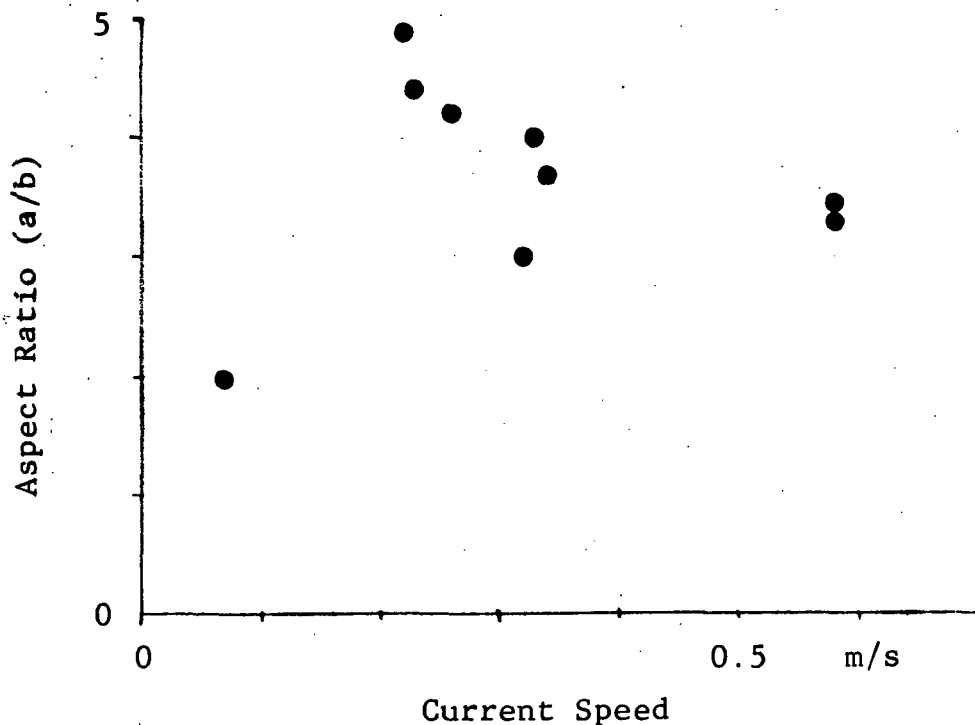
FIG. 7.1   ASPECT RATIO VERSUS SPEED
            OF PREVAILING CURRENT

        Much more hydrographic data was collected during the
associated NASA programs than was available to or could be
employed in this analysis. It is possible that with more complete
ambient data, some pattern might be discerned in the coefficients
of Table 7.1. At present, it appears we may only conclude that
we have a good average value of E_x and E_y for near-calm
conditions in Trinity Bay. The lateral diffusivities probably
represent more closely the effects of "pure" turbulence (i.e.
not being corrupted by shear effects or local currents). It is
interesting to note that the means of these lateral diffusivities
are consistent with the 4/3 fit given by Okubo (1971) for diffusion

on this scale (10^4 cm); this is especially surprising considering
the difference between conditions on these missions and those
usually encountered in the open ocean. It is also of interest
to compare the longitudinal values with that estimated by the
Taylor-Elder formula suggested in NASA (1971). This is

$$E = 77 \, n \, U \, R^{5/6}$$

where   n   is the Manning coefficient,   U   the vertical-mean
current and   R   the hydraulic radius, all in British units.
(We note in passing that this formula applies strictly to one-
dimensional unidirectional flow in which dispersion is solely
due to the shear effect. Application in a two-dimensional model
of Trinity Bay is strictly invalid, but this seems an appropriate
first estimate for the longitudinal coefficient.) Taking   n = .025,
U = 1 fps ($\cong$ .3 m/s which is representative for the data of this
study), and   R = 6 feet , the computed coefficient becomes
8.5 ft^2/s = 8. x 10^{-1} m^2/s , in good agreement with the mean
measured longitudinal coefficient. This comparison neglects
the factor of scale though. Had E_x been scaled to 100 m using
the major axis of the patch, the Taylor-Elder value would be too
high by more than an order of magnitude.

The model calculations performed by NASA (1971) employed
dispersion coefficients on the order of 500-1000 ft^2/min orthogonal
to the discharge canal axis and 1000-3000 ft^2/min parallel to the
canal axis, the precise values being determined by the magnitude
of the discharge current. These coefficients were determined in
earlier verification studies at the P. H. Robinson Generating
Station by TRACOR. The spatial increment used in these model
calculations is about 600 ft, which is an appropriate measure
of the smallest scale of motion that can be resolved by the
model. When the geometric means of Table 7.1 are scaled up to
this (200 m for convenience), the corresponding values are

$E_y = 115 \text{ ft}^2/\text{min}$ and $E_x = 1250 \text{ ft}^2/\text{min}$ ($E_y = 190$ and $E_x = 2000$ if the "poor" data are not neglected). It appears from this comparison that the dispersion coefficients used in the model computations are too large by about a factor of three. Before one accepts this categorically, he should bear in mind two observations: (i) the P. H. Robinson temperature data, from which the model coefficients were developed, were obtained in rougher conditions than the near-calm conditions of this study, so that the difference in coefficients may merely reflect the difference in ambient conditions. The model coefficients may not be "wrong" but rather merely inapplicable to the conditions extant for the Cedar Bayou data. (ii) The coefficients of Table 7.1 were obtained in water well out of the thermal plume, since the objective here was the study of ambient turbulence and mixing processes. The mechanics of the plume itself is comparable to a high-volume jet, and it is unlikely that dispersion coefficients representing the external mixing processes can be used to characterize entrainment and dilution in the plume itself. As the model coefficients were obtained from a similar plume, they may very well represent this kind of process better than coefficients measured in the open water.

7.2 Some Conclusions and Recommendations

With regard to procedures to be followed in future EOD studies involving surface dye releases, the proper balance between aerial photography and surface measurements could not be determined from this work because the photography in the last two missions was unsuccessful. Nevertheless, it remains our conviction that NASA's aerial photography possesses the capability of providing the principal data source for this kind of exercise, and that surface fluorometry should be used only to establish verification or calibration, insofar as the horizontal config-

116

uration is concerned. Unfortunately, potential problems in
obtaining quantitative information from remote photography cannot
be addressed until sufficient data are on hand. However, the
immense capabilities at NASA for obtaining and processing remote
sensing data should enable these problems to be overcome.

Some specific recommendations concerning operational
procedures follow:

(i) More control is required in the photographs. In
most of the helicopter frames from Mission 186 it
is impossible to determine either orientation or
scale. Identifiable markers in the water may
eliminate this difficulty.

(ii) Surface traverses run between markers whose
absolute positions are known yield definitely
superior data to those traverses identified only
by boat course and velocity. When surface fluoro-
metry is a secondary data source, it is recommended
that only two such traverses be run, orthogonals
say, as the dye boat can then deploy and retrieve
the markers itself. If surface fluorometry is
the primary data source, it is recommended that a
second boat be employed to handle the markers,
freeing the dye boat to traverse the patch.

(iii) During a given mission, more dye releases should
be performed than was the case in this work. This
can only be accomplished if the exigent tasks of
the dye boat be relieved freeing the time for
more releases. The employment of aerial photo-
graphy as the primary data source will obviously

117

aid enormously. Also, it is essential to shorten
the search time for patches (which becomes quite
a time-consumer when the dye dilutes to marginal
visibility or less). A second boat supporting
the fluorometer boat will help. In addition, we
suggest marking the releases with flagged drogues
whose vanes are at one foot.

The analysis methods based on Gaussian distributions
(Section 3.2) used in this report, although conventional, involve
too many a priori assumptions and approximations. They are
probably commensurate with the quality of the data presented
here, but with the adoption of more sophisticated sensing tech-
niques, the data analysis should be similarly improved. Hopefully,
a procedure could be developed based only upon the eddy-flux
hypothesis and appropriate integral flux theorems (e.g. the
divergence theorem). This would require much more vertical
detail than acquired in this study, but this could be easily
obtained by the on-board fluorometer. (Fortunately we are
dealing with a shallow estuary, not a lake or ocean, so this is
not impractical.)

Some features of these data sets have been given little
attention in this report, notably the anomalous behavior of some
of the patches. These, however, may be potential sources for more
hydrodynamic information than is derived from the "well-behaved"
patches. Patch B of 8 October 1971 (Mission 186), for example,
remained at its release point and exhibited little development,
while its neighbor at A moved out with the ebbing current
($\sim$.33 m/s) and dispersed dramatically. We might speculate
whether the easterly wind in conjunction with the southerly
(ebb) current may have produced a gyre in Trinity Bay whose
center happened to lie near release point B. Another example
is release B_2 of 7 October 1971 which appears to have been

subjected to a local convergence, discussed in Section 4.3. Although the data available here are inadequate to explicate these behaviors, future programs should be capable of taking advantage of similar phenomena whenever they occur, as they might constitute excellent test cases for verifying the hydro-dynamic model or, at least, illuminate some aspects of the circulations in this complex system.

REFERENCES

Bowden, K. F. (1965), Horizontal Mixing in the Sea due to a
      Shearing Current, *Journal Fluid Mechanics*, 21 (2),
      pp. 83-95.

De Fériet, J. K. (1951), Averaging Processes and Reynolds
      Equations in Atmospheric Turbulence, *Journal Meteor-*
      ology, 8 (October), pp. 358-361.

Diachishin, A. N. (1963), Dye Dispersion Studies, *Proc. ASCE*,
      89, SA-1, pp. 29-49.

Kullenberg, G. E. B. (1969), Measurements of Horizontal and
      Vertical Diffusion in Coastal Waters, *Acta Regiae*
      Soc. Scien. Litt. Gothoburgensis, *Geophysica* 2.

Kullenberg, G. E. B. (1971), *Results of Diffusion Experiments*
      in the Upper Region of the Sea, Univ. of Copenhagen,
      Inst. Phys. Ocean., Report No. 12.

Kullenberg, G. (1972), Apparent Horizontal Diffusion in
      Stratified Vertical Shear Flow, *Tellus*, 24 (1),
      pp. 17-28.

Mood, A. M. (1950), *Introduction to the Theory of Statistics*,
      New York, McGraw-Hill.

National Aeronautics and Space Administration (1971), *Trinity*
      Bay Study: Status Report 5, Earth Observations Division,
      Manned Spacecraft Center, Houston, Texas.

Okubo, A. (1962), <u>Horizontal Diffusion from an Instantaneous Point-Source due to Oceanic Turbulence</u>, Chesapeake Bay Institute, Technical Report 32, Reference 62-22.

Okubo, A. (1962), A Review of Theoretical Models for Turbulent Diffusion in the Sea, <u>Jnl. Oceanographical Soc. Japan</u>, 20th Anniversary Volume, pp. 286-320.

Okubo, A. (1968), <u>A New Set of Oceanic Diffusion Diagrams</u>, Chesapeake Bay Institute, Technical Report 38, Reference 68-6.

Okubo, A. (1971), Oceanic Diffusion Diagrams, <u>Deep-Sea Research</u>, <u>18</u>, pp. 789-802.

Phillips, O. M. (1966), <u>The Dynamics of the Upper Ocean</u>, London: Cambridge University Press.

Ward, G. H. (1972), Some Gaussian Methods of Analyzing Two-Dimensional Dye Distributions for Dispersion Coefficients, Technical Memorandum, Ocean Sciences and Water Resources Department, TRACOR, Inc., Austin, Texas.